Contents lists available at ScienceDirect

Applied Geochemistry

journal homepage: http://www.elsevier.com/locate/apgeochem

Interactive PHREEQ-N-AMDTreat water-quality modeling tools to evaluate performance and design of treatment systems for acid mine drainage

Charles A. Cravotta III

Research Hydrologist, U.S. Geological Survey, Pennsylvania Water Science Center, 215 Limekiln Rd, New Cumberland, PA, 17070, USA

ARTICLE INFO

ABSTRACT

The PHREEQ-N-AMDTreat aqueous geochemical modeling tools described herein simulate changes in pH and solute concentrations resulting from passive and active treatment of acidic or alkaline mine drainage (AMD). The "user-friendly" interactive tools, which are publicly available software, utilize PHREEQC equilibrium aqueous and surface speciation models and kinetics models for O_2 ingassing and CO_2 outgassing, iron and manganese oxidation and precipitation, limestone dissolution, and organic carbon oxidation combined with reduction of nitrate, sulfate, and ferric iron. Reactions with synthetic caustic chemicals (CaO, Ca(OH)$_2$, NaOH, Na$_2$CO$_3$) or oxidizing agents (H$_2$O$_2$) also may be simulated separately or combined with sequential kinetic steps. A user interface facilitates input of water chemistry data for one or two (mixed) influent AMD solutions and adjustment of kinetic variables. Graphical and tabular output indicates the changes in pH, metals and other solute concentrations, total dissolved solids, and specific conductance of treated effluent plus the cumulative quantity of precipitated solids as a function of retention time or the amount of caustic agent added. By adjusting kinetic variables or chemical dosing, the effects of independent or sequential treatment steps that have different retention time (volume/flow rate), aeration rate, quantities of reactive solids, and temperature can be simulated for the specified influent quality. The size (land area) of a treatment system can then be estimated using reaction time estimates (volume for a corresponding treatment step is the product of reaction time and flow rate; area is volume divided by depth). Given the estimated system size, the AMDTreat cost-analysis model may be used to compute approximate costs for installation (capital) and annual operations and maintenance. Thus, various passive and/or active treatment strategies can be identified that could potentially achieve the desired effluent quality, but require different land area, equipment, and costs for construction and operation.

1. Introduction

Contaminated drainage and associated metal-rich precipitates from abandoned coal and metal mines degrade aquatic habitats and affect the potential utilization of water resources in mining regions worldwide. The mine effluents can have a wide range of pH values (2–8) along with elevated concentrations of SO$_4$, Fe, Al, Mn, and other constituents (Blowes et al., 2014; Cravotta, 2008a; Feng et al., 2014; Gombert et al., 2018; Li, 2018; Nordstrom, 2011a, 2011b). Although various trace elements, such as Zn, Cd, Co, Cu, Pb, Ni, As, Se, and others, can be present at concentrations that approach or exceed aquatic toxicity thresholds, dissolved concentrations of Fe, Al, and Mn account for most metals loading from coal mines (Cravotta, 2008a; Cravotta and Brady, 2015; Feng et al., 2014; Gombert et al., 2018). Metal-mine drainage generally overlaps the composition of coal-mine drainage and produces similar precipitates but can have more extreme values for pH, sulfate, and

trace-element concentrations (Nordstrom, 2011a). After exposure to atmospheric conditions, dissolved Fe, Al, and Mn tend to precipitate as ochreous encrustations composed of amorphous to poorly crystalline Fe^{III}- and Al-hydroxide and hydroxysulfate compounds, including ferrihydrite (Fe(OH)$_3$), schwertmannite (Fe$_8$O$_8$(OH)$_6$SO$_4$), goethite (FeOOH), boehmite (AlOOH), gibbsite (Al(OH)$_3$), and basaluminite (Al$_4$(OH)$_{10}$SO$_4$) (Bigham et al., 1996; Bigham and Nordstrom, 2000; Cravotta, 2005, 2008a, 2008b; Kairies et al., 2005; Lozano et al., 2020; Robbins et al., 1999a; Sánchez-España et al., 2016; Winland et al., 1991), plus locally important Mn^{III-IV} hydroxides and oxides (Cravotta and Trahan, 1999; Cravotta and Watzlaf, 2003; Kairies et al., 2005; Santelli et al., 2010; Tan et al., 2010).

Treatment of acidic or alkaline mine drainage (AMD) to attenuate dissolved metals can decrease acidity (Kirby and Cravotta, 2005) and contaminant loadings to streams, potentially mitigating aquatic impacts. At active mining operations, aggressive aeration and/or the addition of

alkaline (caustic) chemicals (NaOH, CaO, Ca(OH)$_2$) or oxidizing agents (H$_2$O$_2$) may be used along with polymers to facilitate the precipitation and settling of metal-rich (Al, Fe, Mn) solids (Cravotta and Brady, 2015; Cravotta et al., 2015; Skousen et al., 2017, 2019; U.S. Environmental Protection Agency, 1983). At abandoned mines, passive treatment using natural substrates, such as limestone and organic-rich compost, may be combined with aeration cascades to increase alkalinity, pH, and O$_2$ with associated attenuation of metals concentrations (Geroni et al., 2012; Hedin et al., 1994; Johnson and Hallberg, 2005; Watzlaf et al., 2004). Decreased concentrations of trace metals concomitant with increased pH during mine-water treatment are consistent with their attenuation by coprecipitation or adsorption with hydrous Fe^{III} oxides (HFO), hydrous Al^{III} oxides (HAO), and hydrous Mn^{III-IV} oxides (HMO) (Burrows et al., 2017; Cravotta et al., 2015; Cravotta and Brady, 2015; Cravotta and Trahan, 1999; Cravotta and Watzlaf, 2003; Kairies et al., 2005). These hydrous metal oxides (HMeO) in AMD treatment systems and associated aquatic environments may be present as discrete phases or combined with other sorbent materials as components of particulate matter, sediments, and biofilms (e.g. Ashby, 2017; Burgos et al., 2012; Chen and Thompson, 2018; Coston et al., 1995; Hedin et al., 2019; Kairies et al., 2005; Lofts and Tipping, 1998; Munk et al., 2002; Tipping et al., 2011; Webster et al., 1998; Winland et al., 1991).

A specific water-treatment strategy may be appropriate for a mine effluent depending on variations in its flow rate and chemistry, site characteristics, funding, and operational logistics plus the chemical and biological characteristics of the receiving water body (Pennsylvania Department of Environmental Protection, 2016). Empirical testing of aeration rate, chemical dosing, and/or contact time with limestone or other substrates can (1) demonstrate the potential effectiveness of a treatment method to meet criteria for discharge and the protection of aquatic life and (2) be useful to indicate system sizing and estimate associated costs (e.g. Cravotta, 2003; 2007; 2008; 2015; Cravotta and Watzlaf, 2003; Cravotta et al., 2008; 2015; Means and Hilton, 2004; Watzlaf and Hedin, 1993; Watzlaf et al., 2004). However, the empirical data, if available, may not demonstrate variations in treatment resulting from changes in the flow rate, water quality, temperature, and other environmental conditions. Geochemical modeling coupled with cost-analysis software, such as AMDTreat (Office of Surface Mining Reclamation and Enforcement, 2017; Cravotta et al., 2015), may be applied to identify and evaluate treatment strategies for the potential range of variations in influent water quality and to compare costs for construction and operation of different treatment methods that produce the desired effluent quality.

In this paper, a novel geochemical tool set is presented that couples aqueous and surface complexation equilibrium with kinetics models to simulate potential changes in water quality during passive and active treatment of AMD. The reactions considered may occur in various environmental settings and affect a wide range of major and trace elements; however, the current scope of modeling and this paper are limited to those constituents (acidity, Al, Fe, Mn, and SO$_4$, plus total dissolved solids and specific conductance) that are the focus of pollutant discharge regulations at coal mines in the USA. Although the geochemical tool set can be used independently, it was developed for eventual incorporation with AMDTreat, which is currently (2018–2020) being recoded from FoxPro to C++ (Cravotta, 2018). This paper provides background on the software development, describes relevant rate expressions and associated sources of information, explains some of the options for adjusting variables, and provides examples for the potential application and interpretation of modeling results.

2. Materials and methods

The PHREEQ-N-AMDTreat water-quality modeling tools, accessible in the U.S. Geological Survey software release (Cravotta, 2020) and with supplemental data, were developed by building on previous PHREEQC (Parkhurst and Appelo, 2013) geochemical codes reported by Cravotta

(2015) and Burrows et al. (2017). The modified PHREEQC code was adapted to run using IPhreeqcCOM (Charlton and Parkhurst, 2011) with an expanded thermodynamic database and a user interface (UI) for input and adjustment of the modeled variables. The code combines equilibrium aqueous and surface speciation and kinetics equations for gas exchange, aqueous Fe^{II} and Mn^{II} oxidation, limestone dissolution, and organic carbon oxidation coupled with reduction of NO$_3$, SO$_4$, and Fe^{III}. Other reported models considered Fe^{II} and Mn^{II} oxidation kinetics and may also have considered adsorption and neutralization processes that are important for AMD treatment (Antoniou et al., 2013; Vries et al., 2017; Burrows et al., 2017). Nevertheless, the executable PHREEQ-N-AMDTreat tools were specifically designed to facilitate simulations of water-quality effects from AMD treatment processes.

Modeled variables include initial solution chemistry and important physical and chemical parameters that may affect the water quality during treatment (Table 1 and S1). For the current effort, the phreeqc. dat database (provided with Phreeqc Interactive 3.6.2.15100 January 2020), which includes diffusivity coefficients for computation of specific conductance (SC), was supplemented with thermodynamic data for solubilities of Fe, Al, Mn, or SO$_4$ solids (Table S2), surface speciation involving HFO, HMO, and HAO sorbents (Tables S3 and S4), and rate models for kinetic reactants (Table S5). To prevent unrealistic instantaneous equilibration to oxidized or reduced species, relevant equilibrium expressions were replicated for "decoupled" redox species of Fe (+2, +3), Mn (+2, +3), N (−3, +5), and S (−2, +6), which are involved in kinetic (disequilibrium) reactions (e.g. Antoniou et al., 2013; Bethke, 2008; Parkhurst and Appelo, 2013; Vries et al., 2017). Oxidation or reduction reactions for the decoupled species occur only through the rate models. All the rate models included in phreeqc.dat (provided with Phreeqc Interactive 3.6.2.15100 January 2020) were modified; the modified rate models plus additional rate models, described below, include adjustment factors that are multiplied by the rate constants. Hereinafter, the expanded thermodynamic database including the rate models, which are used by the PHREEQ-N-AMDTreat modeling tools, is identified as phreeqcAMDTreat.dat.

The UI, which was generated with Visual Studio (2019), is illustrated for each of the PHREEQ-N-AMDTreat tools with different case-study examples in the Results and Discussion and in the supplementary data. The UI facilitates the input, adjustment, and saving of values for water-quality and kinetic variables and permits selection of on-screen graphical displays of results as well as output reports. Instead of "hard-coded" numeric values within the PHREEQC code, which would require modification of the code each time a value is changed, the IPhreeqcCOM code that is linked to the UI incorporates text variables. Numeric values for these text variables, which are displayed in the UI and saved in xml files, are specified for input solution chemistry, kinetics parameters, and sorbent characteristics.

2.1. Kinetics

The PHREEQ-N-AMDTreat modeling tools consider time-dependent chemical reactions that are affected by variations in the temperature, pH, concentrations of dissolved gases and solutes, the availability of sorbent surfaces or reactive substrates, and/or catalysis by iron-oxidizing bacteria (FeOB). All the rate expressions and rate constants for the kinetics models were adapted from the literature. The literature rate constants are automatically corrected for temperature effects and may be further adjusted by user-selected multiplication factors, explained below.

2.1.1. Atmospheric exchange

Because aeration affects the aqueous concentrations of O$_2$ and CO$_2$ and, consequently, pH and aqueous ion activities (e.g. Cravotta, 2015; Geroni et al., 2012; Kirby et al., 2009), the kinetics of gas exchange can affect numerous equilibrium and kinetics processes. A generalized first-order asymptotic expression is used to estimate the rates of CO$_2$

Table 1

Abbreviated description of variables used in PHREEQ-N-AMDTreat modeling tools.

Variable description	Variable on User Interface
Solutions A and B[a]	
Design flow	Design flow (gpm)[a]
Mix fraction	Mix Fraction
Water temperature, Celsius	Temp (C)
Specific conductance at 25°C	SC (uS/cm)
Dissolved oxygen	DO (mg/L)
pH	pH
Acidity	Acidity (mg/L)
Net acidity, calculated	Estimate NetAcidity
Alkalinity	Alk (mg/L)
Total inorganic carbon	TIC (mg/L as C)
Total inorganic carbon, calculated	Estimate TIC
Total iron	Fe (mg/L)
Ferrous iron	Fe2 (mg/L)
Ferrous iron, calculated	Estimate Fe2
Aluminum	Al (mg/L)
Manganese	Mn (mg/L)
Sulfate	SO4 (mg/L)
Chloride	Cl (mg/L)
Calcium	Ca (mg/L)
Magnesium	Mg (mg/L)
Sodium	Na (mg/L)
Potassium	K (mg/L)
Silicon	Si (mg/L)
Nitrate	NO3N (mg/L)
Total dissolved solids	TDS (mg/L)
Dissolved organic carbon	DOC (mg/L as C)
Humate	Humate (mg/L as C)
Hydrogen peroxide, calculated (after conservative mixing of A and B)	Estimate H2O2.mol/L
Kinetic adjustment factor (multiplied by rate constant) applied equally to all steps of ParallelTreatment or TreatTrainMix2 tools	
Factor kCO2, multiplied by CO2 outgassing rate constant (kLaCO2)	factr.kCO2
Factor kO2, multiplied by CO2 outgassing rate constant to estimate O2 ingassing rate constant	factr.kO2
Factor kFeHOM, multiplied by homogeneous Fe2 oxidation rate constant	factr.kFeHOM
Factor kFeHET, multiplied by heterogeneous Fe2 oxidation rate constant	factr.kFeHET
Factor kFeIIMnOx, multiplied by heterogeneous Fe2 oxidation rate constant	factr.kFeIIMnOx
Factor kbact, multiplied by microbial rate constant (assumes Fe oxidizing bacteria MPN = 5.3e11 cells/L)	factr.kbact
Factor kFeNO3, multiplied by homogeneous Fe2 oxidation rate constant	factr.kFeNO3
Factor kMnHOM, multiplied by homogeneous Mn2 oxidation rate constant	factr.kMnHOM
Factor kMnHFO, multiplied by heterogeneous Mn2_HFO oxidation rate constant	factr.kMnHFO
Factor kMnHMO, multiplied by heterogeneous Mn2_HMO oxidation rate constant	factr.kMnHMO
Factor kSHFO, multiplied by FeIII reduction-sulfide oxidation rate constant	factr.kSHFO
Factor kSOC, multiplied by sedimentary organic carbon oxidation rate constant	factr.kSOC
Factor kDOC, multiplied by dissolved organic carbon oxidation rate constant	factr.kDOC
Factor kH2O2, peroxide Fe2 oxidation rate constant	factr.kFeH2O2
Exponential factor for calcite dissolution rate model	EXPcc
Kinetic adjustment and equilibrium variables used in CausticTitration tool	
Time, in seconds, for pre-aeration step	Time0
kCO2, CO2 mass-transfer rate for pre-aeration step; see Table S6	kLaCO2.1/s
Steady-state log PCO2, used with kCO2 in CO2 mass-transfer rate expression	Steady-state logPCO2
Concentration of caustic soda (NaOH) solution in weight percent	NaOH wt%soln

Table 1 (*continued*)

Variable description	Variable on User Interface
Equilibrium value (solid-phase precipitation limit) for all steps in CausticTitration, ParallelTreatment, or TreatTrainMix2 tools	
Saturation index for calcite precipitation as equilibrium phase	SI_CaCO3
Saturation index for siderite precipitation as equilibrium phase	SI_FeCO3
Saturation index for Fe(OH)3 precipitation as equilibrium phase; see Table S2	SI_Fe(OH)3
Saturation index for schwertmannite precipitation as equilibrium phase; see Table S2	SI_Schwertmannite
Saturation index for Al(OH)3 precipitation as equilibrium phase; see Table S2	SI_Al(OH)3
Saturation index for basaluminite precipitation as equilibrium phase; see Table S2	SI_Basaluminite
Kinetic adjustment factor applied differently to each step of ParallelTreatment or TreatTrainMix2 tools, i = (1:11)	
Target pH specified for caustic addition at steps 1-5	– > pH
Hours total for step (1:11)	Time.hrs
Water temperature at end of step (1:11)	Temp2.C
Hydrogen peroxide at beginning of step (1:11)	H2O2.mol
kCO2, CO2 mass-transfer rate at beginning of step (1:11); see Table S6	kLaCO2.1/s
Steady-state log PCO2, used with kCO2 in CO2 mass-transfer rate expression for each step (1:11)	Lg(PCO2.atm)
Calcite unit surface area at beginning of step (1:11); see Table S7	SAcc.cm2/mol
Calcite mass fraction in limestone at beginning of step (1:11)	M/M0cc
Sedimentary organic carbon mass at beginning of step (1:11)	SOC.mol
Sorbent mass at beginning of step (1:11)	HMeO.mg
Sorbent content as percent iron at beginning of step (1:11)	Fe%
Sorbent content as percent manganese at beginning of step (1:11)	Mn%
Sorbent content as percent aluminum at beginning of step (1:11)	Al%
Description of step (1:11)	Description

[a] Input values for two different solutions, A and B, may be entered. Suffix "B" applies to variable names for solution B.

outgassing and O_2 ingassing:

$$d[C]/dt = -k_{L,C}a \cdot K_C \cdot (Pc - Pc_S) = -k_{L,C}a \cdot ([C] - [C]_S) \qquad (1)$$

where C is either CO_2 or O_2, [C] is the molar concentration of the dissolved gas, $k_{L,C}a$ is the mass-transfer coefficient in units of inverse time, K_C is the temperature-adjusted Henry's Law solubility constant, P_C is the gas partial pressure, and P_{CS} is the steady-state partial-pressure value at equilibrium with the ambient atmosphere ($[C]_S = Kc \times Pc_S$), typically assuming Pco_{2S} is $10^{-3.4}$ atm and Po_{2S} is $10^{-0.67}$ atm. The gas mass-transfer rate is adjusted for variations in temperature relative to a reference temperature of 20 °C (Dempsey et al., 2001; Rathbun, 1998).

$$k_{L,C}a_T = k_{L,C}a \cdot (1.0241)^{T-20} \qquad (2)$$

where T is degrees Celsius.

For generalized application of the gas-exchange kinetics, empirical data were collected on the rates of O_2 ingassing and CO_2 outgassing during an aeration experiment at one AMD site described by Cravotta (2015) and at several active or passive treatment AMD sites in Pennsylvania that employed various aeration or other treatment technologies (Means et al., 2015; this paper). Values for $k_{L,}co_2$ and $k_{L,}o_2$ were estimated from the linear slope of $Ln(C_0-C_S)/(C_t-C_S)]$ versus t, where t is elapsed time during the aeration experiment or travel time between measurement points. For aeration cascades and ditches, travel time for intentionally dislodged HMeO sediment was measured for the distance traveled. For a pond, wetland, or limestone bed, the travel time

(residence time) was computed by dividing the estimated water volume by the measured flow rate on the date of sampling. No attempt was made to explicitly consider the effects of water depth, wind, and other hydrodynamic parameters on the gas exchange rates or solute transport (e. g. Rathbun, 1998; Zappa et al., 2003). The empirical values corrected to 20 °C for $k_{L,CO2}$ ranged from 0.000001 s^{-1} to 0.05 s^{-1} (Table S6); values of $k_{L,O2}$ were a factor of approximately 2.1 times those of $k_{L,CO2}$ on average, which corresponds to a $k_{L,CO2}$: $k_{L,O2}$ ratio of 0.48 and indicates CO_2 outgassing is approximately half the rate of O_2 ingassing. Dempsey et al. (2001) reported $k_{L,CO2}$: $k_{L,O2}$ ratios for passive mine water treatment ponds and channels they investigated ranged from 0.30 to 0.65.

2.1.2. Kinetics of iron oxidation

The iron oxidation rate models directly consider the effects of pH and concentrations of dissolved oxygen (DO), nitrate, and aqueous Fe^{2+} (homogeneous oxidation) plus catalysis by adsorption of Fe^{2+} to HFO and HMO surfaces (heterogeneous oxidation) and/or microbial activity (biotic oxidation).

The homogeneous Fe^{II} oxidation rate law of Stumm and Lee (1961), expressed in terms of $[O_2]$ and $\{H^+\}$ $(=10^{-pH})$ by Stumm and Morgan (1996, p. 683–685), describes the abiotic oxidation of aqueous Fe^{2+}:

$$d[Fe^{II}]/dt = -k_{HOM} \cdot [O_2] \cdot \{H^+\}^{-2} \cdot [Fe^{2+}] \qquad (3)$$

where { } indicates aqueous activity, [ ] indicates aqueous concentration in mol/L, and at pH 5 to 8 and 20 °C, the homogeneous rate constant $k_{HOM} = 5.0 (\pm 1.56) \times 10^{-14}$ mol L^{-1} s^{-1} (Singer and Stumm, 1970; Stumm and Morgan, 1996). The uncertainty range corresponds to 0.7 to 1.3 times the reported reference value of k_{HOM}. Oxidation of Fe^{II} by nitrate $[NO_3^-]$, which has been reported to be one-fourth the rate by $[O_2]$ (Appelo and Postma, 2005), was computed by replacing $[O_2]$ in Eq. (3) with $0.25 \times [NO_3^-]$. The homogeneous Fe^{II} oxidation rate model, shown as Eq. (3), is commonly expressed in terms of P_{O2} and $\{OH^-\}$:

$$d[Fe^{II}]/dt = -k_{HOM-OH} \cdot P_{O2} \cdot \{OH^-\}^2 \cdot [Fe^{2+}] \qquad (4)$$

with a corresponding rate constant of 1.33×10^{12} (mol/L)$^{-2}$ atm^{-1} s^{-1} $(= k_1 \cdot Ko_2/Kw^2)$ at 20 °C, which includes factors for the hydrolysis of water ($Kw = 10^{-14.168} = \{OH^-\} \cdot \{H^+\}$) and the Henry's Law constant for O_2 solubility in water ($Ko_2 = 10^{-2.854} = [O_2]/P_{O2}$ adjusted from 25 °C to 20 °C using polynomial expressions in phreeqc.dat and phreeqcAMDTreat.dat). The rate expressions given in Eqs. (3) and (4) are interchangeable in PHREEQC and provide the same results, provided the relevant rate constants and the temperature corrections for Kw and Ko$_2$ are applied.

By using the reported activation energy of 96.2 kJ mol^{-1} (23 kcal mol^{-1}) for Eq. (3) (Stumm and Morgan, 1996, p. 684) with the Arrhenius equation (Appelo and Postma, 2005), the rate constant is automatically adjusted in the PHREEQ-N-AMDTreat model from the reference temperature to lower or higher temperatures:

$$k_{HOM-T2} = k_{HOM-T1} / \exp\{E_a /(R) \cdot (1/TK_2 - 1/TK_1)\} \qquad (5)$$

where TK_1 is the reference temperature of 20 °C expressed in absolute temperature (degrees Kelvin, 293.15 K), TK_2 is the modeled temperature, k_{HOM-T2} is the temperature-adjusted value of the rate constant, k_{HOM-T1} is the reference value of the rate constant, E_a is the activation energy, and R is the ideal gas constant.

The heterogeneous oxidation rate model for Fe^{II} is expressed in terms of the concentrations of adsorbed Fe^{II} and dissolved oxygen (Tamura et al., 1976):

$$d[Fe^{II}_{ads}]/dt = -k_{HET} \cdot [O_2] \cdot [Fe^{II}_{ads}] \qquad (6)$$

where the rate constant k_{HET} has a value of 73 (mol/L)$^{-1}$ s^{-1} at 25 °C and the activation energy is 179 kJ mol^{-1} (Dempsey et al., 2001; Sung and Morgan, 1980). The amount of adsorbed Fe^{II}, which is computed as a function of the pH, explained later, is the sum of Fe^{II} on strong and weak adsorption sites of HFO (Dzombak et al., 1990) plus analogous x- and

y-adsorption sites of HMO (Tonkin et al., 2004). Increasing the available mass of sorbent, for example by recirculating HFO solids or by accumulation of HFO on submerged surfaces, increases the corresponding surface area and potential for adsorption of the dissolved Fe^{2+} and other ions at a given pH, with corresponding heterogeneous oxidation (e.g. Davison and Seed, 1983; Dempsey et al., 2001; Jones et al., 2014; Dietz and Dempsey, 2017).

Although Eq. (6) does not distinguish between HFO and HMO as the sorbent, the catalytic oxidation of Fe^{II} by HMO may, in fact, be coupled with the reductive dissolution of the sorbent $Mn^{III,IV}$ oxide (Postma and Appelo, 2000). Through this process, Mn^{2+} is released into solution and HMO is replaced by HFO, with the net result, if any, being a minor change in the total sorbent and sorbed-Fe^{II} and a corresponding increase in dissolved Mn^{II}. The "pyrolusite" reduction rate model in PHREEQ-N-AMDTreat uses the rate constant, k_P of value of 6.98×10^{-5} (mol/L)$^{-1}$ s^{-1} at 25 °C (Parkhurst and Appelo, 2013; Postma and Appelo, 2000, Eq. (12)), with the computed mass of HMO as MnOOH instead of pyrolusite; temperature correction is not applied.

Microbial catalysis of Fe^{II} oxidation is computed as a function of the concentration of FeOB (microbes), pH, DO, and temperature. Acidophilic and neutrophilic FeOB contributions are considered separately. The acidophilic FeOB rate increases as pH decreases from 5 to 2.8 and generally exceeds the abiotic Fe^{II} oxidation rate at these low pH values (Kirby et al., 1999; Kirby and Elder-Brady, 1998; Pesic et al., 1989). In the PHREEQ-N-AMDTreat model, the acidophilic FeOB oxidation rate is added to the homogeneous rate:

$$d[Fe^{II}]/dt = -k_{bio} \cdot C_{bact} \cdot [Fe^{2+}] \cdot [O_2] \cdot \{H^+\} \qquad (7)$$

In Eq. (7) the rate constant k_{bio} is 5.15×10^{-2} L^3 mol^{-2} mg^{-1} s^{-1} at 25 °C (given the pre-exponential factor of 1.02×10^{-2} and activation energy of 58,770 J mol^{-1} reported by Kirby et al., 1999), C_{bact} is the concentration of iron-oxidizing bacteria in mg L^{-1} (dry weight) (Kirby et al., 1999; Pesic et al., 1989), and other variables are as previously defined. Because the most-probable number (MPN) method is traditionally used for enumeration of FeOB (Alexander, 1982; Greenberg et al., 1982), the MPN value of 5.3×10^{11} cells per liter, which equals Cbact of 150 mg L^{-1} ($= MPN \times 2.8 \times 10^{-10}$ mg cell^{-1}), is the default, constant value used in PHREEQ-N-AMDTreat. Increasing the FeOB adjustment factor (factr. kbact) from the default of 1 implies greater FeOB activity than predicted by Eq. (7), whereas decreasing this factor to 0 results in the abiotic homogeneous rate. For rate computations, the same MPN value and factr.kbact are assumed without distinction for the acidophilic or neutrophilic FeOB rate models.

Catalysis by neutrophilic FeOB generally involves adsorption of Fe^{II} by HFO and increases with the amount of HFO-sorbed Fe^{II} (van Beek et al., 2012). Thus, the neutrophilic FeOB contribution is added to the heterogeneous rate in the PHREEQ-N-AMDTreat model. The neutrophilic FeOB rate generally does not exceed the abiotic oxidation rate, except at optimum pH and DO conditions. Eggerichs et al. (2014) showed that at optimum conditions of near-neutral pH (6.5–7.5) and low DO (1.9–2.2 mg L^{-1}), the neutrophilic FeOB rate was approximately a factor of 20 times the abiotic heterogeneous Fe^{II} oxidation rate of Davies and Morgan (1989). Thus, based on the data distributions of Eggerichs et al. (2014, Figs. 4 and 8 therein), an estimate of the overall rate contribution by neutrophilic FeOB is obtained herein by combining adjustment factors for pH and DO.

The combined effects of pH and DO on the neutrophilic FeOB rate are computed as the product of two rate adjustment factors, which yields a value of approximately 20 under optimum conditions (e.g. $4.6 \times 4.5 = 20.7$) that is then multiplied by the temperature-adjusted heterogeneous rate constant, k_{HET} (Eq. (6)). The neutrophilic FeOB adjustment factor for pH is:

$$pH\_factor = -1.605(pH)^2 + 22.383(pH) - 73.351 \qquad (8)$$

at $5.25 < pH < 8.5$; the pH_factor is null for pH values outside this range.

Eq. (8) indicates that the pH rate factor is greatest, ~4.6, at pH 6.8 to 7.2. The neutrophilic FeOB adjustment factor for DO is:

$$DO\_factor = 4.22 \times 10^{12}[O_2]^3 - 1.59 \times 10^9[O_2]^2 + 1.50 \times 10^5[O_2] + 0.282 \quad (9)$$

at $[O_2] < 1.9 \times 10^{-4}$ mol L^{-1} (6.1 mg L^{-1}); the DO_factor is 0.3 for greater DO values. Eq. (9) indicates the greatest DO factor, ~4.5, at $[O_2]$ of 6.0×10^{-5} mol L^{-1} (1.9 mg L^{-1}) to 6.9×10^{-5} mol L^{-1} (2.2 mg L^{-1}).

In addition to the above models for Fe^{II} oxidation by oxygen or nitrate, an additional kinetic expression for the oxidation of Fe^{II} by hydrogen peroxide (H_2O_2) is included in the PHREEQ-N-AMDTreat model. The rate expression is first order with respect to molar concentrations of H_2O_2 and total aqueous Fe^{II} (Hardwick, 1957; Millero et al., 1987; Millero and Sontolongo, 1989):

$$d[H_2O_2]/dt = -k_{H2O2} \cdot [H_2O_2] [Fe^{II}] \quad (10)$$

The total $[Fe^{II}]$ oxidized is computed as $0.5 \times [H_2O_2]$ on the basis of the following stoichiometry:

$$Fe^{2+} + 0.5 \, H_2O_2 + H^+ = Fe^{3+} + H_2O \quad (11)$$
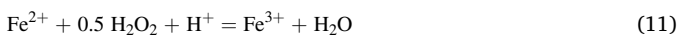
Empirical tests on near-neutral mine drainage indicate that upon the addition of H_2O_2, Fe^{II} oxidation and subsequent Fe^{III} hydrolysis are practically instantaneous, occurring within seconds, while Mn^{II} is unaffected (Cole et al., 1977; Burrows et al., 2017; Cravotta, 2015; Means et al., 2013). Although Mn^{II} is not oxidized by H_2O_2 (Sato, 1960), H_2O_2 can oxidize dissolved sulfide and organic carbon (Hoffman, 1977; Millero and Sotolongo, 1989). PHREEQ-N-AMDTreat computes the quantity of $[H_2O_2]$ needed to oxidize only the aqueous concentration of Fe^{II} on the basis of the stoichiometry of Eq. (11); this computed value may be deficient for actual treatment where sulfide and/or organic carbon compounds are present in the water or where the pH is very low.

Millero and Sontolongo (1989) reported the rate constant for Eq. (10) increases dramatically with pH from 3.5 to 8.5 but is independent of pH at values less than 3.5. The value of k_{H2O2} as a function of pH is estimated herein using a linear regression equation for log(k) versus pH for freshwater at 5 °C based on Figure 13 of Millero and Sotolongo (1989):

$$\log k_{H2O2} = 0.72 \, pH - 1.02 \quad (12)$$

The corresponding rate constant is automatically adjusted to higher or lower temperature using the Arrhenius equation with an activation energy of 56 kJ mol^{-1} (Millero and Sotolongo 1989). Eq. (12) yields values of k_{H2O2} at 5 °C of 109,650 (mol/L) $^{-1}$ s^{-1} at pH 7 and 31.6 (mol/L) $^{-1}$ s^{-1} at pH $\leq$ 3.5. The latter value corrected to 20 °C is 109.2 (mol/L) $^{-1}$ s^{-1}, which is similar in magnitude to the rate of 42.6 (mol/L) $^{-1}$ s^{-1} for dilute sulfuric acid solution at 20 °C reported by Hardwick (1957).

2.1.3. Kinetics of manganese oxidation

The oxidation rate models for Mn^{II} in PHREEQ-N-AMDTreat consider homogeneous and heterogeneous contributions such as those for Fe^{II}; however, the applicable Mn^{II} oxidation rate expressions do not explicitly consider biological catalysis. The kinetics equation for the homogeneous Mn^{II} oxidation rate law is adopted from Davies and Morgan (1989) with P_{O2}:

$$d[Mn^{II}]/dt = -k_{1Mn} \cdot P_{O2} \cdot \{OH^-\}^{2.56} \cdot [Mn^{2+}] \quad (13)$$

Davies and Morgan (1989) reported the rate model for P_{O2} of 1 atm with the rate constant k_{1Mn} value of 2.08×10^{-2} (mol/L) $^{-2.56}$ s^{-1} atm^{-1} at 25 °C and activation energy of 272 kJ mol^{-1}; they used the homogeneous rate model given in Eq. (13) to correct the rate constant values for the much faster heterogeneous Mn^{II} oxidation rate.

The heterogeneous Mn^{II} oxidation rate model incorporates pH-dependent adsorption of Mn^{2+} by HFO (Davies and Morgan, 1989) and/or HMO (Morgan, 2005):

$$d[Mn^{II}ads]/dt = -k_{2Mn} \cdot P_{O2} \cdot [Mn^{II}ads] \quad (14)$$

where the rate constant k_{2Mn} has a value of 2.1×10^{-4} s^{-1} atm^{-1} and the activation energy is approximately 100 kJ mol^{-1} as reported by Davies and Morgan (1989). The amount of adsorbed Mn^{II} $\cdot(Mn^{II}ads)$, which is computed in PHREEQ-N-AMDTreat as a function of the pH and the composition and mass of sorbent, is the sum of that sorbed on strong and weak sites of HFO (Dzombak and Morel, 1990) and on analogous x- and y-adsorption sites of HMO (Tonkin et al., 2004). The default Mn^{II}-HMO heterogeneous oxidation rate constant is estimated as 0.5 that reported for Mn^{II} on HFO by Davies and Morgan (1989). This Mn^{II}-HMO rate estimate accounts for the spontaneous disproportionation of MnOOH to yield 0.5 MnO_2 and 0.5 aqueous Mn^{II} (Bricker, 1965). Despite the slower heterogeneous oxidation rate for Mn^{II}-HMO, half of that for Mn^{II}–HFO, Mn^{II} adsorption on HMO greatly exceeds that by HFO of equivalent mass at moderately acidic to near-neutral pH (see Tables S3 and S4).

Increasing the available surface area of HFO or HMO, for example by accumulation of HMO coatings on limestone particles in a Mn-removal bed (e.g. Means and Rose, 2005), increases potential for attenuation of dissolved Mn at a given pH. Eventually, the adsorbed Mn may oxidize in place, adding to the HMO sorbent. Although microbial catalysis is not modeled explicitly, increasing the available HFO and/or HMO surface area (mass of sorbent) or increasing the respective multiplication factors for the heterogeneous Mn^{II} oxidation rate (factr.kMnHFO, factr. kMnHMO) may be applied to account for the enhanced biological catalysis of Mn oxidation in passive AMD treatment (Cravotta and Trahan, 1999; Means and Rose, 2005; Robbins et al., 1999b; Santelli et al., 2010; Tan et al., 2010; Vail and Riley, 2000).

2.1.4. Kinetics of limestone dissolution

The calcite dissolution kinetics model in PHREEQ-N-AMDTreat is adapted from the oft-cited Plummer, Wigley, and Parkhurst ("PWP") calcite-dissolution rate model, which considers pH, partial pressure of CO_2, and proximity of solution to calcite equilibrium (Plummer et al., 1978). The PWP model indicates the rate of calcite dissolution is a function of three dissolution reactions (forward; k_1, k_2, k_3) and the precipitation reaction (backward; k_4).

$$r = (k_1 \cdot a_{H+} + k_2 \cdot a_{H2CO3*} + k_3 \cdot a_{H2O}) - k_4 \cdot a_{Ca2+} \cdot a_{HCO3-} \quad (15)$$

At equilibrium, the backward and combined forward reactions occur at an equal rate. For the above expression, Plummer et al. (1978) reported the forward rate constants in millimoles calcite per centimeter squared per second (mmol cm^{-2} s^{-1}) as a function of temperature (T, in K):

$$\log k_1 = 0.198 - 444 / T; \quad (16)$$

$$\log k_2 = 2.84 - 2177 / T; \quad (17)$$

$$\log k_3 = -5.86 - 317 / T \text{ for } T \leq 298; \log k_3 = -1.10 - 1737 / T \text{ for } T > 298 \quad (18)$$

Appelo et al. (1998) and Appelo and Postma (2005) adapted the PWP model to consider physical characteristics of the system as well as solution chemistry:

$$R_{CC} = k \cdot (A / V) \cdot (1 - \Omega)^n \quad (19)$$

where A is calcite surface area, V is volume of solution, Ω is saturation ratio (IAP/K = 10^{SIcc}; where SIcc is the saturation index for calcite) and n is an empirical coefficient (typically set to 0.67) that accounts for variations in particle shape. For the PWP model applied to 1-L solution, the overall rate of calcite dissolution becomes:

$$R_{CC} = (k_1 \cdot a_{H+} + k_2 \cdot a_{H2CO3*} + k_3 \cdot a_{H2O}) \cdot (A) \cdot (1 - 10^{(n \bullet SIcc)}) \quad (20)$$

Generally, the dissolution rate increases with increased values of A (decreased particle size) and/or decreased values of SIcc (distance from equilibrium). For the PHREEQ-N-AMDTreat model, limestone particle
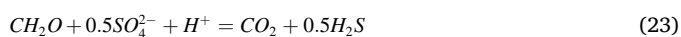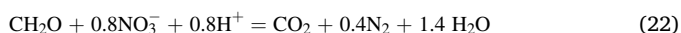
surface area and corresponding particle volume are estimated for standard dimensions of various aggregate sizes assuming an ellipsoid shape (e.g. Cravotta et al., 2008; Pennsylvania Department of Environmental Protection, 2012; Santomartino and Webb, 2007). Using the same dimension and shape information, the approximate volume and mass of HMeO surface coating per liter of water in a limestone bed (void volume) can be estimated given the thickness and density of the coating and the porosity of the limestone bed. Table S7 in the supplementary data is provided for the computations of limestone particle surface area and coating thickness.

Although the rate model does not consider the effects of hydrodynamics or surface coatings on limestone dissolution (e.g. Cravotta, 2008c; Huminicki and Rimstidt, 2008; Palomino-Ore et al., 2019; Rose, 1999; Santomartino and Webb, 2007), the model includes an adjustment factor, M/M_0, that can account for inefficiency of dissolution or impurity of the limestone (Tables 1 and S1). A value of 1 for M/M_{0CC} implies efficient dissolution of pure calcite; values less than 1 indicate decreased availability of $CaCO_3$ for reaction. Likewise, the M/M_{0CC} factor can be used to define the mass fraction of limestone in a mixture with organic matter. For example, a value of 0.25 for M/M_{0CC} indicates the compost mix contains 25% limestone, with the remainder being solid organic carbon (examples are given in Results and Discussion and in supplementary data).

2.1.5. Organic carbon oxidation

Solid organic matter and dissolved organic carbon are essential microbial substrates in bioreactors, anaerobic wetlands, and reducing and alkalinity producing systems. The compositions of organic materials used in such systems vary widely, but frequently include compost mixtures containing 20–25% dispersed limestone fines, bivalve shells, or other calcareous material. Dissolution of the calcareous materials within the compost layer helps (1) to maintain a pH environment favorable to biological sulfate reduction (McCauley et al., 2009; Neculita et al., 2011; Reeder et al., 2010) and (2) to facilitate the precipitation of HAO and HFO solids within the organic-rich layer (Carballo et al., 2011; Rose, 2004; Skousen et al., 2017; Thomas and Romanek, 2002a, 2002b).

Solid organic carbon (SOC) of the compost mixture, represented as CH_2O, may be oxidized by aqueous oxygen, nitrate, and/or sulfate:

$$CH_2O + O_2 = CO_2 + H_2O \tag{21}$$

$$CH_2O + 0.8NO_3^- + 0.8H^+ = CO_2 + 0.4N_2 + 1.4\ H_2O \tag{22}$$

$$CH_2O + 0.5SO_4^{2-} + H^+ = CO_2 + 0.5H_2S \tag{23}$$

Considering the above reactions, the overall rate model for solid organic carbon oxidation is:

$$d[SOC]/dt = -\ k_{SOC} \cdot [SOC] \cdot R_{OX} \tag{24}$$

where [SOC] is the concentration (mol/kg), k_{SOC} is the first-order decay constant with a value of $1.57 \times 10^{-9}\ s^{-1}$, and R_{OX} is the oxidant multiplier in the form of an additive Monod kinetics expression modified from Appelo and Postma (2005):

$$R_{OX} = 1.0[O_2]/(2.94 \times 10^{-4} + [O_2]) + 0.01\ [NO_3^-]/(1.55 \times 10^{-4} + [NO_3^-])$$
$$+ 6.4 \times 10^{-5}[SO_4^{2-}]/(1 \times 10^{-4} + [SO_4^{2-}])\ (arctan(0.42\ (pH - 4.75)) + 5) \tag{25}$$

The factor 1.0, 0.01, or 6.4×10^{-5} in the numerator for the O_2, NO_3^-, or SO_4^{2-} contribution, respectively, indicates the maximum rate (s^{-1}) when multiplied by k_{SOC}. The value in the respective denominators is the half-saturation constant, $K_{1/2}$, which is the concentration (mol L^{-1}) where the rate is half the maximum value. The arctan term in Eq. (25) accounts for the inhibition of sulfate reduction at low pH (Peiffer, 2016).
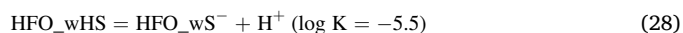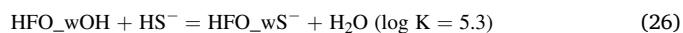
The Monod parameters in Eq. (25) are empirical values for the oxidation of natural organic carbon in soils by the specified oxidants (Eckert and Appelo, 2002). Appelo and Postma (2005) explained that

the overall oxidation rate may be decreased to account for slower decay of recalcitrant organic carbon in sedimentary rock aquifers, or increased, if appropriate. For example, Eckert and Appelo (2002) found the rate of degradation of dissolved organic carbon (DOC) in a contaminated aquifer was 10^7 faster than that for natural organic matter in soil. Likewise, the rate of oxidation is expected to be higher for relatively labile SOC sources, such as fresh or composted manure, compared to sedimentary organic carbon. Thus, in PHREEQ-N-AMDTreat, the default adjustment factor for k_{SOC} is set to 100, which results in a value of k_{OC} equal to $1.57 \times 10^{-7}\ s^{-1}$ that is 100 times faster than that for soil organic carbon. The default adjustment factor for k_{DOC} is set to 1, to reproduce the relatively rapid DOC degradation rate of Eckert and Appelo (2002).

Degradation of SOC and DOC mainly affects the availability of oxidants in the PHREEQ-N-AMDTreat model; aqueous and surface complexation by the uncharacterized SOC and DOC are not considered. Although concentrations of DOC are not routinely measured for AMD samples, untreated AMD may contain $\sim$1 mg L^{-1} (0.5–3.2 mg L^{-1}) of uncharacterized DOC (Cravotta and Brady, 2015), which could decrease or increase through a treatment system depending on microbial CH_2O degradation rates and input from algae, aquatic plants, and leaf litter. Humate is included in the PHREEQ-N-AMDTreat model as a surrogate for natural organic matter (NOM) and other uncharacterized aqueous components of DOC that have varying capacities to form metal-organic complexes. As reported by Burté et al. (2019), aqueous complexation of Fe^{II} and Fe^{III} by humate has the potential effect of decreasing the activity (availability) of Fe^{2+} and slowing the rate of Fe^{II} oxidation. The concentration of humate specified for influent is assumed to be non-degradable; the initial concentration of humate is assumed to be 10% of the initial concentration of DOC unless a non-zero value for humate is specified.

2.1.6. Reduction of Fe^{III} and oxidation of sulfide

In a reducing and alkalinity producing system, also known as a vertical flow wetland (VFW) or vertical flow pond (VFP), water transports solutes down through the organic-rich layer before reaching the underlying bed of limestone aggregate (Rose, 2004; Skousen et al., 2017; Watzlaf et al., 2000, 2004). Reduction of solid or aqueous Fe^{III} to Fe^{II} within the anoxic organic-rich layer of the VFP decreases potential for HFO accumulation within the underlying limestone bed, which otherwise could coat limestone particles or decrease porosity and flow through the bed. In the PHREEQ-N-AMDTreat model, the reductive dissolution of HFO by surface-adsorbed sulfide is included as the relevant kinetic process for the conversion of Fe^{III} to Fe^{II} (dos Santos Alfonso and Stumm, 1992; Peiffer et al., 1992; Poulton, 2003). The rate of Fe^{III} reduction coupled with the oxidation of adsorbed sulfide is faster than that for the microbial reduction of Fe^{III} oxyhydroxides coupled with organic carbon oxidation (e.g. Bonneville et al., 2009; Lovley et al., 1991). In the model, aqueous sulfide, which is produced by sulfate reduction coupled with organic carbon oxidation (Eq. (23)), may adsorb to HFO, if present, or precipitate as mackinawite (FeS). The concentrations of HFO-adsorbed sulfide species on weak and strong sorption sites (HFO_wOH and HFO_sOH, respectively) are computed as a function of pH (Peiffer et al., 1992; Poulton, 2003):

$$HFO\_wOH + HS^- = HFO\_wS^- + H_2O\ (log\ K = 5.3) \tag{26}$$

$$HFO\_wOH + HS^- + H^+ = HFO\_wHS + H_2O\ (log\ K = 10.82) \tag{27}$$

$$HFO\_wHS = HFO\_wS^- + H^+\ (log\ K = -5.5) \tag{28}$$

The adsorbed sulfide then chemically reduces solid Fe^{III} to aqueous Fe^{II}, which is represented by the rate model below, adapted from dos Santos Alfonso and Stumm (1992):

$$d[HS^-]/dt = -\ (k_{e1} \cdot [HFO\_wS^-] + k_{e2} \cdot [HFO\_wHS])\ /\ A_{HFO} \tag{29}$$

where the rate constant k_{e1} is 30 m^2 h^{-1} (8.33×10^{-3} m^2 s^{-1}) for the

oxidation of HS^- on the neutral surface (HFO_wS^-) (mol L^{-1}), the rate constant k_{e2} is 400 m² h⁻¹ (1.11×10^{-1} m² s⁻¹) for the oxidation of HS^- on the protonated surface (HFO_wHS) (mol L^{-1}), and A_{HFO} is the surface area of HFO per liter of solution (m² L^{-1}). Peiffer et al. (1992) reported the rate of oxidation of adsorbed sulfide is approximately 15 times faster than the rate of Fe^{II} dissolution. Thus, $[Fe^{II}]$ released is computed as 1/15 (0.0667) of total $[H_2S]$ oxidized.
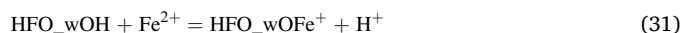
2.2. Adsorption by hydrous metal oxides

The PHREEQ-N-AMDTreat model accounts for surface-catalyzed oxidation kinetics as functions of adsorbed Fe^{2+} and Mn^{2+} on HFO and HMO surfaces (e.g. Chen and Thompson, 2018; Davies and Morgan, 1989; Stumm and Morgan, 1996; Tamura et al., 1976) and HS^- on HFO (dos Santos Alfonso and Stumm, 1992; Peiffer et al., 1992; Poulton, 2003). Thus, surface-complexation equilibria for cations and anions are included in phreeqcAMDTreat.dat (Tables S3 and S4) to model the potential interactions among Fe^{2+}, Mn^{2+}, and other aqueous ions with HMeO surfaces. The inclusion of a broad array of surface speciation reactions is important to indicate potential competition among major and trace ions for available surface sites. The PHREEQ-N-AMDTreat model does not consider sorption of Fe^{3+} and Mn^{3+} or the oxidation of Mn^{3+}. Instead, the concentrations of Fe^{3+} and Mn^{3+} are controlled only by their kinetic production and the consequent precipitation of amorphous $Fe(OH)_3$ or schwertmannite and MnOOH. In addition to all the published HFO, HMO, and HAO equilibrium equations and associated binding constants from the primary works, equilibrium expressions for the adsorption of Fe^{2+} by HFO (Appelo et al., 2002), Al^{3+} by HFO (Burrows et al., 2017; Hiemstra and van Riemsdijk, 2007), HS^- by HFO (Peiffer et al., 1992; Poulton, 2003), and Fe^{2+} by HMO (computed from reported linear free energy (LFER) relations reported by Tonkin et al., 2004) also are included in phreeqcAMDTreat.dat. Other potential mineral sorbents, including various oxides, carbonates, or clay minerals or solid organic matter, which are considered with the Windermere Humic Aqueous Model (Lofts and Tipping, 1998; Tipping et al., 2011) and Visual MINTEQ (Gustafsson, 2013) equilibrium models, were not included in the PHREEQ-N-AMDTreat model.

The adsorption expressions for HFO and HMO employ the diffuse double-layer concept, which considers a monoprotic sorbent with a small number of strong binding sites and a larger number of weak binding sites (Appelo and Postma, 2005; Dzombak and Morel, 1990; Tonkin et al., 2004; Parkhurst and Appelo, 2013). A single binding site is considered for monoprotic HAO (Karamalidis and Dzombak, 2010). Instead of goethite (FeOOH), birnessite (MnO_2), and gibbsite ($Al(OH)_3$), for which the original binding constants were developed, the PHREEQ-N-AMDTreat model defines amorphous ferric hydroxide (Fe$(OH)_3$), manganite (MnOOH), and amorphous $Al(OH)_3$ as the HFO, HMO, and HAO phases, respectively, which are presumed to have the same number of sorption sites per mole and unit surface areas as the original solids, but have different molar mass. In aqueous systems where pH and other conditions change rapidly, the modeled sorbent compounds tend to precipitate readily upon reaching equilibrium (saturation), removing Fe^{3+}, Mn^{3+}, and Al^{3+} from solution and forming fresh surface coatings (e.g. Bigham and Nordstrom, 2000; Chen and Thompson, 2018). For example, Nordstrom (2020) modeled effects of variations in solubility of Fe^{III} and Al phases on the attenuation of the dissolved metals in neutralized AMD and concluded that precipitation of amorphous Fe^{III} and Al compounds controlled the aqueous concentrations. Because the modeled sorbents are more soluble than the crystalline reference compounds, the default equilibrium condition determined by the PHREEQ-N-AMDTreat model results in supersaturation with respect to goethite, birnessite, and/or gibbsite. To consider different precipitates that may limit Fe or Al concentrations, the PHREEQ-N-AMDTreat models permit a user to specify the saturation index at which relevant phases precipitate, which is equivalent to adjusting the solubility constant (Table S2).

Total sorbent mass in the PHREEQ-N-AMDTreat model includes contributions from (1) the precipitation of amorphous $Fe(OH)_3$, MnOOH, and $Al(OH)_3$ to maintain equilibrium (autocatalytic fraction) upon reaching saturation, plus (2) an optional specified mass of previously formed HFO, HMO, and HAO that may be present as surface coatings (previously accumulated fraction) or suspended particles (recirculated sludge). For the autocatalytic fraction, the mass of sorbent will increase to a maximum concentration equal to the initial dissolved metal concentration, following kinetic oxidation of dissolved Fe^{2+} and Mn^{2+}. For the specified additional sorbent fraction, the PHREEQ-N-AMDTreat model requires input on the quantity and composition of the solids expressed as the metal mass per liter of solution (HMeO.mg, Fe %, Mn%, Al%). The model uses these input data with literature values for specific surface area, site densities, and formula weights for the respective sorbents (Table S3) to compute the moles of combined autocatalytic and previously formed sorption sites on HFO, HMO, and HAO for surface-speciation computations.

Surface-equilibrium computations consider the mass of sorbent plus the effects of protons and complexing ligands on the surface charge and the consequent distribution of surface and aqueous species. For example, the distribution of aqueous and adsorbed Fe^{2+} on HFO is determined by the pH and the availability of sorbent with corresponding equilibrium expressions:

$$HFO\_sOH + Fe^{2+} = HFO\_sOFe^+ + H^+ \tag{30}$$

$$HFO\_wOH + Fe^{2+} = HFO\_wOFe^+ + H^+ \tag{31}$$

$$HFO\_wOH + Fe^{2+} + H_2O = HFO\_wOFeOH + 2H^+ \tag{32}$$
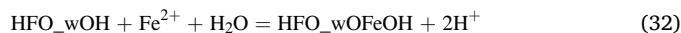
where HFO_s indicates strong sites, and HFO_w indicates weak sites, consistent with Eqs. 26–28. The binding constant for Eq. (30) is $10^{-0.95}$ (Appelo et al., 2002) and those for Eqs. (31) and (32) are $10^{-2.98}$ and $10^{-11.55}$, respectively (Liger et al., 1999; Parkhurst and Appelo, 2013). Although the equilibrium constants to compute activities of aqueous species are corrected for temperature, the binding constants for HFO, HMO, and HAO used in the PHREEQ-N-AMDTreat models are not adjusted for temperature variations.

2.3. Empirical data for model development and calibration

Available data from case studies were used to develop and calibrate simulations using the PHREEQ-N-AMDTreat models. The empirical data had been collected during prior studies to evaluate the attenuation of AMD contaminants (e.g. Ashby, 2017; Burrows et al., 2017; Cravotta, 2015; Cravotta and Brady, 2015; Cravotta and Trahan, 1999; Cravotta et al., 2014; R. Beam, 2020, Pennsylvania Department of Environmental Protection, written commun.). In general, grab samples representing increased reaction time or travel time were collected at points along flow paths in locations where flow was concentrated; integrated depth or width sampling was not attempted. Water temperature, SC, DO, redox potential (Eh), pH, and alkalinity were measured in the field. Field-filtered (0.20 or 0.45-μm) samples were analyzed in the laboratory for dissolved concentrations of major and trace elements. In a few instances, travel times between sample points were measured directly, in order to estimate the CO_2 outgassing rate for aeration steps (Eq. (1)). However, in most cases, travel times or retention times corresponding to the empirical data were computed later using volume estimated from engineering designs divided by the inflow or outflow rate on the date of sampling. Given the retention time for a treatment step (which ranged from seconds to days), other variables in the model, such as CO_2 outgassing rate, limestone particle size, and/or sorbent mass and composition, were adjusted to "calibrate" simulation results to measured water-quality values. Model fit was visually evaluated for multiple variables including pH, P_{CO_2}, P_{O_2}, and concentrations of Fe, Al, Mn, SO_4, and other solutes and was considered acceptable if simulation results were within a factor of ~2 of most measured values (which commonly

varied over an order of magnitude to the end of a flow path).

3. Results and Discussion—Simulation of observed changes in chemistry of AMD

Input variable values and model results for the three complementary PHREEQ-N-AMDTreat tools (CausticTitration, ParallelTreatment, and TreatTrainMix2) are presented below and in supplementary data for multiple case studies. The simulation results are compared to empirical observations in order to calibrate and "validate" the PHREEQ-N-AMDTreat models. Subsequently, the models are used to evaluate potential water-quality effects from different hypothetical treatment strategies.

3.1. Caustic titration case

The "CausticTitration" tool simulates the incremental addition of a caustic chemical (NaOH, Ca(OH)$_2$, CaO, or Na$_2$CO$_3$) to net-acidic or net-alkaline AMD (Fig. 1). The results include the quantity of the selected caustic titrant required to increase pH by 0.25 unit up to 11.0; the concentrations of dissolved Fe, Mn, Al, and other solutes plus net acidity, total dissolved solids (TDS), and SC; the mass of solids precipitated; and saturation indices for relevant solid phases. Although caustic agents may be added without prior treatment steps, aeration of AMD to outgas CO$_2$

before the addition of caustic chemicals has been reported to decrease chemical usage, sludge volume, and treatment costs (Jageman et al., 1988; Means et al., 2015). Thus, the PHREEQ-N-AMDTreat caustic titration model was expanded from the equilibrium titration tool in AMDTreat 5.0 (Cravotta et al., 2015) to include the option for pre-aeration ("decarbonation") before addition of caustic chemicals. For the no-aeration and equilibrium-aeration options, all reactions are assumed instantaneous equilibrium processes, whereas for the pre-aeration simulation, CO$_2$ outgassing, O$_2$ ingassing, and redox reactions are simulated as kinetics processes.

Figs. 1 and 2 show input data and simulation results for caustic titration of the St. Michael AMD with CaO (pebble quick lime) considering scenarios without aeration and with pre-aeration. According to data collected August 2020 (R. Beam, 2020, Pennsylvania Department of Environmental Protection, written commun.), the St. Michael AMD is characterized as a large volume (19,684 L min^{-1}, 5200 gal min^{-1}), anoxic, net-acidic coal-mine discharge (net acidity 223 mg L^{-1} as CaCO$_3$; alkalinity 50.8 mg L^{-1} as CaCO$_3$) that has pH 5.7 with elevated concentrations of dissolved CO$_2$ (Pco$_2$ 10$^{-1.0}$ atm) and Fe^{II} (148 mg L^{-1}) and lower concentrations of Mn^{II} (3.6 mg L^{-1}) and Al (0.34 mg L^{-1}). Cravotta (2008a) reported similar composition of the AMD in 1999. In 2014, Means et al. (2015) evaluated the potential benefits of pre-aeration to outgas CO$_2$ before addition of lime to the AMD: The original lime treatment plant, which began operations in 2013, was

Fig. 1. User interface (UI) for PHREEQ-N-AMDTreat "CausticTitration" modeling tool. Input values for one initial solution (A) or two solutions (A and B mixture) may be entered. Data shown are for simulated pre-aeration before caustic addition at the St. Michael AMD, August 2020 (R. Beam, 2020, Pennsylvania Department of Environmental Protection, written commun.). Selected output results are displayed as a pH matrix in Fig. 2. Detailed descriptions of the model variables are given in Table S1 of supplementary data. Although solution B has zero flow, non-zero values must always be entered for temperature and dissolved oxygen (DO) and values for all other parameters must be provided (blanks are not acceptable).

A. CausticTitration.exe: Not aerated (CaO reacted to achieve pH 8.5 is 675 mg/L as CaCO3)

pH	Caustic asCaCO3mg	Fe_mg	Fe2_mg	Al_mg	Mn_mg	TDS_mg	NetAcidity_mg	SolidsPPT_mg	CO2_mg	O2_mg
5.699391	0.000000	148.253946	148.184017	0.340583	3.606177	1,844.993285	219.160655	0.000000	184.696702	0.000000
5.698863	0.000000	148.192824	148.184017	0.340583	3.606188	1,844.843522	219.051235	0.116997	184.743198	0.000000
6.000000	36.694286	148.189513	148.184989	0.340591	3.606212	1,881.558706	182.288486	0.125192	152.974763	0.000000
6.500000	112.570987	148.188619	148.186989	0.125352	3.606260	1,956.151328	106.359043	0.753005	87.623936	0.000000
7.000000	171.880310	148.189212	148.188493	0.204352	3.606297	2,016.003903	47.027779	0.526362	37.108986	0.000000
7.500000	304.913856	148.187159	148.186724	0.340595	3.606254	1,955.324734	108.502893	194.644240	8.208932	0.000000
8.000000	420.943189	148.184464	148.184105	0.340589	3.606190	1,859.127523	204.623649	406.792768	0.939037	0.000000
8.500000	674.529768	31.972639	31.972263	0.340599	3.606297	1,671.810545	44.644131	687.418049	0.074199	0.000000
9.000000	737.552245	3.319670	3.319157	0.340602	3.606323	1,629.448665	1.378623	753.285879	0.007021	0.000000
9.500000	752.060641	0.379644	0.378671	0.340601	3.606321	1,629.762183	-7.720410	763.426508	0.000694	0.000000
10.000000	767.704290	0.055916	0.053479	0.340601	2.441687	1,639.455711	-21.535525	767.660752	0.000068	0.000000
10.500000	1,067.563230	0.018483	0.011410	0.340618	0.266277	1,695.835449	-39.623063	935.930409	0.000005	0.000000
11.000000	1,171.884112	0.027497	0.005748	0.055888	0.034796	1,729.690739	-65.761207	987.130878	0.000000	0.000000

B. CausticTitration.exe: Pre-aerated, CO2 decreased almost 90% (CaO reacted to achieve pH 8.5 is 290 mg/L as CaCO3)

pH	Caustic asCaCO3mg	Fe_mg	Fe2_mg	Al_mg	Mn_mg	TDS_mg	NetAcidity_mg	SolidsPPT_mg	CO2_mg	O2_mg
5.700000	0.000000	148.253944	148.253944	0.340583	3.606177	1,796.954955	218.906769	0.000000	184.683994	0.010018
6.697709	0.000000	148.153294	148.152157	0.131429	3.606182	1,795.523678	218.803412	0.797321	17.796470	10.215814
6.000000	-28.616060	148.152569	148.151421	0.131434	3.606169	1,766.883972	247.467641	0.000009	42.257085	10.215762
6.500000	-7.568373	148.153121	148.151973	0.122499	3.606183	1,787.899450	226.379052	0.025841	24.223205	10.215800
7.000000	9.055535	148.153108	148.152391	0.131435	3.606193	1,804.585382	209.741323	0.000836	10.263163	10.215829
7.500000	18.349692	148.152996	148.152562	0.131435	3.606191	1,813.885563	200.442332	0.001376	3.580427	10.215841
8.000000	35.672893	148.152651	148.152292	0.131435	3.606191	1,810.601897	203.719540	20.603783	0.958068	10.215822
8.500000	289.472888	32.288226	32.287850	0.131439	3.606297	1,660.197303	45.284262	302.427612	0.075796	10.216122
9.000000	352.483745	3.743785	3.743272	0.131440	3.606322	1,626.972166	2.424687	368.515322	0.007173	10.216195
9.500000	367.272893	0.673854	0.672881	0.131440	3.606321	1,628.061164	-6.846925	378.974003	0.000709	10.216191
10.000000	383.349079	0.123433	0.122284	0.131440	2.431956	1,637.645626	-21.058240	383.628171	0.000070	10.216184
10.500000	683.966927	0.020465	0.019316	0.131446	0.264708	1,694.073381	-39.188404	552.424752	0.000005	10.216705
11.000000	786.717176	0.007691	0.006542	0.060071	0.034620	1,730.957523	-65.661659	598.666335	0.000000	10.216884

Fig. 2. Matrix output display (cropped and highlighted) for CausticTitration tool. Results are shown for simulated treatment of St. Michael discharge with CaO, (A) without and (B) with pre-aeration to drive off CO_2 (input data values are given in Fig. 1). For this example, the dissolved CO_2 concentration is decreased by 90% and the caustic requirement to attain a pH 8.5 is decreased by 57% through aggressive aeration for 54 s with a Maelstrom Oxidizer® ($k_{L,CO2} = 0.05$ s^{-1}) prior to lime addition. For A and B, CaO reacted to achieve pH 8.5 is 675 mg/L as CaCO₃ and 290 mg/L as CaCO₃, respectively. Empirical treatment evaluation by Means et al. (2015) indicated similar results.

retrofitted with a Maelstrom Oxidizer® (plug-flow, coarse-bubble diffuser), and aggressive aeration was conducted for 46 s prior to the lime dosing. The pre-aeration step decreased dissolved CO_2 from 189 mg L^{-1} to 18 mg L^{-1} and the pebble lime dose from 10.1 tons/day to 3.8 tons/day (63% decrease). Using the water chemistry data from August 2020 and assuming $k_{L,CO2} = 0.05$ s^{-1}, which is the highest value of aeration technologies evaluated in this study (Table S6), the PHREEQ-N-AMDTreat simulations indicate a result consistent with empirical data—pre-aeration decreased CO_2 from 185 mg L^{-1} to 18 mg L^{-1} and decreased the theoretical caustic requirement for treatment to pH 8.5 by 57%. Additional treatment steps, including recirculation of solids, which improved performance, are evaluated later in this paper using the TreatTrainMix2 tool.

An additional caustic titration case study at the Nittanny mine discharge where NaOH was added to strongly acidic, metal-laden AMD without aeration is included in the supplementary data (Figs. S1-S3). The Nittanny treatment case, previously reported by Cravotta et al. (2015) and Cravotta and Brady (2015), demonstrates consistency among changes in pH and associated solute concentrations between the empirical titration measurements and simulation results.

3.2. Parallel treatment case

The "ParallelTreatment" tool simulates simultaneous treatment of the same starting water composition and is useful to evaluate effects on treatment resulting from different values for "system" variables. Relevant variables include temperature, caustic or H_2O_2 addition, and kinetics variables such as CO_2 mass-transfer (outgassing/ingassing) rate, limestone particle size, and/or sorbent availability. The tool is used herein to simulate complex interactions among CO_2 outgassing, pH, Fe^{II} oxidation, and the attenuation of associated metals, which were observed during aeration of net-alkaline AMD at the Oak Hill boreholes (Burrows et al., 2017; Cravotta, 2015; Henry, 2015). Such vertical boreholes, installed from a low-elevation surface location into underlying mine workings to prevent AMD discharging at higher elevation into buildings and other infrastructure, are a challenge to remediate because of their anoxic character and proximity to streams (e. g. Cravotta et al., 2014). The untreated AMD had pH 6.4 with concentrations of DO < 0.5 mg L^{-1} and dissolved Fe^{II}, Mn^{II}, and Al of 19.7, 3.6, and 0.056 mg L^{-1}, respectively. The side-by-side batch tests, which were conducted for 5–5.5 h duration, evaluated a control (Aer0), three progressively higher aeration rates (Aer1, Aer2, Aer3), and an initial dose of H_2O_2 without aeration (Figs. 3 and 4). As explained by Cravotta (2015) and Burrows et al. (2017), the field experiments demonstrated higher rates of aeration promoted CO_2 outgassing, thereby increasing pH and the rate of Fe^{II} oxidation; the results of field aeration experiments were consistent with in-stream changes. In contrast, H_2O_2 added without aeration instantaneously oxidized Fe^{II} and caused a precipitous decline in pH; thereafter pH remained relatively stable and paralleled that of the control (Fig. 4). The concentrations of dissolved Al, which were initially at equilibrium with amorphous Al(OH)₃, decreased to values below equilibrium for the H_2O_2 treatment at pH 6.2 and for the aeration treatments as the pH increased to ~7 and newly formed (autocatalytic) suspended HFO particles accumulated. Burrows et al. (2017) modeled the Al trends by adsorption to HFO; the same Al–HFO binding constant is assumed in phreeqcAMDTreat.dat. Concentrations of Mn^{II} were unaffected by H_2O_2 and decreased slightly with aeration. The trends in Mn also could be explained by adsorption to suspended HFO particles, with a higher pH required for binding than that for Al.

The parallel kinetics simulations of the pH, Fe^{II}, Mn^{II}, Al, alkalinity, DO, Pco₂, and Po₂ (curves in Fig. 4) generally reproduced the non-linear trends for the measured values (point symbols in Fig. 4). Note that error bars (not shown) are approximately twice the size of point symbols shown in Fig. 4; details are given by Burrows et al. (2017). Except for adjusting values of $k_{L,CO2}$ and H_2O_2 for the simulations, default values were used for all the kinetic parameters. The model results are consistent with abiotic, homogeneous oxidation of Fe^{II}, whereas the attenuation of a small fraction of the dissolved Mn^{II} concentration is consistent with its

Fig. 3. UI for PHREEQ-N-AMDTreat "ParallelTreatment" modeling tool exhibiting input values for simulations of batch aeration experiments at the Oak Hill Boreholes. Results of simulations are shown in Fig. 4; kinetic adjustment parameters and other input variables in the model are described in Tables 1 and S1.

adsorption by suspended particles of HFO (produced by Fe^{II} oxidation) and, possibly, heterogeneous Mn^{II} oxidation. Although other model scenarios are not shown, setting the rate adjustment factor to 0 (e.g. Fig. 3) for FeOB (factr.kbact) or heterogeneous (factr.kHET) contributions to Fe^{II} oxidation or homogeneous oxidation of Mn^{II} (factr. kMnHOM) did not affect simulation results.

An additional case study, using the ParallelTreatment tool for simulations, is given in supplemental data (Figs. S4 and S5). For that case, the tool was used to evaluate effects of different limestone particle sizes and quantities of HMeO sorbent on water quality during AMD treatment in an oxic limestone drain (OLD) with retention time less than 6 h. As previously reported by Cravotta and Trahan (1999) and Cravotta and Watzlaf (2003), influent pH of 3.5 increased to 5.5 within 1.5 h and to 6.5 within 6 h; Fe^{III} and Al precipitated at pH < 5.5 near the inflow while dissolved Fe^{II} and Mn^{II} were transported relatively conservatively through the OLD during the first 6 months of operation (<6 mos in Figs. S4 and S5). After approximately 6 months of operation, HMeO had accumulated in the downflow part of the OLD where elevated pH (>6) promoted sorption and coprecipitation of dissolved Mn, Cu, Co, Ni, and Zn as indicated by decreased concentrations of the metals in effluent and their enrichment relative to Fe in HMeO suspended solids and coatings on limestone. Simulation results demonstrate the importance of particle size on limestone dissolution rate and of HMeO and pH on the attenuation of Mn (Fig. S5).

3.3. Sequential treatment cases

The "TreatTrainMix2" modeling tool, which combines the capabilities of the CausticTitration and ParallelTreatment tools, simulates progressive changes in water quality resulting from sequential passive or active treatment steps that typically involve neutralization, oxidation, and solids precipitation processes. To demonstrate model validity, empirical data for case studies, where field and laboratory water-quality measurements were obtained at multiple points through passive and active treatment systems, are presented with simulation results as a function of retention time (computed as the void volume of the treatment component divided by the flow rate).

3.3.1. Passive treatment case

The Pine Forest passive AMD treatment system consists of an anoxic limestone drain (ALD), oxidation/settling pond, and three aerobic wetlands, in series, with aeration steps in between (Figs. 5 and 6). The untreated AMD (690 gal min^{-1}, 43.5 L s^{-1}), sampled during winter 2015 (Ashby, 2017), had pH 5.8 with DO < 0.5 mg L^{-1} and dissolved concentrations of Fe^{II}, Mn^{II}, and Al of 14.0, 3.1, and 0.09 mg L^{-1}, respectively. The treated effluent had pH ~7 with Fe and Mn < 2 mg L^{-1}. After its first year of operation (2006), the ALD began to clog with gelatinous, Fe-rich precipitate. Although equipped with flushing pipes, manual activation of flushing was not attempted during the first year.

For the simulated "biofouling" scenario, the FeOB rate factor was increased from 1 to 2 and a pre-existing (accumulated) sorbent mass (HMeO.mg) of 116 mg was specified for the ALD (Fig. 5). This sorbent mass in the ALD is consistent with a 0.5-μm thick coating on the limestone particles (72 cm^2/mol) in contact with 1 L water volume, assuming 35% bed porosity and sorbent density of 1.25 g/cm^3 (Table S7). The assumed bed porosity, which represents partial clogging by accumulated sludge, is less than values of 42–53% for well-sorted limestone fragments (e.g. Cravotta and Watzlaf, 2003; Cravotta et al., 2008). For subsequent steps, the specified sorbent mass was only 1–3 mg, representing suspended particles or coatings on rock or plant surfaces.

The sequential model results for pH, Fe^{II}, Mn^{II}, Al, P_{CO_2}, and P_{O_2}, shown as a function of the retention time for the biofouling simulation, generally reproduce the longitudinal trends for measured constituent values (Fig. 6, red dashed curves). The simulated Fe^{II} concentration decreased by 30% within the ALD because of microbial oxidation combined with sorption and heterogeneous oxidation. Despite less mass of sorbent indicated for wetlands, progressively increased pH and greater Mn content of sorbent promoted attenuation of dissolved Mn^{II} in wetlands. Simulation results for a reference scenario (Fig. 6, black dotted curves) demonstrate abiotic, homogeneous processes are not adequate to explain observations at the Pine Forest ALD. The reference simulation uses the same aeration coefficients and retention times as the biofouling simulation, but the existing sorbent and FeOB rate factor were set to 0, equivalent to the abiotic homogeneous Fe^{II} oxidation rate model. This reference scenario underpredicts removal of Fe, Mn, and Al in the upper stages of the system where most chemical changes occur
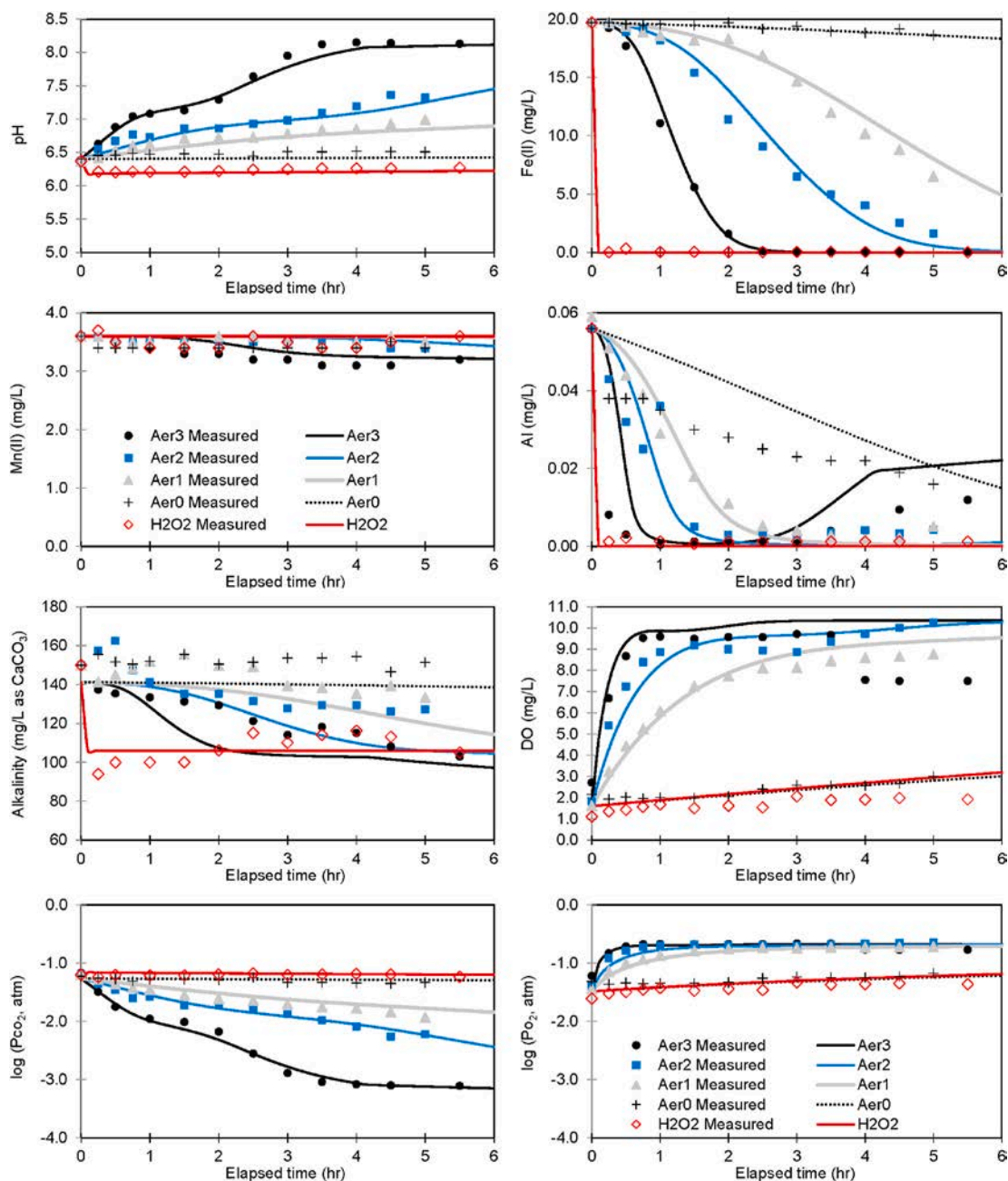
Fig. 4. Comparison of measured (symbols) and simulated (curves) values for pH, Fe^{II}, Mn^{II}, Al, alkalinity, DO, Pco_2, and Po_2 during batch aeration experiments on AMD from the Oak Hill Boreholes. Simulations used the ParallelTreatment tool with the same initial water chemistry and default values for kinetic adjustment factors, and different values for k_{L,CO_2} and $[H_2O_2]$, given in Fig. 3.

and does not indicate observed Mn^{II} attenuation. Thus, a combination of abiotic, microbial, and surface processes account for the attenuation of Fe within the limestone bed. Considering the reference model results, one may hypothesize that frequent flushing of the limestone bed immediately after construction may be effective to avoid sludge accumulation and associated biofouling (e.g. Wolfe et al., 2010).

In supplemental data, the TreatTrainMix2 tool is also used to simulate effects of passive treatment at the Silver Creek aerobic wetlands using data collected by Ashby (2017) and Cravotta (this study) under high-flow (December 2015) and low-flow (August 2016) conditions (Figs. S8-S11). In addition to data on water temperature, DO, pH, alkalinity, and solute concentrations used to calibrate these models, sediment chemistry data at the outflow of each treatment step at the

Silver Creek system were available to estimate the sorbent composition (Ashby, 2017). For the Silver Creek models, the CO_2 outgassing rate (k_{La, CO_2}) and sorbent mass and composition (HMeO.mg, Fe%, Mn%, Al%) at each step were the only kinetics variables adjusted to achieve a reasonable match between empirical and simulated values for dynamic changes in pH, Fe, Mn, Al, and associated solute concentrations. Shallow, wide aeration cascades and long riprap runs were highly effective at facilitating gas exchange and rapid increases in pH, followed by Fe^{II} oxidation in large ponds with long retention times where gas exchange was limited by minimal advection. Greater mass and/or Mn content of sorbent increased Fe^{II} and Mn^{II} attenuation; most Mn was attenuated in wetlands at later treatment steps.

Fig. 5. UI for TreatTrainMix2 sequential model exhibiting input values for simulation of water-quality changes through the Pine Forest treatment system, December 2015, which consists of a "biofouled" anoxic limestone drain (ALD), oxidation/settling pond, and three aerobic wetlands, with aeration steps in between. The values shown represent enhanced FeOB activity (factr.kbact = 2, instead of default value of 1) and a specified sorbent mass of 116 mg in the ALD and smaller sorbent mass with progressively greater Mn content downstream. Results of simulations are shown in Fig. 6.

3.3.2. Active treatment case

The active treatment of St. Michael AMD, described previously, involves pre-aeration and lime dosing (Fig. 1) plus, importantly, the recirculation of high-density sludge (9.5 L s^{-1}, 150 gal min^{-1}), which consists of HMeO precipitate and unreacted lime, followed by settling of solids in a clarifier before discharge. Using August 2020 data on dissolved and total concentrations of metals and associated constituents in the untreated AMD and at points through the treatment process, the TreatTrainMix2 tool was set up and calibrated to simulate observed changes in pH, alkalinity, and dissolved metals concentrations (Figs. 7 and 8). During the first simulation step, (1) pre-aeration with the Maelstrom Oxidizer® for 54 s increased the pH from 5.7 to 6.7 and decreased aqueous CO_2 by 90 percent (as described previously). Next, the target pH of approximately 8.5 in the mix tank (continuously receiving slaked lime) was maintained for a duration of ~15 min by the addition of CaO over *three simulation steps* to (2) instantaneously precipitate $Fe(OH)_2$ and $Al(OH)_3$ as equilibrium phases, (3) sorb and heterogeneously oxidize Fe^{II} and Mn^{II} with the consequent precipitation of $Fe(OH)_3$ and MnOOH, and (4) adjust the pH of effluent exiting the caustic mix tank. Although the clarifier step (5) that followed involved more than 14 h for settling the solids precipitated during prior steps, the solute concentrations were relatively unchanged in the clarifier; nearly all oxidation and precipitation reactions had taken place during the 15 min of retention in prior steps.

The previous examples and others in supplemental data demonstrate that the PHREEQ-N-AMDTreat water-quality modeling tools can be used to quantify effects of factors that could increase or decrease the rates of Fe^{II} oxidation and Fe^{III} hydrolysis. Factors that can increase Fe-attenuation rates include increased temperature, increased pH, increased availability of sorbent HMeO, and increased FeOB activity. On the other hand, Rose and Waite (2003) reported that natural organic-matter-Fe^{II}-complex formation occurs on a similar time scale as Fe^{II} oxidation, and the formation of stable aqueous complexes (e.g. Fe^{II}-humate) can decrease Fe^{II} attenuation. To evaluate potential effects of NOM complexes on Fe attenuation, initial DOC and humate values may be adjusted from zero to non-zero values. Effects of other variables may also be evaluated by changing their initial values to represent temporal variability in AMD flow rates, chemistry, and system characteristics (e.g. Cravotta et al., 2010; 2014; Gammons et al., 2015).

General agreement between simulated and measured values and the ability to adjust input variables to simulate site-specific conditions support the use of the PHREEQ-N-AMDTreat modeling tools for the evaluation of hypothetical AMD treatment strategies. An expansive supplemental data (section S4) is provided that continues the demonstration of the TreatTrainMix2 tool for the conceptual design and preliminary economic assessment of potential passive and active treatment strategies for AMD. In that section, Figures S12 and S13 show the input data and output results for passive treatment simulation using the TreatTrainMix2 tool to evaluate progressive changes in water quality along the generalized flow sequence through a vertical flow system containing layers of compost and limestone, followed by an aerobic pond, wetland, and finally a manganese removal bed, with aeration steps in between. For the same initial water quality, Figures S14 and S15 show the simulation of active lime treatment, with the "+Caustic?" check box active for a target pH value of 8.5 at step 3, with $Ca(OH)_2$ as the caustic agent. In addition to the water-quality simulations, corresponding system sizing and summary cost estimates are given (Table S8) for evaluation of the cost-effectiveness of the hypothetical passive and active treatments.

4. Conclusions

Three complementary user-friendly geochemical models simulate the treatment of AMD to neutralize acidity and attenuate dissolved metals. The interactive UI for each of the PHREEQ-N-AMDTreat tools facilitates input of initial water chemistry data and adjustment of model variables while avoiding manual revisions to the variable values within the linked PHREEQC code. Graphical and tabular output indicates the changes in pH, solute concentrations, total dissolved solids, and specific conductance of treated effluent plus the cumulative quantity of precipitated solids as a function of retention time or the amount of caustic or oxidizing agent added. By adjusting chemical dosing or kinetic
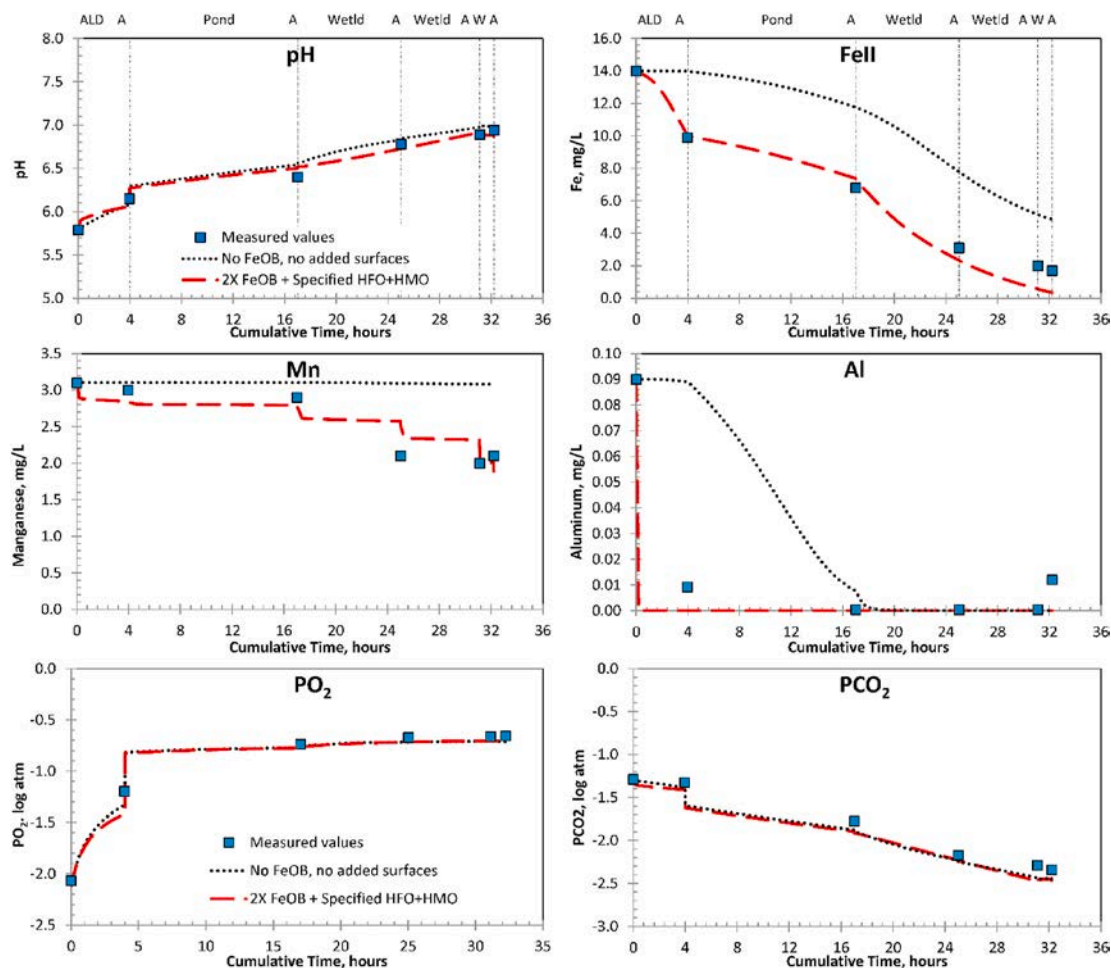
Fig. 6. Comparison of measured (symbols) and simulated (curves) values for pH, Fe^{II}, Mn^{II}, Al, Pco_2, and Po_2 during treatment of AMD at the Pine Forest passive treatment system, December 2015. Simulations used the TreatTrainMix2 sequential model with initial water chemistry, specified values for $k_{L,CO2}a$, FeOB rate factor, and sorbent mass and composition (Fig. 5). The black dotted curves show results for abiotic conditions without specified sorbent. The red dashed curves show results for enhanced FeOB activity (2X default FeOB rate) and specified sorbent mass in the ALD equivalent to 0.5-μm thick coating on limestone surfaces and smaller sorbent mass with progressively greater Mn content in downstream wetlands. Simulation results for additional parameters (alkalinity, net acidity, temperature, specific conductance, accumulated solids, mass of limestone and SOC dissolved, DO, nitrate, DOC, sulfate, and TDS) are included in the supplementary data (Figs. S6-S7). (For interpretation of the references to colour in this figure legend, the reader is referred to the Web version of this article.)

variables, the effects of independent or sequential treatment steps that have different retention time, aeration rate, quantities of reactive solids, and temperature can be simulated. Interactions among different variables and corresponding water-quality effects can be readily evaluated.

The model results indicate that effluent quality can be affected by the interactions of several independent and dependent variables. The key independent variable is the time specified for kinetic steps; this variable is essentially the travel time or retention time (volume/flow rate) for individual treatment steps. For most rate models, increased time generally results in greater reaction progress. However, forward reactions may be limited by atmospheric or solubility equilibrium, with diminished benefit from increased time for reaction as the system approaches equilibrium. One of the key dependent variables is pH, which affects aqueous and surface speciation and the rates of kinetic reactions. Importantly, the PHREEQ-N-AMDTreat models account for processes that may increase or decrease the pH. For example, the pH of treated effluent varies in response to atmospheric exchange (CO_2 outgassing), limestone dissolution, oxidation Fe^{II} and hydrolysis of Fe^{III}, and oxidation of organic carbon and can be modified through the addition of caustic agents or sorptive capacity. The geochemical models indicate potential for solids to precipitate or dissolve, but do not consider physical processes that could affect treatment performance such as particle settling, clogging of voids, or consumption of reactive substrates.

This paper demonstrates the models (1) to gain an understanding of the relative effects and importance of certain water-quality and system variables affecting AMD treatment and (2) to evaluate potential treatment strategies for cost-effective mitigation of Fe, Al, Mn, and associated contaminants from AMD. First, the CausticTitration tool quantifies the effects of commonly used caustic chemicals to increase pH and precipitate solids. Using this tool, preliminary treatment scenarios may be considered for caustic addition before or after aeration to drive off CO_2. Second, the ParallelTreatment tool considers the same starting water composition but with different possible values for kinetics variables such as CO_2 outgassing rate, limestone particle size, and/or sorbent availability. Field experiments that evaluated the effects of aeration or H_2O_2 treatment on the pH and Fe^{II} oxidation rate were accurately simulated with the parallel reactions tool. Third, the TreatTrainMix2 sequential treatment tool, which combines the capabilities of the caustic titration and parallel kinetics tools, simulates progressive changes in water quality resulting from passive or active treatment steps that typically involve neutralization, oxidation, and solids precipitation processes. The TreatTrainMix2 tool was applied to indicate observed changes in pH, dissolved O_2, metals, and associated solute concentrations in passive and active AMD treatment systems that had a range of retention times, aeration rates, and system components. Using this sequential treatment
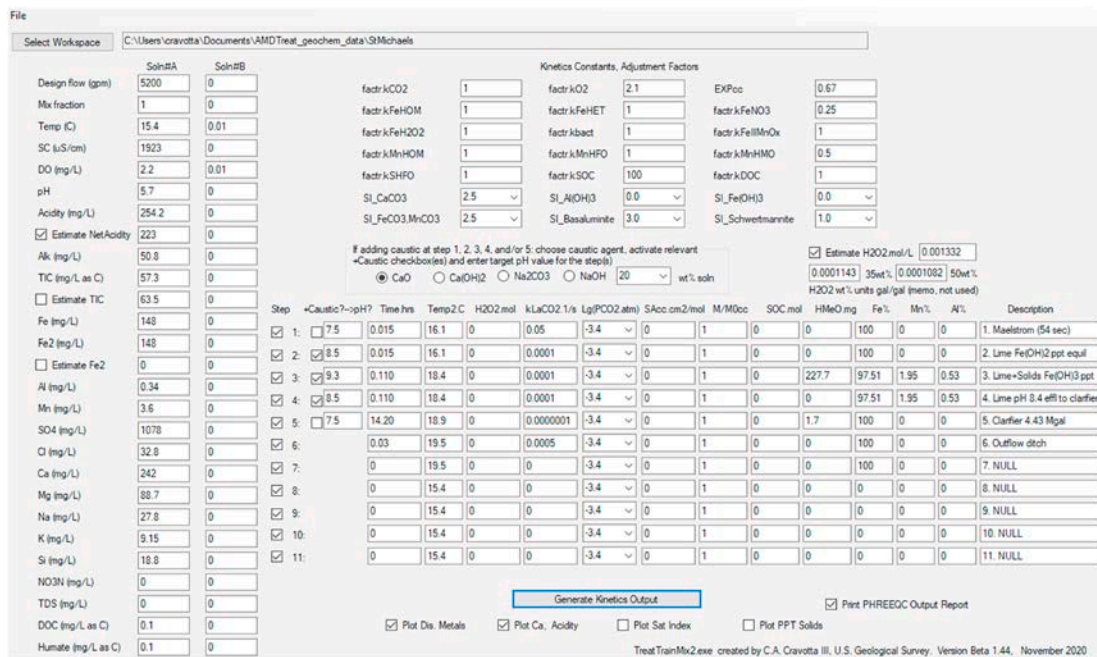
Fig. 7. TreatTrainMix2 input values for simulation of St. Michael active treatment system, which involves pre-aeration, continuous lime dosing with high-density sludge recirculation, and sludge settling steps. Results of simulations are shown in Fig. 8. Note the concentration and composition of HMeO sorbent specified for step (3) were computed as the sum of suspended Fe + Mn + Al concentrations (measured total minus dissolved concentration) exiting the mix tank (step 4). To prevent calcite precipitation and improve alkalinity simulation, the modeled calcite saturation index was increased from the default of 0.3–2.5; calcite was not detected (precipitated solids did not effervesce on reaction with HCl).
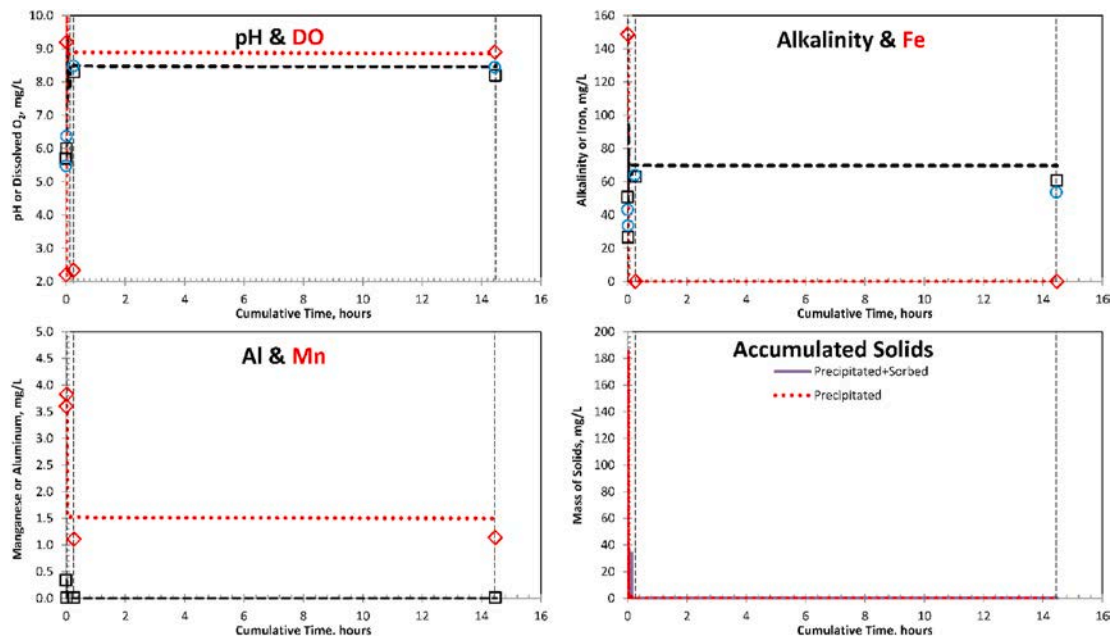
Fig. 8. Comparison of measured (symbols) and TreatTrainMix2 simulation results (curves) for pH, alkalinity, dissolved O_2, Fe, Al, and Mn, plus estimated concentration of accumulated solids at the St. Michael active treatment system. Input values for starting water quality and other model variables are shown in Fig. 7.

tool with chemistry and flow data for one or two AMD sources plus user-specified retention time and other system characteristics, various passive and/or active treatment strategies can be identified that achieve the desired effluent quality. Thus, considering land area and other requirements for installation, operation, and maintenance of the alternatives, potentially cost-effective, feasible treatment methods can be identified.

In conclusion, the PHREEQ-N-AMDTreat modeling tools effectively simulate dynamic interactions between dissolved Fe, Al, Mn, and other solutes in complex aqueous environments that exhibit gradients in pH, redox, and solute concentrations. The modeling capability of PHREEQC, including aqueous and surface speciation coupled with kinetics of oxidation-reduction and dissolution reactions, provides a quantitative framework for synthesis and application of laboratory rate data to field settings. The PHREEQ-N-AMDTreat UI facilitates application of the models to evaluate the performance and design of a wide variety AMD

treatment systems. Uncertainty in water-quality data, rate data, sorbent quantities and properties, and other system variables can be evaluated by changing values in the UI to identify critical parameters and document potential variations in results. Although publicly available, the models are not "smart," and practitioners may lack experience in water-quality analysis or engineering concepts. A user must choose appropriate values for system variables and treatment steps in the models. Site-specific information is essential for feasibility analysis and design.

Nordstrom and Campbell (2014) offered several relevant conclusions and recommendations on the sort of modeling presented herein: "Expert judgment, developed over long time periods and involving many mistakes, along with carefully acquired empirical observations in the field and in the laboratory, will ultimately guide our models from possibility to probability." They added, "Future efforts should be directed toward developing standardized test cases for a wide variety of processes against which code performance can be compared and tested." To this end, additional data collection is underway at several active and passive treatment facilities. The data collection is targeted to improve our knowledge of important variables or processes and associated effects on effluent quality at those facilities. Accordingly, revisions to improve the software may be anticipated. Additionally, efforts are underway to integrate the PHREEQ-N-AMDTreat water-quality modeling tools with the AMDTreat cost analysis model. The integrated models will facilitate feasibility and cost analysis.

Declaration of competing interest

The authors declare that they have no known competing financial interests or personal relationships that could have appeared to influence the work reported in this paper.

Acknowledgments

Appendix A. Supplementary data

Supplementary data to this article can be found online at https://doi.org/10.1016/j.apgeochem.2020.104845.

References

Alexander, M., 1982. Most probable number method for microbial populations. In: Page, A.L., Miller, R.H., Keeney, D.R. (Eds.), Methods of Soil Analysis, Part 2. Chemical and Microbiological Properties (2nd): Madison, Wis, vol. 9. American Society of Agronomy Monograph, pp. 815–820.

Antoniou, E.A., Stuyfzand, P.J., van Breukelen, B.M., 2013. Reactive transport modeling of an aquifer storage and recovery (ASR) pilot to assess long-term water quality improvements and potential solutions. Appl. Geochem. 35, 173–186. https://doi.org/10.1016/j.apgeochem.2013.04.009.

Appelo, C.A.J., Postma, D., 2005. Geochemistry, Groundwater and Pollution (2nd). Balkema, Leiden, p. 678.

Appelo, C.A.J., Van Der Weiden, M.J.J., Tournassat, C., Charlet, L., 2002. Surface complexation of ferrous iron and carbonate on ferrihydrite and the mobilization of arsenic. Environ. Sci. Technol. 36, 3096–3103.

Appelo, C.A.J., Verweij, E., Schäfer, H., 1998. A hydrogeochemical transport model for an oxidation experiment with pyrite/calcite/exchangers/organic matter containing sand. Appl. Geochem. 13, 257–268.

Ashby, E.J., 2017. Biogeochemical Mechanisms of Rare Earth Element Enrichment in Mining-Affected Aqueous Environments. University of Ottawa, Canada, M.S. thesis, p. 133.

Bethke, C.M., 2008. Geochemical and Biogeochemical Reaction Modeling, 2nd. Cambridge University Press, p. 543.

Bigham, J.M., Nordstrom, D.K., 2000. Iron and aluminum hydroxysulfates from acid sulfate waters. In: Alpers, C.N., Jambor, J.L., Nordstrom, D.K. (Eds.), Sulfate Minerals – Crystallography, Geochemistry, and Environmental Significance. Mineral. Soc. Amer. 40, Washington, DC, pp. 351–403.

Bigham, J.M., Schwertmann, U., Traina, S.J., Winland, R.L., Wolf, M., 1996. Schwertmannite and the chemical modeling of iron in acid sulfate waters. Geochem. Cosmochim. Acta 60, 2111–2121. https://doi.org/10.1016/0016-7037(96)00091-9.

Blowes, D.W., Ptacek, C.J., Jambor, J.L., Weisener, C.G., Paktunc, D., Gould, W.D., Johnson, D.B., 2014. The geochemistry of acid mine drainage. In: Holland, H.D., Turekian, K.K. (Eds.), Treatise on Geochemistry (2nd) 9. Elsevier, Oxford, pp. 131–190.

Bonneville, S., Behrends, T., Van Cappellen, P., 2009. Solubility and dissimilatory reduction kinetics of iron(III) oxyhydroxides: a linear free energy relationship. Geochem. Cosmochim. Acta 73, 5273–5282.

Bricker, O.P., 1965. Some stability relations in the system Mn-O$_2$-H$_2$O at 25 °C and one atmosphere total pressure. Am. Mineral. 50, 1296–1354.

Burgos, W.D., Borch, T., Troyer, L.D., Luan, F., Larson, L.N., Brown, J.F., Lambson, J., Shimizu, M., 2012. Schwertmannite and Fe oxides formed by biological low-pH FeII oxidation versus abiotic neutralization: impact on trace metal sequestration. Geochem. Cosmochim. Acta 76, 29–44. https://doi.org/10.1016/j.gca.2011.10.015.

Burrows, J.E., Cravotta III, C.A., Peters, S.C., 2017. Enhanced Al and Zn removal from coal-mine drainage during rapid oxidation and precipitation of Fe oxides at near-neutral pH: Appl. Geochem. (Tokyo. 1967) 78, 194–210. https://doi.org/10.1016/j.apgeochem.2016.12.019.

Burté, L., Cravotta III, C.A., Bethencourt, L., Farasin, J., Pédrot, M., Dufrense, Al, Gérard, M.-F., Baranger, C.C., Le Borgne, T., Aquilina, L., 2019. Kinetic study on clogging of a geothermal pumping well triggered by mixing-induced biogeochemical reactions. Environ. Sci. Technol. 53, 5848–5857. https://doi.org/10.1021/acs.est.9b00453.

Charlton, S.R., Parkhurst, D.L., 2011. Modules based on the geochemical model PHREEQC for use in scripting and programming languages. Comput. Geosci. 37, 1653–1663.

Chen, C., Thompson, A., 2018. Ferrous iron oxidation under varying pO$_2$ levels: the effect of Fe^{III}/Al^{III} oxide minerals and organic matter. Environ. Sci. Technol. 52, 597–606. https://doi.org/10.1021/acs.est.7b05102.

Cole, C.A., Molinski, A.E., Rieg, N., Backus, F., 1977. Oxidation of iron in coal mine drainage. Wat. Pollut. Control Fed. 49, 1616–1620.

Coston, J.A., Fuller, C.C., Davis, J.A., 1995. Pb^{2+} and Zn^{2+} adsorption by a natural aluminum- and iron-bearing surface coating on an aquifer sand. Geochem. Cosmochim. Acta 59, 3535–3547. https://doi.org/10.1016/0016-7037(95)00231-n.

Cravotta III, C.A., 2003. Size and performance of anoxic limestone drains to neutralize acidic mine drainage. J. Environ. Qual. 32, 1277–1289. https://doi.org/10.2134/jeq2003.1277.

Cravotta III, C.A., 2005. Effects of abandoned coal-mine drainage on streamflow and water quality in the mahanoy Creek basin, schuylkill, columbia, and northumberland counties, Pennsylvania, 2001. U.S. Geol. Surv. Sci. Inv. Rep. 2004–5291, 60.

Cravotta III, C.A., 2007. Passive aerobic treatment of net-alkaline, iron-laden drainage from a flooded underground anthracite mine, Pennsylvania, USA. Mine Water Environ. 26, 128–149.

Cravotta III, C.A., 2008a. Dissolved metals and associated constituents in abandoned coal-mine discharges, Pennsylvania, USA – 1. Constituent concentrations and correlations. Appl. Geochem. 23, 166–202.

Cravotta III, C.A., 2008b. Dissolved metals and associated constituents in abandoned coal-mine discharges, Pennsylvania, USA – 2. Geochemical controls on constituent concentrations. Appl. Geochem. 23, 203–226.

Cravotta III, C.A., 2008c. Laboratory and field evaluation of a flushable oxic limestone drain for treatment of net-acidic, metal-laden drainage from a flooded anthracite mine, Pennsylvania, USA. Appl. Geochem. 23, 3404–3422.

Cravotta III, C.A., 2015. Monitoring, field experiments, and geochemical modeling of FeII oxidation kinetics in a stream dominated by net-alkaline coal-mine drainage, Pennsylvania. U.S.A. Appl. Geochem. 62, 96–107.

Cravotta III, C.A., 2020. Interactive PHREEQ-N-AMDTreat Water-Quality Modeling Tools to Evaluate Performance and Design of Treatment Systems for Acid Mine Drainage (Software Download). https://doi.org/10.5066/P9QEE3D5. U.S. Geological Survey Software Release. https://code.usgs.gov/water/phreeq-n-amdtreat/-/archive/v1.44/phreeq-n-amdtreat-v1.44.zip.

Cravotta III, C.A., Trahan, M.K., 1999. Limestone drains to increase pH and remove dissolved metals from acidic mine drainage. Appl. Geochem. 14, 581–606.

Cravotta III, C.A., Ward, S.J., Hammarstrom, J,M, 2008. Downflow limestone beds for treatment of net-acidic, oxic, iron-laden drainage from a flooded anthracite mine, Pennsylvania, USA–Laboratory evaluation. Mine Water Environ. 27, 86–99. https://doi.org/10.1007/s10230-008-0031-y.

Cravotta III, C.A., Watzlaf, G.R., 2003. Design and performance of limestone drains to increase pH and remove metals from acidic mine drainage. In: Naftz, D.L., Morrison, S.J., Fuller, C.C., Davis, J.A. (Eds.), Handbook of Groundwater Remediation Using Permeable Reactive Barriers–Application to Radionuclides, Trace Metals, and Nutrients. Academic Press, San Diego, Ca, pp. 19–66. https://doi.org/10.1016/B978-012513563-4/50006-2.

Cravotta III, C.A., Brightbill, R.A., Langland, M.J., 2010. Abandoned mine drainage in the swatara creek basin, southern anthracite coalfield, Pennsylvania, USA–1. Streamwater-quality trends coinciding with the return of fish. Mine Water Environ. 29, 176–199. https://doi.org/10.1007/s10230-010-0112-6.

Cravotta III, C.A., Goode, D.J., Bartles, M.D., Risser, D.W., Galeone, D.G., 2014. Surface-water and groundwater interactions in an extensively mined watershed, upper Schuylkill River, Pennsylvania, USA. Hydrol. Process. 28, 3574–3601. https://doi.org/10.1002/hyp.9885.

Cravotta III, C.A., Means, B., Arthur, W., McKenzie, R., Parkhurst, D.L., 2015. AMDTreat 5.0+ with PHREEQC titration module to compute caustic chemical quantity, effluent quality, and sludge volume. Mine Water Environ. 34, 136–152.

Davies, S.H.R., Morgan, J.J., 1989. ManganeseII oxidation kinetics on metal oxide surfaces. J. Colloid Interface Sci. 129, 63–77.

Davison, W., Seed, G., 1983. The kinetics of the oxidation of ferrous iron in synthetic and natural waters. Geochem. Cosmochim. Acta 47, 67–79.

Dempsey, B.A., Roscoe, H.C., Ames, R., Hedin, R., Byong-Hun, J., 2001. Ferrous oxidation chemistry in passive abiotic systems for the treatment of mine drainage. Geochem. Explor. Anal. 1, 81–88.

Dietz, J.M., Dempsey, B.A., 2017. Heterogeneous oxidation of Fe(II) in AMD. Appl. Geochem. 81, 90–97.

dos Santos Alfonso, M., Stumm, W., 1992. Reductive dissolution of iron(III) (hydr)oxides by hydrogen sulfide. Langmuir 8, 1671–1675.

Dzombak, D.A., Morel, F.M.M., 1990. Surface Complexation Modeling: Hydrous Ferric Oxide. John Wiley and Sons, New York, NY, USA.

Eckert, P., Appelo, C.A.J., 2002. Hydrogeochemical modeling of enhanced benzene, toluene, ethylbenzene, xylene (BTEX) remediation with nitrate. Water Resour. Res. 38 (8) https://doi.org/10.1029/2001WR000692, 1130, 5.1-5.11.

Eggerichs, T., Opel, O., Otte, T., Ruck, W., 2014. Interdependencies between biotic and abiotic ferrous iron oxidation and influence of pH, oxygen and ferric iron deposits. Geomicrobiol. J. 31, 461–472.

Feng, Q., Li, T., Qian, B., Zhou, L., Gao, B., Yuan, T., 2014. Chemical characteristics and utilization of coal mine drainage in China. Mine Water Environ. 33, 276–286. https://doi.org/10.1007/s10230-014-0271-y.

Gammons, C.H., Nimick, D.A., Parker, S.R., 2015. Diel cycling of trace elements in streams draining mineralized areas–A review. Appl. Geochem. 57, 35–44.

Geroni, J.N., Cravotta III, C.A., Sapsford, D.J., 2012. Evolution of the chemistry of Fe bearing waters during CO_2 degassing. Appl. Geochem. 27, 2335–2347.

Gombert, P., Sracek, O., Koukouzas, N., Gzyl, G., Tuñon Valladares, S., Frączek, R., Klinger, C., Bauerek, A., Álvarez Areces, J.E., Chamberlain, S., Paw, K., Pierzchała, L., 2018. An overview of priority pollutants in selected coal mine discharges in Europe. Mine Water Environ. 38, 16–23. https://doi.org/10.1007/s10230-018-0547-8.

Iron and sulfur bacteria. In: Greenberg, A.E., Clesceri, L.S., Eaton, A.D., Franson, M.A.H. (Eds.), 1992. Standard Methods for the Examination of Water and Wastewater (18th). American Public Health Association, Washington, D.C.. Section 9240.

Gustafsson, J.P., 2013. Visual MINTEQ Version 3.1. Stockholm, Sweden. https://vminteq.lwr.kth.se/. December 21, 2013 (accessed January 23, 2019).

Hardwick, T.J., 1957. The rate constant of the reaction between ferrous ions and hydrogen peroxide in acidic solution. Can. J. Chem. 35, 428–436.

Hedin, B.C., Capo, R.C., Stewart, B.W., Hedin, R.S., Lopano, C.L., Stuckman, M.Y., 2019. The evaluation of critical rare earth element (REE) enriched treatment solids from coal mine drainage passive treatment systems. Int. J. Coal Geol. 208, 54–64.

Hedin, R.S., Nairn, R.W., Kleinmann, R.L.P., 1994. Passive Treatment of Coal Mine Drainage, vol. 9389. U.S. Bureau of Mines Information Circular, p. 35.

Henry, Jill E., 2015. Geochemical Factors Controlling the Fate of Fe, Al, and Zn in Coal-Mine Drainage in the Anthracite Coal Region. Ph.D. thesis. Lehigh University, Pennsylvania, USA, p. 195. http://preserve.lehigh.edu/etd/2633.

Hiemstra, T., van Riemsdijk, W.H., 2007. Adsorption and surface oxidation of Fe(II) on metal hydroxides. Geochem. Cosmochim. Acta 71, 5913–5933.

Hoffman, M.R., 1977. Kinetics and mechanism of oxidation of hydrogen sulfide by hydrogen peroxide in acidic solution. Environ. Sci. Technol. 11, 61–66.

Huminicki, D.M.C., Rimstidt, J.D., 2008. Neutralization of sulfuric acid solutions by calcite dissolution and the application to anoxic limestone drain design. Appl. Geochem. 23, 148–165.

Jageman, T.C., Yokley, R.A., Heunisch, H.E., 1988. The Use of Preaeration to Reduce the Cost of Neutralizing Acid Mine Drainage. U.S. Bureau of Mines Information Circular 9183, Pittsburgh, PA, pp. 131–135.

Jones, A.M., Griffin, P.J., Collins, R.N., Waite, T.D., 2014. Ferrous iron oxidation under acidic conditions – the effect of ferric oxide surfaces. Geochem. Cosmochim. Acta 145, 1–12.

Kairies, C.L., Capo, R.C., Watzlaf, G.R., 2005. Chemical and physical properties of iron hydroxide precipitates associated with passive treated coal mine drainage in Bituminous Region of Pennsylvania and Maryland. Appl. Geochem. 20, 1445–1460.

Karamalidis, A.K., Dzombak, D.A., 2010. Surface Complexation Modeling: Gibbsite. John Wiley & Sons, Inc., Hoboken, NJ, USA.

Kirby, C.S., Cravotta III, C.A., 2005. Net alkalinity and net acidity 2: practical considerations. Appl. Geochem. 20, 1941–1964.

Kirby, C.S., Elder-Brady, J.A., 1998. Field determination of Fe^{2+} oxidation rates in acid mine drainage using a continuously-stirred tank reactor. Appl. Geochem. 13, 509–520.

Kirby, C.S., Thomas, H.M., Southam, G., Donald, R., 1999. Relative contributions of abiotic and biological factors in Fe(II) oxidation in mine drainage. Appl. Geochem. 14, 511–530.

Kirby, C.S., Dennis, A., Kahler, A., 2009. Aeration to degas CO_2, increase pH, and increase iron oxidation rates for efficient treatment of net alkaline mine drainage. Appl. Geochem. 24, 1175–1184.

Li, Peiyue, 2018. Mine water problems and solutions in China. Mine Water Environ. 37, 217–221. https://doi.org/10.1007/s10230-018-0543-z.

Liger, E., Charlet, L., Van Cappellen, P.V., 1999. Surface catalysis of uranium(VI) reduction by ironII. Geochem. Cosmochim. Acta 63, 2939–2955.

Lofts, S., Tipping, E., 1998. An assemblage model for cation binding by natural particulate matter. Geochem. Cosmochim. Acta 62, 2609–2625.

Lovley, D.R., Phillips, E.J.P., Lonergan, D.J., 1991. Enzymic versus nonenzymic mechanisms for iron(III) reduction in aquatic sediments. Environ. Sci. Technol. 25, 1062–1067.

Lozano, A., Ayora, C., Fernández-Martínez, A., 2020. Sorption of rare earth elements on schwertmannite and their mobility in acid mine drainage treatments. Appl. Geochem. 113, 104499. https://doi.org/10.1016/j.apgeochem.2019.104499.

McCauley, C.A., O'Sullivan, A.D., Milke, M.W., Weber, P.A., Trumm, D.A., 2009. Sulfate and metal removal in bioreactors treating acid mine drainage dominated with iron and aluminum. Water Res. 43, 961–970.

Means, B., Rose, A.W., 2005. Manganese removal in limestone bed systems. In: Proceedings of the 2005 National Meeting of the American Society of Mining and Reclamation, pp. 702–717.

Means, B., Beam, R., Charlton, D., 2013. Operational and financial studies of hydrogen peroxide versus hydrated lime and hydrogen peroxide versus sodium hydroxide at two Pennsylvania mine drainage treatment sites. In: West Virginia Mine Drainage Task Force, 2013 Symposium. https://wvmdtaskforce.files.wordpress.com/2016/01/13-means-paper.doc.

Means, B., Parker, B., Beam, R., 2015. Decarbonating at the St. Michael Treatment plant: effect on cost, sludge, and sedimentation. In: West Virginia Mine Drainage Task Force, 2013 Symposium. https://wvmdtaskforce.files.wordpress.com/2016/01/15-means-paper.docx.

Millero, F.J., Sotolongo, S., 1989. The oxidation of Fe(II) with H_2O_2 in seawater. Geochem. Cosmochim. Acta 53, 1867–1873.

Millero, F.J., Sotolongo, S., Izaguirre, M., 1987. The oxidation kinetics of Fe(II) in seawater. Geochem. Cosmochim. Acta 51, 793–801.

Morgan, J.J., 2005. Kinetics of reaction between O_2 and Mn(II) species in aqueous solutions. Geochem. Cosmochim. Acta 69, 35–48.

Munk, L., Faure, G., Pride, D.E., Bigham, J.M., 2002. Sorption of trace metals to an aluminum precipitate in a stream receiving acid rock-drainage; Snake River, Summit County, Colorado. Appl. Geochem. 17, 421–430. https://doi.org/10.1016/s0883-2927(01)00098-1.

Neculita, C.M., Yim, G.-J., Lee, G., Ji, S.-W., Jung, J.W., Park, H.-S., Song, H., 2011. Comparative effectiveness of mixed organic substrates to mushroom compost for treatment of mine drainage in passive bioreactors. Chemosphere 83, 76–82.

Nordstrom, D.K., 2011a. Mine waters: acidic to circumneutral. Elements 7, 393–398.

Nordstrom, D.K., 2011b. Hydrogeochemical processes governing the origin, transport and fate of major and trace elements from mine wastes and mineralized rock to surface waters. Appl. Geochem. 26, 1777–1791.

Nordstrom, D.K., 2020. Geochemical modeling of iron and aluminum precipitation during mixing and neutralization of acid mine drainage. Minerals 10, 547. https://doi.org/10.3390/min10060547.

Nordstrom, D.K., Campbell, K.M., 2014. Modeling low-temperature geochemical processes. In: Holland, H.D., Turekian, K.K. (Eds.), Treatise on Geochemistry (2nd) 7. Elsevier, Oxford, pp. 27–68.

Office of Surface Mining Reclamation and Enforcement, 2017. AMDTreat.(last updated 2017). https://amd.osmre.gov/ accessed August 24, 2020.

Palomino-Ore, S.B., Rimstidt, J.D., Chermak, J.A., Schreiber, M.E., Seal II, R.R., 2019. Aluminum hydroxide coatings in limestone drains. Appl. Geochem. 103, 23–30.

Parkhurst, D.L., Appelo, C.A.J., 2013. Description of input and examples for PHREEQC version 3—a computer program for speciation, batch-reaction, one-dimensional transport, and inverse geochemical calculations. U.S. Geol. Surv. Techniques Methods 6-A43, 497. https://pubs.er.usgs.gov/publication/tm6A43 https://www.usgs.gov/software/phreeqc-version-3/.

Peiffer, S., dos Santos Afonso, M., Wehrli, B., Gachter, R., 1992. Kinetics and mechanism of the reaction of H_2S with lepidocrocite. Environ. Sci. Technol. 26, 2408–2412.

Peiffer, S., 2016. Reaction time scales for sulphate reduction in sediments of acidic pit lakes and its relation to in-lake acidity neutralization. Appl. Geochem. 73, 8–12.

Pennsylvania Department of Environmental Protection, 2012. Erosion and Sediment Pollution Control Program Manual: Harrisburg. Pennsylvania Dept. Environmental Protection Bureau of Watershed Management. Document No. 363-2134-008, 563 pp. (tables 6.6 and 6.7).

Pennsylvania Department of Environmental Protection, 2016. Acid Mine Drainage Set-Aside Program Implementation Guidelines. Pennsylvania Department of Environmental Protection, Bureau of Abandoned Mine Reclamation, p. 70. Document 546-5500-001.

Pesic, B., Oliver, D.J., Wichlacz, P., 1989. An electrochemical method of measuring the oxidation rate of ferrous to ferric iron with oxygen in the presence of Thiobacillus ferrooxidans. Biotechnol. Bioeng. 33, 428–439.

Plummer, L.N., Wigley, M.L., Parkhurst, D.L., 1978. The kinetics of calcite dissolution in CO_2-water systems at 5° to 60°C and 0.0 to 1.0 atm CO_2. Am. J. Sci. 278, 179–216.

Postma, D., Appelo, C.A.J., 2000. Reduction of Mn-oxides by ferrous iron in a flow system: column experiment and reactive transport modeling. Geochem. Cosmochim. Acta 64, 1237–1247.

Poulton, S.W., 2003. Sulfide oxidation and iron dissolution kinetics during the reaction of dissolved sulfide with ferrihydrite. Chem. Geol. 202, 79–94.

Rathbun, R.E., 1998. Transport, behavior, and fate of volatile organic compounds in streams. U. S. Geol. Surv. Prof. Pap. 1589, 151.

Reeder, M.D., Branam, T.D., Olyphant, G.A., 2010. Assessment of two field-scale sulfate reducing bioreactors using sulfur isotopes. In: The 2010 National Meeting of the American Society of Mining and Reclamation, pp. 813–827.

Robbins, E.I., Cravotta III, C.A., Savela, C.E., Nord Jr., G.L., 1999a. Hydrobiogeochemical interactions in "anoxic" limestone drains for neutralization of acidic mine drainage. Fuel 78, 259–270.

Robbins, E.I., Brant, D.L., Ziemkiewicz, P.F., 1999b. Microbial, algal, and fungal strategies for manganese oxidation at a Shade Township coal mine, Somerset County, Penna. In: Proceedings American Society of Mining and Reclamation, Scottsdale, AZ, August 13-19, 1999, pp. 634–640. https://doi.org/10.21000/JASMR99010634.

Rose, A.L., Waite, T.D., 2003. Kinetics of iron complexation by dissolved natural organic matter in coastal waters. Mar. Chem. 84, 85–103. https://doi.org/10.1016/S0304-4203(03)00113-0.

Rose, A.W., 1999. Chemistry and kinetics of calcite dissolution in passive treatment systems. In: Proceedings American Society of Mining and Reclamation, Scottsdale, AZ, August 13-19, 1999, pp. 634–640. https://doi.org/10.21000/JASMR99010599.

Rose, A.W., 2004. Vertical flow systems-Effects of time and acidity relations. In: Proceedings American Society of Mining and Reclamation, Morgantown, WV, April 18-24, 2004, pp. 1595–1616. https://doi.org/10.21000/JASMR04011595.

Sánchez-España, J., Usta, I., Gray, J., Burgos, W.D., 2016. Geochemistry of dissolved aluminum at low pH: extent and significance of Al-Fe(III) co-precipitation below pH 4.0. Geochem. Cosmochim. Acta 175, 128–149. https://doi.org/10.1016/j.gca.2015.10.035.

Santelli, C.M., Pfiser, D.H., Lazarus, D., Sun, L., Burgos, W.D., Hansel, C.M., 2010. Promotion of Mn(II) oxidation and remediation of coal mine drainage in passive treatment systems by diverse fungal and bacterial communities. Appl. Environ. Microbiol. 76, 4871–4875. https://doi.org/10.1128/AEM.03029-99.

Santomartino, S., Webb, J.A., 2007. Estimating the longevity of limestone drains in treating acid mine drainage containing high concentrations of iron. Appl. Geochem. 22, 2344–2361.

Sato, M., 1960. Oxidation of sulfide ore bodies 1. Geochemical environments in terms of Eh and pH. Econ. Geol. 55, 928–961.

Skousen, J.G., Zipper, C.E., Rose, A.W., Ziemkiewicz, P.F., Nairn, R., McDonald, L.M., Kleinmann, R.L., 2017. Review of passive systems for acid mine drainage treatment. Mine Water Environ. 36, 133–153.

Skousen, J.G., Ziemkiewicz, P.F., McDonald, L.M., 2019. Acid mine drainage formation, control and treatment: approaches and strategies. The Extractive Industries and Society 6, 241–249.

Stumm, W., Lee, G.F., 1961. Oxygenation of ferrous iron. Ind. Eng. Chem. 53, 143–146.

Stumm, W., Morgan, J.J., 1996. Aquatic Chemistry-Cchemical Equilibria and Rates in Natural Waters, 3rd). Wiley-Interscience, New York, p. 1022.

Sung, W., Morgan, J.J., 1980. Kinetics and product of ferrous iron oxygenation in aqueous systems. Environ. Sci. Technol. 14, 561–568.

Tamura, H., Goto, K., Nagayama, M., 1976. The effect of ferric hydroxide on the oxygenation of ferrous iron in neutral solutions. Corrosion Sci. 16, 197–207.

Tan, H., Zhang, G., Heaney, P.J., Webb, S.M., Burgos, W.D., 2010. Characterization of manganese oxide precipitates from Appalachian coal mine drainage treatment systems. Appl. Geochem. 25, 389–399. https://doi.org/10.1016/j.apgeochem.2009.12.006.

Thomas, R.C., Romanek, C.S., 2002a. Passive treatment of low-pH, ferric dominated acid rock drainage in a vertical flow wetland–I. Acidity neutralization and alkalinity generation. In: Proceedings American Society of Mining and Reclamation, Lexington, Kentucky, June 9-13, 2002, pp. 723–748. https://doi.org/10.21000/JASMR02010723.

Thomas, R.C., Romanek, C.S., 2002b. Passive treatment of low-pH, ferric dominated acid rock drainage in a vertical flow wetland–II. Metal removal. In: Proceedings American Society of Mining and Reclamation, Lexington, Kentucky, June 9-13, 2002, pp. 752–775. https://doi.org/10.21000/JASMR02010752.

Tipping, E., Lofts, S., Sonke, J.E., 2011. Humic ion-binding model VII: a revised parameterisation of cation-binding by humic substances. Environ. Chem. 8 (3), 225–235.

Tonkin, J.W., Balistrieri, L.S., Murray, J.W., 2004. Modeling sorption of divalent metal cations on hydrous manganese oxide using the diffuse double layer model. Appl. Geochem. 19, 29–53.

Vail, W.J., Riley, R.K., 2000. The Pyrolusite Process®: a bioremediation process for the abatement of acid mine drainage. Green Lands. Fall 40–47, 2000.

van Beek, C.G.E.M., Hiemstra, T., Hofs, B., Nederlof, M.M., van Paaassen, J.A.M., Reijnen, G.K., 2012. Homogeneous, heterogeneous and biological oxidation of iron (II) in rapid sand filtration. J. Water Supply Res. Technol. - Aqua 61, 1–10.

Visual Studio, 2019. 16.2.3. Microsoft Visual Studio Community 2019 Version 16.2.3 (Accessed 29 July 2019).

Vries, D., Bertelkamp, C., Schoonenberg Kegel, F., Hofs, B., Dusseldorp, J., Bruins, J.H., de Vet, J.H., van den Akker, B., 2017. Iron and manganese removal: recent advances in modelling treatment efficiency by rapid sand filtration. Water Res. 109, 35–45.

Watzlaf, G.R., Schroeder, K.T., Kairies, C., 2000. Long-term performance of alkalinity-producing passive systems for the treatment of mine drainage. In: Proc. 2000 National Meeting of the American Society for Surface Mining and Reclamation, pp. 262–274.

Watzlaf, G.R., Schroeder, K.T., Kleinmann, R.L.P., Kairies, C.L., Nairn, R.W., 2004. The Passive Treatment of Coal Mine Drainage. U.S. Department of Energy DOE/NETL-2004/1202 (accessed June 15, 2020 at. http://www.bobkleinmann.com/images/2004_DOEPassiveTreatment_of_Coal_Mine_Drainage_NETL-1202.pdf.

Webster, J.G., Swedlund, P.J., Webster, K.S., 1998. Trace metal adsorption onto an acid mine drainage iron(III) oxy hydroxy sulfate. Environ. Sci. Technol. 32 (10), 1361–1368. https://doi.org/10.1021/es9704390.

Winland, R.L., Traina, S.J., Bigham, J.M., 1991. Chemical composition of ochreous precipitates from Ohio coal mine drainage. J. Environ. Qual. 20, 452–460. https://doi.org/10.2134/jeq1991.00472425002000020019x.

Wolfe, N., Hedin, R.S., Weaver, T., 2010. Sustained treatment of AMD containing Al and Fe^{3+} with limestone aggregate. In: International Mine Water Association 2010 Symposium. Nova Scotia, Canada, Sydney, pp. 237–241. https://www.imwa.info/docs/imwa_2010/IMWA2010_Hedin_490.pdf.

Zappa, C.J., Raymond, P.A., Terray, E.A., McGillis, W.R., 2003. Variations in surface turbulence and the gas transfer velocity over a tidal cycle in a macro-tidal estuary. Estuaries 26, 1401–1415.

Supplementary Data:

Interactive PHREEQ-N-AMDTreat Water-Quality Modeling Tools to Evaluate Performance and Design of Treatment Systems for Acid Mine Drainage

Charles A. Cravotta III, Research Hydrologist,

U.S. Geological Survey, Pennsylvania Water Science Center,

215 Limekiln Rd, New Cumberland, PA 17070

cravotta@usgs.gov

This supplementary data file augments the article by the same title (Cravotta, 2020a). It includes 8 tables, 21 figures, expanded explanation of the user interface for the PHREEQ-N-AMDTreat software (Cravotta, 2020b), and additional case-study simulations using the PHREEQ-N-AMDTreat modeling tools that were excluded from the journal article to reduce the paper length.

Supplementary Tables:

Table S1. Expanded description of variables used in PHREEQ-N-AMDTreat modeling tools (Excel file with expanded information from table included in main text).

Table S2. Solubility reactions and equilibrium constants used with PHREEQC database for PHREEQ-N-AMDTreat models (phreeqcAMDTreat.dat). (Excel file)

Table S3. Surface complexation model parameters for hydrous metal oxides (HMeO) used with phreeqcAMDTreat.dat database for PHREEQ-N-AMDTreat models. (Excel file)

Table S4. Surface species for hydrous ferric oxide (HFO), hydrous manganese oxide (HMO), and hydrous aluminum oxide (HAO) in phreeqcAMDTreat.dat database (Excel file)

Table S5. Rate models in phreeqcAMDTreat.dat database coded for use by PHREEQ-N-AMDTreat software. (Excel file)

Table S6. Typical empirical values of rate constants for CO_2 outgassing and O_2 ingassing. (Excel file)

Table S7. Surface area and volume estimates for various coarse aggregates used in limestone beds. (Excel file)

Table S8. Estimated size of passive or active treatment systems for Morea AMD based on retention times used in TreatTrainMix2 and 90th percentile flow (Excel file).

Supplementary Figures:

Figure S1. UI for PHREEQ-N-AMDTreat model exhibiting input values for simulations of caustic titration of Nittanny mine effluent.

Figure S2. Concentration of NaOH added and corresponding pH and solute concentrations indicated for simulated titration of effluent at the Nittanny mine.

Figure S3. Measured and simulated titrant and chemical concentrations as a function of pH during titration of Nittanny mine effluent with NaOH.

Figure S4. UI for PHREEQ-N-AMDTreat parallel model exhibiting input values for simulations of different limestone particle size and sorbent for Orchard oxic limestone drain.

Figure S5. Comparison of measured (symbols) and simulated (curves) values for pH, alkalinity, Ca, Fe, Al, Mn, P_{CO_2}, and calcite saturation index during treatment of AMD at the Orchard oxic limestone drain, 1995-2000.

Figure S6. UI for PHREEQ-N-AMDTreat sequential model exhibiting input values for simulation of water-quality changes through the Pine Forest treatment system, December 2015, which consists of a "biofouled" anoxic limestone drain (ALD), oxidation/settling pond, and three aerobic wetlands, with aeration steps in between.

Figure S7. Comparison of measured (symbols) and simulated (curves) values for pH, Fe^{II}, Mn^{II}, Al, P_{CO_2}, and P_{O_2} during treatment of AMD at the Pine Forest passive treatment system, December 2015.

Figure S8. UI for PHREEQ-N-AMDTreat model exhibiting input values for simulations of sequential treatment steps at the Silver Creek treatment system, December 2015, which consists of a small sedimentation pond, two large oxidation/settling ponds, and two aerobic wetlands, with aeration cascades in between.

Figure S9. Comparison of measured (symbols) and simulated (curves) values for pH, Fe^{II}, Mn^{II}, Al, P_{CO_2}, and P_{O_2} during treatment of AMD at the Silver Creek passive treatment system, December 2015.

Figure S10. UI for PHREEQ-N-AMDTreat sequential model exhibiting input values for simulations of sequential steps at the Silver Creek treatment system, August 2016.

Figure S11. Comparison of measured (symbols) and simulated (curves) values for pH, Fe^{II}, Mn^{II}, Al, P_{CO_2}, and P_{O_2} during treatment of AMD at the Silver Creek passive treatment system, August 2016.

Figure S12. UI for TreatTrainMix2 simulation of passive treatment of net-acidic AMD at Morea Mine through (1) sedimentation pond; (2-4) vertical flow pond (VFP); (6, 8) oxidation/settling ponds; (10) aerobic wetlands; and (11) manganese removal bed with intermediate aeration steps (5 7 9 11).

Figure S13. TreatTrainMix2 simulation results for passive treatment of Morea AMD by (1) VFP (consisting of a 0.61-m (2-ft) deep water layer, 0.61-m (2-ft) thick compost layer composed of 25 % limestone fines and 75% organic matter having 45% porosity, 0.91-m (3-ft) thick limestone layer having 45% porosity), (2) 1.52-m (5-ft) deep aerobic pond, (3) 0.30-m (1-ft) deep wetlands, and (3) 0.30-m (0.5-ft) deep "manganese" removal limestone bed

Figure S14. UI for TreatTrainMix2 simulation of active treatment of net-acidic AMD at Morea Mine through (1) sedimentation pond; (3) lime dosing and sludge recirculation; (4) aerobic pond; and (6) aerobic wetlands with aeration steps (2 5 7).

Figure S15. TreatTrainMix2 input and simulation results for active treatment of AMD at Morea Mine by (1) hydrated lime dosing and recirculation of sludge, including HMeO solids and unreacted lime, (2) 1.52-m (5-ft) deep aerobic pond, and (3) 0.30-m (1-ft) deep wetlands.

Figure S16. UI for PHREEQ-N-AMDTreat model exhibiting input values for simulations of hypothetical treatment using passive aeration after mixing of AMD from the Oak Hill boreholes (Soln#A) and Pine Knot tunnel (Soln#B).

Figure S17. Simulation results for passive treatment of combined Oak Hill boreholes + Pine Knot tunnel AMD by aeration cascades, oxidation+settling pond, aerobic wetlands, and Mn-removal bed.

Figure S18. UI for PHREEQ-N-AMDTreat model exhibiting input values for simulations of hypothetical treatment using aggressive aeration after mixing of AMD from the Oak Hill boreholes (Soln#A) and Pine Knot tunnel (Soln#B).

Figure S19. Simulation results for passive treatment of combined Oak Hill boreholes + Pine Knot tunnel AMD by Maelstrom Oxidizer®, oxidation+settling pond, aerobic wetlands, and Mn-removal bed.

Figure S20. UI for PHREEQ-N-AMDTreat model exhibiting input values for simulations of hypothetical treatment using H_2O_2 after mixing of AMD from the Oak Hill boreholes (Soln#A) and Pine Knot tunnel (Soln#B).

Figure S21. Simulation results for passive treatment of combined Oak Hill boreholes + Pine Knot tunnel AMD by H_2O_2 without sludge recirculation, oxidation+settling pond, aerobic wetlands, and Mn-removal bed.

S1. Access, Installation, and Use of PHREEQ-N-AMDTreat Software

The executable PHREEQ-N-AMDTreat program files including example input and output files are accessible in the U.S. Geological Survey software release (Cravotta, 2020b). Instructions for installation and use of the software are provided in the document, "Instructions_PHREEQ-N-AMDTreatGeochemicalModels.docx," included with the software.

S2. User Interface for PHREEQ-N-AMDTreat

The PHREEQ-N-AMDTreat water-quality modeling tools consider dynamic reactions that take place in AMD treatment systems and other aquatic environments. The CausticTitration and ParallelTreatment tools consider treatment of one or a mixture of two water samples, whereas the TreatTrainMix2 sequential tool may be used for evaluation of progressive changes for the same initial water chemistry over as many as eleven sequential treatment steps, where water chemistry after reactions from the prior step is passed to the next step. Each step can have a different specified reaction (residence) time, temperature, aeration rate, mass of limestone and/or organic matter, and mass and composition of hydrous metal oxide (HMeO) sorbent plus added caustic agent or H_2O_2. Values for variables used in the PHREEQ-N-AMDTreat tools (Tables 1 and S1) are displayed and adjusted in the user interface (UI) that is linked to the PHREEQC code for each of the three tools. After entering or selecting values for each variable in the UI, the input data may be saved to a file "water_quality_input_values.xml" for re-use.

Check boxes on the UI screen permit the activation of selected computations. Specifically, the user can input the values for acidity (hot acidity or net acidity), total inorganic carbon (TIC), and Fe^{II}, or select the relevant option to estimate values for one or more of these parameters from other input dat. Likewise, check boxes are used to activate sequential kinetic steps or addition of caustic agents. Later in this document, the UI for various treatment simulations is displayed with input values. For example, Figure S1 shows the UI for the CausticTitration tool, with radio button activated for direct addition of NaOH without pre-aeration or other pre-treatment steps. The UI for the ParallelTreatment tool (Fig. S4) is identical to that for the TreatTrainMix2 tool (e.g. Figs. S6, S8, S10, S12, S14, S16, S18, and S20). Each step for the ParallelTreatment simulation is

independent of the others, whereas the TreatTrainMix2 simulations use water chemistry results from the prior step at the beginning of the next step.

The mass of precipitated solids is computed as the mass of precipitated minerals plus the adsorbed metals, expressed as the relevant hydroxides. Including the adsorbed metals considers that they could eventually oxidize in situ, with infinite time for reaction. To compute the sludge mass produced by treatment, Fe, Al, Mn, and Mg are assumed to precipitate as $Fe(OH)_3$, $Al(OH)_3$, $Mn(OH)_2$, and $Mg(OH)_2$, respectively, and SO_4 as gypsum ($CaSO_4 \cdot 2H_2O$), which in addition to the unreacted solid chemicals can make up a large fraction of the sludge (e.g. Means and Hilton 2004).

Changes to rate parameters are implemented by changing multiplication factors in the UI, not the actual rate constants. For example, FeOB (iron-oxidizing bacteria) contributions to the Fe^{II} oxidation rate may be changed from 1 (default) to 0 to yield solely abiotic contributions, or the fixed sorbent mass and composition can be specified as 0 to simulate solely autocatalytic oxidation, or to other positive values to reflect measured chemistry (percentage Fe, Mn, Al) of the sorbent.

Net acidity (as mg/L of $CaCO_3$) is computed for "non-purgeable" constituents in AMD; computed net acidity and measured hot acidity exclude CO_2 acidity, because that can be eliminated simply by aeration (Kirby and Cravotta, 2005). The net-acidity computation considers a negative contribution from alkalinity and positive contributions from H^+ (pH) and concentrations of dissolved Fe^{III}, Fe^{II}, Mn, and Al in milligrams per liter (CFe^{III}, CFe^{II}, C_{Mn}, C_{Al}, respectively):

$$\text{Net Acidity} = 50 \cdot (10^{(3-\text{pH})} + 3 \cdot CFe^{III}/55.85 + 2 \cdot CFe^{II}/55.85 + 2 \cdot C_{Mn}/54.94 + 3 \cdot C_{Al}/26.98) - \text{Alkalinity}$$
(S1)

Kirby and Cravotta (2005) showed that if the AMD is net acidic (net acidity > 0; hot-peroxide acidity > 0), the ultimate pH of oxidized samples will be less than 5.0 and additional alkalinity would be needed to maintain pH greater than or equal to 6.0. If the AMD is net alkaline (net acidity < 0; hot-peroxide acidity < 0), the ultimate pH of the oxidized AMD will be greater than or equal to 6.0. Kirby and Cravotta (2005) also showed that the cold acidity or treatment acidity (prior to complete oxidation and atmospheric equilibration) can be larger than the hot acidity because of contributions by dissolved CO_2 that are excluded from the hot acidity or calculated net acidity. Thus, pre-aeration may be conducted to promote the CO_2 outgassing and reduce the caustic chemical requirement for treatment (Jageman et al., 1988; Means and Hilton, 2004).

Some AMD has low pH and no measurable alkalinity, but may still have elevated concentrations of dissolved CO_2 that is included in treatment acidity. Therefore, the model uses the

TIC concentration instead of alkalinity as input to PHREEQC for carbonate speciation calculations. If selected, the initial TIC can be estimated from input values for alkalinity, pH, and temperature, assuming equilibrium among dissolved carbonate species in accordance with the following:

$$\text{TIC (mg/L as C)} = (\text{Alkalinity}/50000)/K_1 \cdot [H^+] \cdot (1 + K_1/[H+] + K_1 \cdot K_2/[H^+]^2) \tag{S2}$$

where $[H^+] = 10^{-pH}$, and K_1 and K_2 are the temperature-adjusted dissociation constants for carbonate species (Ball and Nordstrom 1991). If alkalinity is 0 and/or pH is less than or equal to 3.9, TIC is assumed to be 0.0001 mol/L (1.2 mg/L), which corresponds to an equilibrium partial pressure of CO_2 (P_{CO2}) of $10^{-2.5}$ atm. AMD samples from 140 coal mines in Pennsylvania had P_{CO2} values from $10^{-2.5}$ to $10^{-0.5}$ atm and were mostly undersaturated with carbonate minerals (Cravotta 2008b).

The initial distribution of Fe^{II} and Fe^{III} species is estimated by PHREEQC using the input values for total dissolved iron (undefined redox state) and Fe^{II}. Thereafter, the PHREEQC titration simulations assume that any Fe^{II} can be oxidized kinetically to consume available DO (without and with pre-aeration, as explained below). However, because data on the initial concentration of Fe^{II} may not be available the initial Fe^{II} concentration can be estimated using the input values for total dissolved Fe and pH:

$$pH > 2.6 \qquad Fe^{III} = Fe \cdot 10(-1.40844 \cdot pH + 3.675995) \tag{S3a}$$

$$pH \leq 2.6 \qquad Fe^{III} = Fe \cdot (0.9999) \tag{S3b}$$

$$Fe^{II} = Fe - Fe^{III} \tag{S3c}$$

These computations yield a greater proportion of Fe^{III} to Fe^{II} at progressively lower pH, until pH < 2.6, where 99.99% of the total dissolved Fe is assumed to be Fe^{III}. The computations are based on an approximation of the empirical relation between the ratio of Fe^{III}/total Fe as a function of pH of AMD in Pennsylvania (Cravotta 2008a).

Input values for the sorbent mass and chemistry in the UI are used with the specific surface area and site densities to compute the moles of sorption sites on HFO, HMO, and HAO for adsorption equilibrium computations (Tables S3 and S4). For HFO, the unit mass was estimated as 107 g/mol for $Fe(OH)_3$ instead of using 89 g/mol for FeOOH, otherwise, specific surface area of 600 m^2/g and densities of strong and weak sites of 0.005 mol/mol and 0.2 mol/mol, respectively, were adopted from Dzombak and Morel (1990). For HMO, the unit mass and surface area were specified as 105 g/mol and 746 m^2/g with densities of strong and weak sites of 0.0141 mol/mol and

0.0794 mol/mol, respectively (Tonkin et al., 2004). For HAO, the unit mass and surface area were specified as 78 g/mol and 32 m^2/g, respectively, with only a single site type having a density of 0.033 mol/mol (Karamalidis and Dzombak, 2010). Estimates for Al-HAO and Al-HMO surface species were computed using linear free energy relations with the first-hydrolysis equilibrium constant after Karamalidis and Dzombak (2010) and Tonkin et al. (2004), whereas that for Al-HFO adsorption was taken from Burrows et al. (2017).

S3. Additional Model Validation--Simulations of Observed Changes in Chemistry of AMD

S3.1. Caustic Titration without Pre-Aeration (Nittanny Mine)

The caustic titration tool is used to simulate field acidity titration (cold, no aeration) of Nittanny mine effluent with NaOH (1.6 N = 6.0 wt%). Detailed empirical water chemistry data were collected at points during the field titration in November 2011 and are used for comparison with simulations. The simulation results for titration with NaOH without aeration are consistent with the empirical data on pH and concentrations of major ions, Fe, Al, and Mn (Figs. S1-S3). Additional information about this site and the water-quality evaluation, including the field titration and the active treatment of the effluent, are reported by Cravotta et al. (2015) and Cravotta and Brady (2015).

File

Select Workspace | C:\Users\cravotta\Documents\AMDTreat_geochem_data\Nittanny

	Soln#A	Soln#B
Design flow (gpm)	50	0
Mix fraction	1	0
Temp (C)	13.5	0.01
SC (uS/cm)	5551	0
DO (mg/L)	4.1	0.01
pH	3.01	0
Acidity (mg/L)	0	0
☑ Estimate NetAcidity	1079.2	0
Alk (mg/L)	0	0
TIC (mg/L as C)	19.2	0
☑ Estimate TIC	1.2	0
Fe (mg/L)	40.7	0
Fe2 (mg/L)	29.58	0
☐ Estimate Fe2	0	0
Al (mg/L)	128	0
Mn (mg/L)	129	0
SO4 (mg/L)	5000	0
Cl (mg/L)	1.9	0
Ca (mg/L)	422	0
Mg (mg/L)	652	0
Na (mg/L)	17.8	0
K (mg/L)	3.48	0
Si (mg/L)	30.8	0
NO3N (mg/L)	0.01	0
TDS (mg/L)	7620	0
DOC (mg/L as C)	1.9	0
Humate (mg/L as C)	1.9	0

Caustic Chemical Treatment Type

○ Hydrated Lime, Ca(OH)2
○ Pebble Quick Lime, CaO
● Caustic Soda, NaOH   [6 ▽] wt% soln
○ Soda Ash, Na2CO3

● Not Aerated
○ Pre-Aerated   TimeSecs [72]
  kLaCO2.1/s   [0.005 ▽]
  factr.kCO2   [1]
  factr.kO2   [2.1]
  H2O2.mol   [0]
  ☑ Estimate H2O2.mol/L   [0.000266]
  [2.28E-05] 35wt% [2.16E-05] 50wt%
  H2O2 wt% units gal/gal (memo, not used)
  factr.kFeH2O2   [1]

○ Aerated to Equilibrium

User Specified "Steady-State" Conditions:

Steady-state logPCO2   [-3.4 ▽]

Saturation Index lg(IAP/K) to Precipitate Selected Solids:

Al(OH)3	0.0 ▽	Basaluminite	3.0 ▽
Fe(OH)3	0.0 ▽	Schwertmannite	1.0 ▽
CaCO3	0.3 ▽	FeCO3 or MnCO3	2.5 ▽

[Generate Titration Output]   ☑ Print PHREEQC Output Report

☑ Plot Dis. Metals   ☑ Plot Ca, Acidity   ☑ Plot Sat Index   ☑ Plot PPT Solids

CausticTitration.exe created by C.A. Cravotta III, U.S. Geological Survey. Version Beta 1.44, November 2020

Figure S1. UI for PHREEQ-N-AMDTreat model exhibiting input values for simulations of caustic titration of Nittanny mine effluent. Results of simulations are shown in Figures S2-S3. The value of 1.2 for "Estimate TIC" for solution A or B corresponds to an assumed P_{CO_2} of $10^{-2.5}$ atm for samples with pH < 3.9 (Eq. S2).

A

pH	Caustic moles	Caustic units	Caustic asCaCO3mg	Fe_mg	Fe2_mg	Al_mg	Mn_mg	Na_mg	Ca_mg	Mg_mg	SO4_mg	Alk_mg	SpCond_uS	TDS_mg	NetAcidity_mg	SolidsPPT_mg	CO2_mg	O2_mg
3.010999	0.000000	0.000000	0.000000	40.963462	29.500570	128.828578	129.835051	17.915224	424.731718	656.220569	5,032.366343	-139.093900	5,381.732596	6,782.110614	1,096.471392	0.000000	4.422939	0.000000
3.010999	0.000000	0.000000	0.000000	40.963479	29.500570	128.828583	129.835062	17.915224	424.731722	656.220569	5,032.366357	-139.093830	5,381.732316	6,782.110746	1,096.471436	0.000000	4.422939	0.000000
4.000000	0.002632	0.001644	131.729299	30.927933	29.499487	128.823854	129.830296	76.427694	423.929334	656.196481	5,030.295835	-16.340967	5,208.996566	6,894.145825	1,016.252790	22.582296	4.400522	0.000000
4.500000	0.002908	0.001817	145.548216	29.676932	29.499393	128.823443	129.829682	84.775487	423.498088	656.194387	5,029.249411	-3.641950	5,198.621912	6,904.236755	1,008.726038	26.822977	4.347788	0.000000
5.000000	0.003079	0.001924	154.091279	29.541372	29.499364	128.823317	129.829754	88.699855	423.149042	656.193741	5,028.409825	4.780329	5,202.110004	6,911.765506	1,002.264595	28.578333	4.189039	0.000000
5.500000	0.014945	0.009336	747.896278	29.512219	29.499739	22.069809	129.831406	361.482400	408.514849	656.202091	4,993.384620	4.529079	5,835.602848	6,824.894963	407.949346	400.172834	3.753572	0.000000
6.000000	0.017254	0.010779	863.450372	29.503809	29.499801	0.965798	129.831677	414.586362	406.034728	656.203458	4,987.448606	2.643948	5,959.340601	6,807.173726	292.238152	471.862082	2.824345	0.000000
6.500000	0.017369	0.010851	869.237714	29.501208	29.499800	0.143455	129.831673	417.224939	405.999566	656.203441	4,987.364231	3.853228	5,965.522307	6,808.046894	286.403850	474.395582	1.581686	0.000000
7.000000	0.017402	0.010871	870.863758	29.500392	29.499797	0.188060	129.831663	417.971879	406.035821	656.203388	4,987.450803	5.726916	5,967.334344	6,810.168680	284.762970	474.112290	0.656795	0.000000
7.500000	0.017432	0.010890	872.388024	29.500134	29.499782	0.526899	129.831645	418.672034	406.069006	656.203296	4,987.529780	9.136713	5,968.658991	6,814.009564	283.233892	472.990332	0.225002	0.000000
8.000000	0.017498	0.010931	875.662622	29.500053	29.499782	1.635557	129.831596	420.176162	406.131010	656.203052	4,987.676895	18.581152	5,970.926733	6,824.606295	279.957437	469.518152	0.067816	0.000000
8.500000	0.017686	0.011049	885.062312	29.500025	29.499745	5.152413	129.831464	424.502940	406.314163	656.202381	4,988.111775	47.572733	5,977.398859	6,857.150958	270.536190	458.561782	0.017282	0.000000
9.000000	0.019022	0.011884	951.956897	7.161506	7.161123	16.282065	129.831196	455.222789	406.377837	656.201041	4,988.256189	136.352637	6,017.228560	6,930.889105	203.655072	462.051008	0.003438	0.000000
9.500000	0.024073	0.015039	1,204.687336	0.785458	0.784729	51.537562	39.647702	571.319656	406.094327	656.198004	4,987.562965	409.548781	6,168.676804	7,153.933034	-49.097383	517.621406	0.000913	0.000000
10.000000	0.044934	0.028071	2,248.687649	0.101922	0.100088	89.624845	4.304857	1,051.239648	250.732682	496.747519	4,840.819347	709.162324	6,677.631397	7,404.052763	-202.378848	1,510.219790	0.000182	0.000000
10.500000	0.084213	0.052609	4,214.335471	0.023208	0.017863	60.901065	0.520543	1,554.969477	123.871022	53.246265	4,700.634506	513.019286	7,872.897102	7,389.928731	-173.114833	3,204.683801	0.000039	0.000000
11.000000	0.089866	0.056141	4,497.233716	0.023228	0.006796	45.935147	0.066962	2,085.261448	58.890600	5.476058	4,627.593805	429.723125	8,061.371739	7,240.294867	-173.919146	3,642.413746	0.000007	0.000000

Display

B

pH	Caustic moles	Caustic units	Caustic asCaCO3mg	Fe_mg	Fe2_mg	Al_mg	Mn_mg	Na_mg	Ca_mg	Mg_mg	SO4_mg	Alk_mg	SpCond_uS	TDS_mg	NetAcidity_mg	SolidsPPT_mg	CO2_mg	O2_mg
3.110592	0.000000	0.000000	0.000000	40.963478	0.763963	128.828627	129.835101	17.915231	424.731880	656.220820	5,032.368252	-164.847370	5,273.793918	6,766.661143	1,110.062723	0.000000	4.422319	0.000000
3.113321	0.000000	0.000000	0.000000	40.963491	0.000006	128.828621	129.835101	17.915229	424.731847	656.220763	5,032.367828	-165.567901	5,271.131100	6,766.272873	1,110.451823	0.000000	0.817309	10.596304
4.000000	0.006088	0.003803	304.664800	1.436339	0.000001	128.823926	63.894837	157.869425	421.173131	656.196845	5,023.691961	-16.433767	5,291.527631	6,800.954609	843.261288	196.417926	0.816936	10.591470
4.500000	0.008456	0.005283	423.179094	0.177923	0.000000	128.822489	6.411334	212.309349	419.105134	656.189524	5,018.690603	-3.775701	5,332.304915	6,760.375843	730.971713	299.714653	0.816904	10.591053
5.000000	0.008833	0.005518	442.015821	0.042017	0.000000	128.822257	0.642033	220.961942	418.607156	656.188342	5,017.489783	4.428532	5,340.808699	6,762.643795	714.348891	311.346959	0.816850	10.590350
5.500000	0.020670	0.012913	1,034.395810	0.012481	0.000000	22.468139	0.066684	493.087885	404.554562	656.196285	4,983.857043	3.919134	5,980.309702	6,677.159336	121.462401	680.210784	0.815568	10.573736
6.000000	0.023009	0.014374	1,151.486648	0.004008	0.000000	0.978835	0.006717	546.877353	402.101674	656.197629	4,977.986164	1.315981	6,106.880154	6,658.589314	4.215240	752.999827	0.815316	10.570474
6.500000	0.023120	0.014443	1,157.005715	0.001408	0.000000	0.143874	0.000672	549.412658	402.061452	656.197617	4,977.889689	2.175655	6,112.779538	6,659.065887	-1.350685	755.595270	0.815304	10.570309
7.000000	0.023184	0.014483	1,160.210309	0.000594	0.000000	0.188078	0.000067	550.884695	402.161564	656.197534	4,978.129131	5.624664	6,116.968019	6,663.072532	-4.570199	755.039698	0.693989	10.570143
7.500000	0.023212	0.014501	1,161.614816	0.000341	0.000000	0.526910	0.000007	551.529828	402.204838	656.197463	4,978.232410	8.914520	6,118.367939	6,666.820759	-5.979448	753.874562	0.244479	10.570067
8.000000	0.023270	0.014537	1,164.500004	0.000271	0.000000	1.635595	0.000001	552.855050	402.291448	656.197255	4,978.438852	17.969617	6,120.720495	6,677.089145	-8.866313	750.296720	0.078935	10.569908
8.500000	0.023439	0.014643	1,172.986733	0.000280	0.000000	5.152584	0.000000	556.753155	402.541665	656.196718	4,979.035164	46.028794	6,127.339865	6,708.874986	-17.354108	739.052015	0.023925	10.569437
9.000000	0.023959	0.014968	1,199.012230	0.000582	0.000000	16.283424	0.000000	568.707196	403.285475	656.195133	4,980.808239	133.996622	6,147.535357	6,808.427943	-43.381516	703.670749	0.006495	10.567992
9.500000	0.025530	0.015949	1,277.633285	0.000729	0.000000	51.536835	0.000000	604.819465	405.199009	656.190747	4,987.461808	406.642463	6,208.975405	7,119.003521	-119.825215	591.932267	0.001103	10.563598
10.000000	0.045079	0.028162	2,255.922109	0.001834	0.000000	89.678781	0.000000	1,054.546167	250.693791	496.858587	4,841.027823	708.741403	6,681.971912	7,400.422109	-209.680858	1,523.174956	0.000182	10.559894
10.500000	0.084231	0.052621	4,215.263473	0.005345	0.000000	60.913266	0.000000	1,955.363524	123.866861	53.247993	4,700.639319	512.916985	7,873.475641	7,389.465396	-173.924908	3,212.032250	0.000039	10.545760
11.000000	0.089869	0.056143	4,497.396164	0.016432	0.000000	45.935330	0.000000	2,085.301685	58.890194	5.476151	4,627.539965	429.701237	8,061.435515	7,240.193553	-174.030432	3,649.133387	0.000007	10.545751

Figure S2. Concentration of NaOH added and corresponding pH and solute concentrations indicated for simulated titration of effluent at the Nittanny mine. Simulations use effluent composition data in Figure S1 for conditions with: A, no gas exchange with atmosphere and B, with equilibrium with atmosphere.
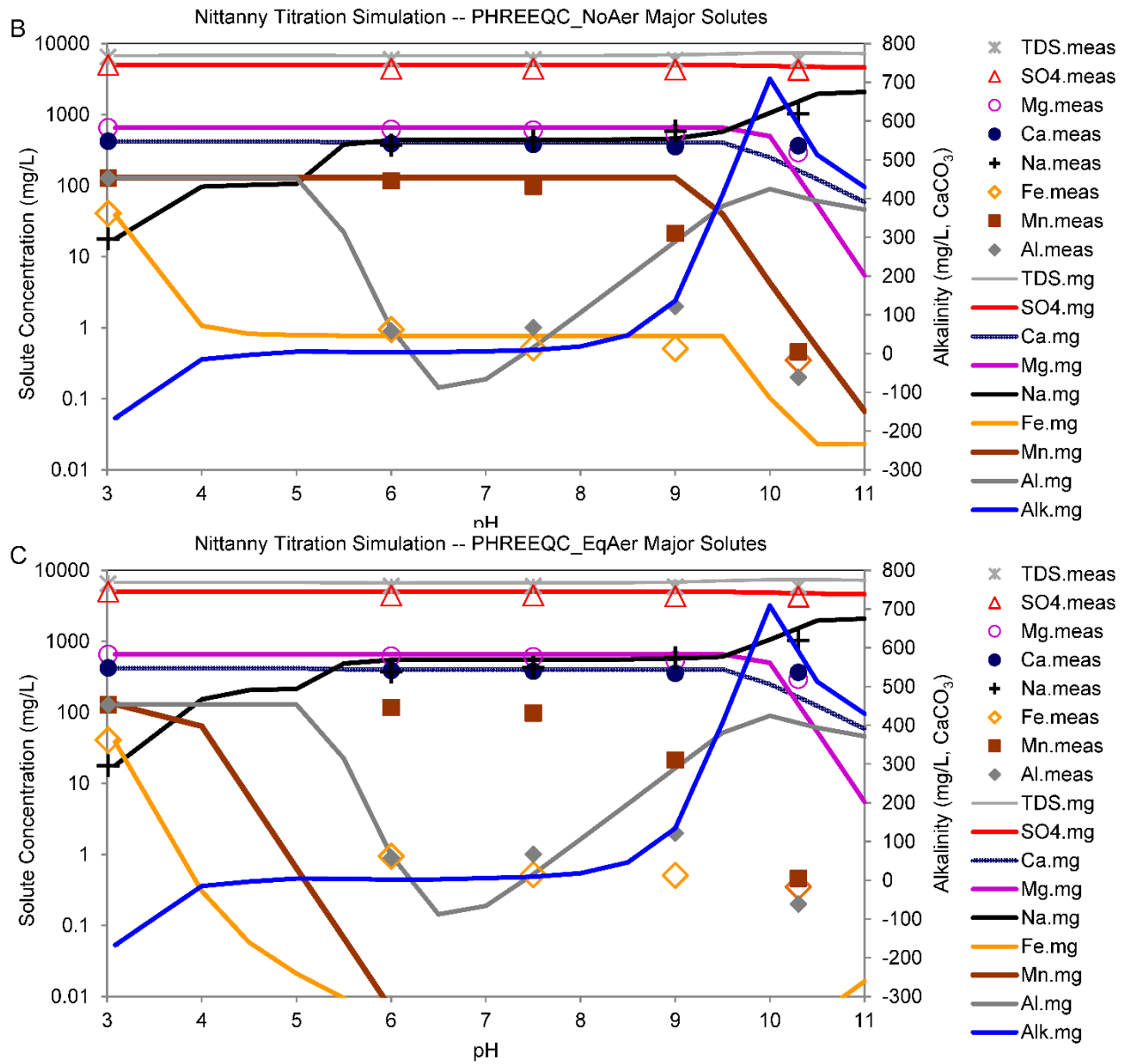
Figure S3. Measured (point symbols) and simulated (lines) titrant and chemical concentrations as a function of pH during titration of Nittanny mine effluent with NaOH. Simulations use effluent composition data shown in Figure S1 for conditions with: B, no gas exchange with atmosphere (PHREEQC_NoAer) and C, with equilibrium with atmosphere (PHREEQC_EqAer). The simulations without atmospheric equilibration are consistent with empirical results where oxidation of Fe^{II} and Mn^{II} are kinetically limited.

S3.2. Parallel Treatment Fragment Size and Coatings (Orchard OLD)

The Orchard limestone drain was constructed in 1995 as a research project to evaluate the efficiency of neutralization of low pH, oxic AMD with relatively low concentrations of dissolved metals (<5 mg/L) by limestone and associated reactions (Figs. S4 and S5). Three parallel "oxic"

limestone drains (OLDs), with access wells at five locations along the length of each drain, were constructed to treat the same influent AMD (Cravotta and Trahan, 1999; Cravotta and Watzlaf, 2003). The untreated AMD (6.9 gal min^{-1}, 0.43 L s^{-1}), sampled during 1995-2000, had median pH 3.5 with DO 2.6 mg/L and dissolved concentrations of Fe, Fe^{II}, Mn^{II}, and Al of 1.8, 0.6, 3.0, and 0.065 mg/L, respectively (Figs. S4 and S5). As reported by Cravotta and Trahan (1999), downgradient trends through the OLDs during the first 6 months of treatment (Fig. S5, Mar95-Aug95) were consistent with those expected for an ALD, with relatively conservative transport of Fe^{II} and Mn^{II}; however, after the first 6 months (Fig. S5, Sep95-May00), the drains began to retain Mn and trace metals consistent with adsorption by HFO and HMO that accumulated in the downstream section of the drains wherein pH was 6-6.5.
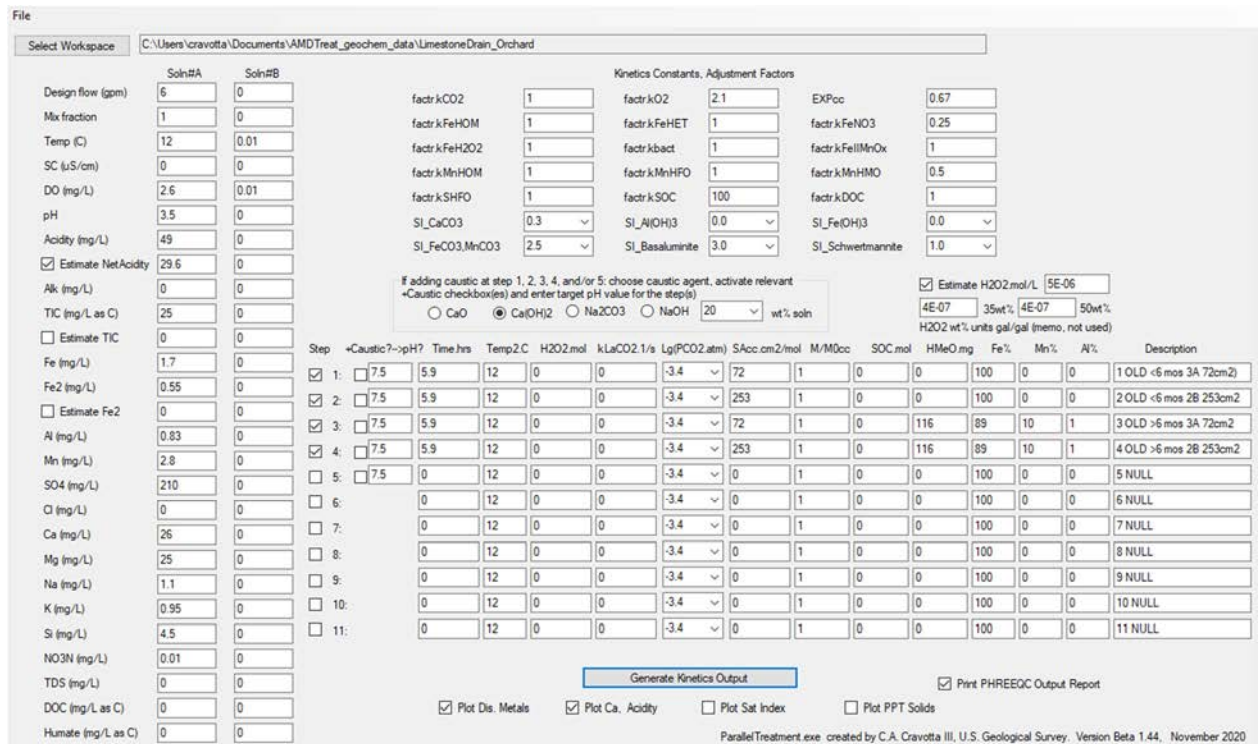
Figure S4. UI for PHREEQ-N-AMDTreat parallel model exhibiting input values for simulations of different limestone particle size and sorbent for Orchard oxic limestone drain. Results are shown in Figure S5
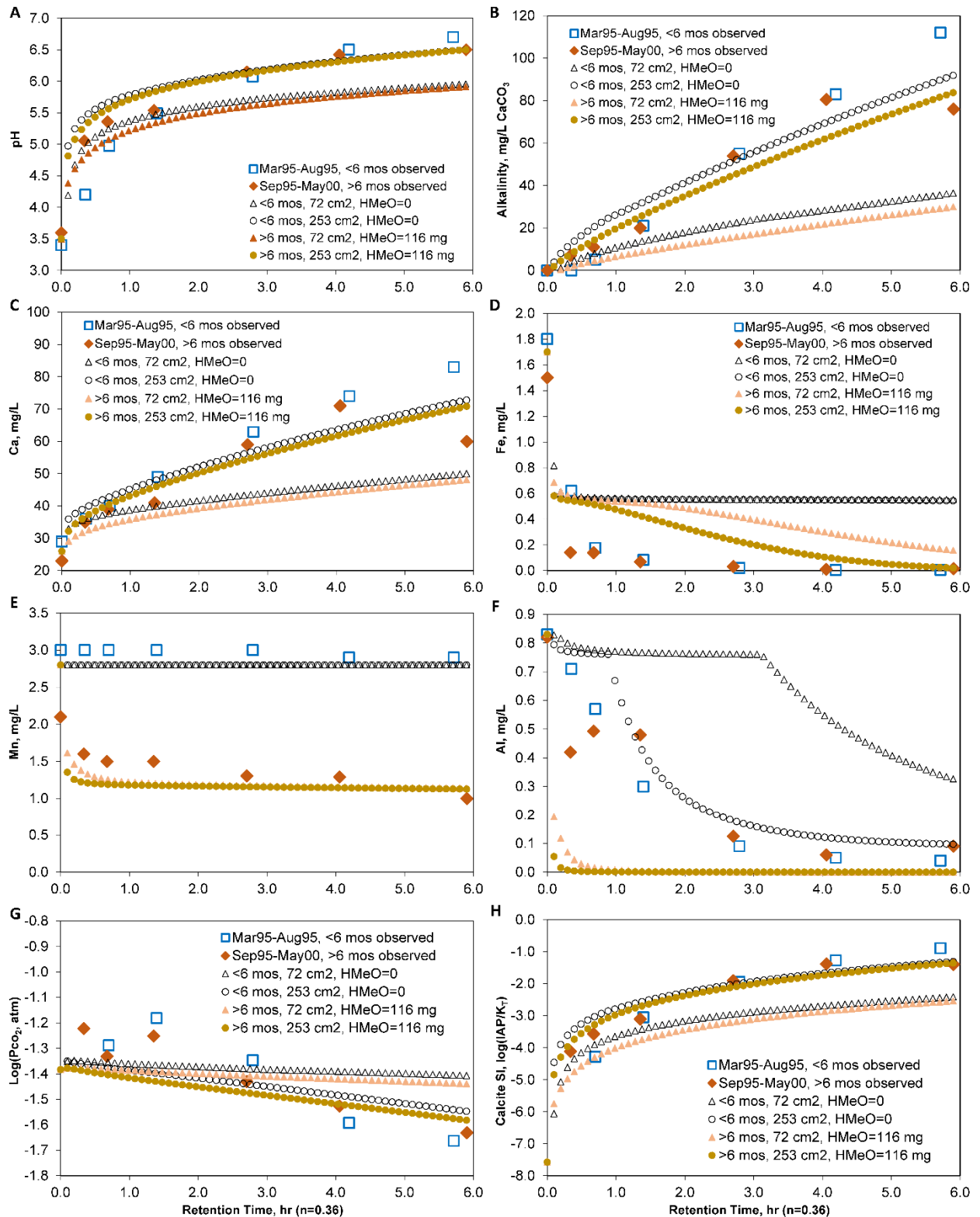
Figure S5. Comparison of measured and simulated values for pH, alkalinity, Ca, Fe, Al, Mn, P_{CO_2}, and calcite saturation index during treatment of AMD at the Orchard oxic limestone drain, 1995-2000.

Travel time through the OLDs increased linearly with distance from the inflow, attaining a total retention time of approximately 6 hrs at the outflow, which assumes a porosity of 35% (Fig. S5). The pH, alkalinity, Ca, and calcite saturation index ($SI_{CALCITE}$) values increased rapidly near the inflow and more gradually toward the outflow (Fig. S5). The asymptotic trends for pH, alkalinity, and Ca with retention time are consistent with rapid rates of limestone dissolution at low pH, and decreasing rates of dissolution as equilibrium with calcite is approached (Plummer et al., 1978).

The simulations consider two different limestone particle sizes consistent with standard aggregate materials (Table S7). The smaller particles correspond to AASHTO 57 or PA 2B size with average axis dimensions of 1.48 cm and estimated surface area of 2.53 cm^2/g (253 cm^2/mol). The larger particles, which correspond to AASHTO 3 or PA 3A size with average axis dimensions of 3.81 cm, have smaller estimated surface area of 0.72 cm^2/g (72 cm^2/mol). The simulated dissolution of the smaller size particles resulted in nearly double the concentrations of Ca and alkalinity (Fig. S5) and matched the observed data values better than simulations with larger particles.

Simulations for the system after 6 months (Sep95-May00) include an accumulated sorbent mass (HMeO.mg) of 116 mg within the OLD that is composed of 89% Fe, 10% Mn, and 1% Al (Fig. S4). This sorbent mass was computed for 0.5-μm thick coating on the limestone particles (72 cm^2/mol) in contact with 1 L water volume, assuming 35% bed porosity and sorbent density of 1.25 g/cm^3 (Table S7). The same mass of sorbent would have a smaller thickness if spread out over the finer particles. The included sorbent in the simulations improved the predictions of Fe and Mn attenuation, but resulted in overestimate of Al attenuation. The simulations do not evaluate potential for HMeO surface coatings to affect the limestone particle dissolution rate. Despite the accumulation of precipitated metals on limestone surfaces in the OLD and elsewhere, Cravotta and Trahan (1999), Cravotta and Watzlaf (2003), Cravotta (2003), and Cravotta et al. (2004, 2008c) showed that limestone theoretically could dissolve throughout the limestone systems they investigated because the water was consistently undersaturated with respect to calcite, attaining $SI_{CALCITE}$ values from -2.4 to -0.3 under the conditions evaluated. Cravotta and Trahan (1999) and Cravotta (2008c) noted etch pits beneath loosely bound surface coatings on limestone as evidence for continued dissolution. Although Palomino-Ore et al. (2019) demonstrated that Al armoring can lower calcite dissolution rates in the lab, Wolfe et al. (2010) demonstrated that automated flushing systems may be designed to effectively remove such solids to sustain the performance of a limestone bed.

S3.3. Sequential Treatment by Anoxic Limestone Drain (ALD), Cascades, Oxidation/Settling Pond, and Aerobic Wetlands

The Pine Forest treatment system consists of an anoxic limestone drain (ALD), oxidation/settling pond, and three aerobic wetlands, in series, with aeration steps in between (Figs. S6 and S7). The untreated AMD (690 gal min^{-1}, 43.5 L s^{-1}), sampled during winter 2015, had pH 5.8 with DO < 0.5 mg/L and dissolved concentrations of Fe^{II}, Mn^{II}, and Al of 14.0, 3.1, and 0.09 mg/L, respectively (Fig. S6). The treated effluent had pH ~7 with Fe and Mn <2 mg/L. After its first year of operation (2006), the ALD began to clog with gelatinous, Fe-rich precipitate. For this "biofouling" scenario, the microbial rate factor was increased from 1 to 2 and a pre-existing (accumulated) sorbent mass (HMeO.mg) of 116 mg was specified for the ALD (Fig. S6). The sorbent mass in the ALD was computed for 0.5-μm thick coating on the limestone particles (72 cm^2/mol) in contact with 1 L water volume, assuming 35% bed porosity and sorbent density of 1.25 g/cm^3 (Table S7). For downstream steps, the specified sorbent mass was only 1 to 3 mg.

The sequential model results for pH, Fe^{II}, Mn^{II}, Al, Pco_2, and Po_2, shown as a function of the retention time (computed as the void volume of the treatment component divided by the flow rate), generally reproduce the longitudinal trends for measured constituent values (Fig. S7). Despite less mass of sorbent indicated for wetlands, progressively increased pH and greater Mn content of sorbent at this stage of the treatment promoted attenuation of dissolved Mn^{II}. Simulation results for a reference scenario are also shown in Figure S7, where the existing sorbent and FeOB rate factor were set to 0, equivalent to the abiotic homogeneous Fe^{II} oxidation rate model. This abiotic reference scenario uses the same aeration coefficients and retention times as the biofouling scenario but underpredicts removal of Fe, Mn, and Al in the upper stages of the system where most chemical changes occur and does not indicate observed Mn^{II} attenuation. Simulation results for additional parameters (alkalinity, net acidity, temperature, specific conductance, accumulated solids, mass of limestone and SOC dissolved, DO, nitrate, DOC, sulfate, and TDS) indicated by the Pine Forest sequential kinetics model are included in the supplementary data (Figs. S6-S7).

Figure S6. UI for PHREEQ-N-AMDTreat sequential model exhibiting input values for simulation of water-quality changes through the Pine Forest treatment system, December 2015, which consists of a "biofouled" anoxic limestone drain (ALD), oxidation/settling pond, and three aerobic wetlands, with aeration steps in between. The values shown represent enhanced FeOB activity (factr.kbact 2, instead of default value of 1) and a specified sorbent mass of 116 mg in the ALD and smaller sorbent mass with progressively greater Mn content downstream. Results of simulations are shown in Figure S7.
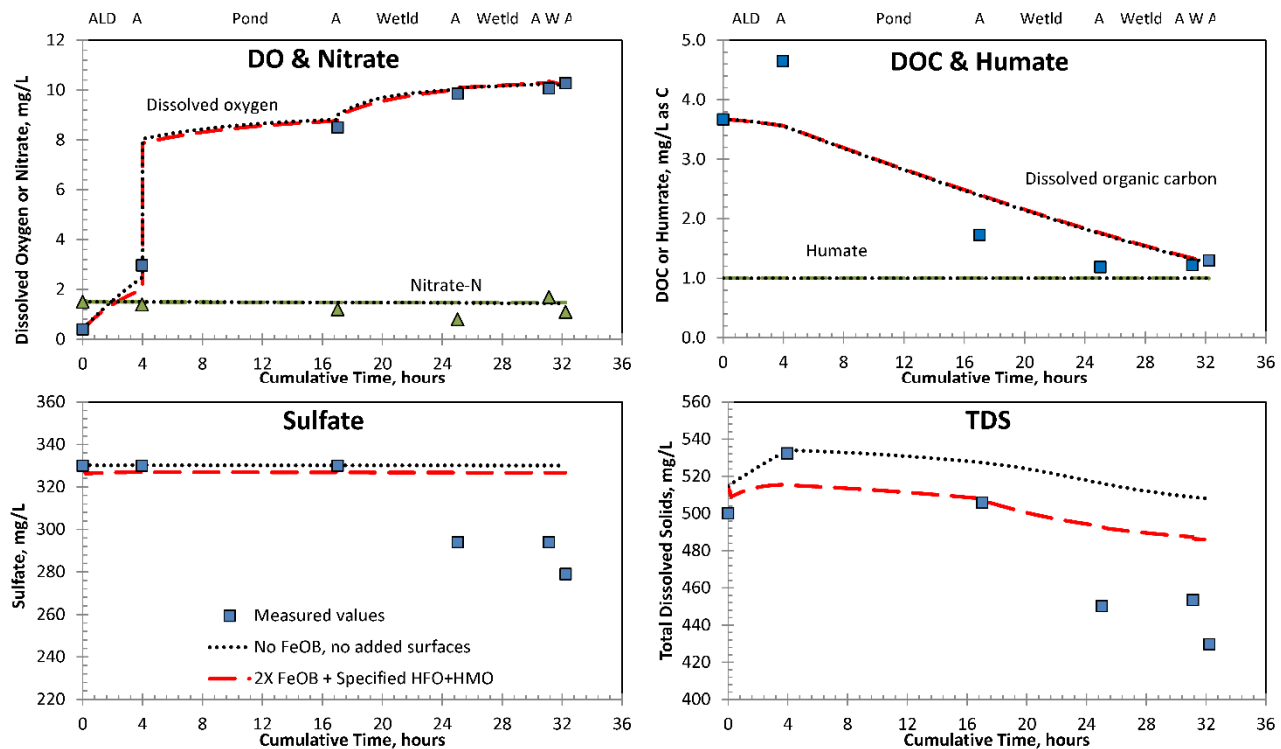
Figure S7. Comparison of measured (symbols) and simulated (curves) values for pH, Fe^{II}, Mn^{II}, Al, P_{CO_2}, and P_{O_2} during treatment of AMD at the Pine Forest passive treatment system, December 2015. Simulations used the PHREEQ-N-AMDTreat sequential model with initial water chemistry, specified values for $k_{L,CO_2}a$, FeOB rate factor, and sorbent mass and composition (Fig. S6). The black dotted curves show results for abiotic conditions without specified sorbent. The red dashed curves show results for enhanced FeOB activity (2X default FeOB rate) and specified sorbent mass in the ALD equivalent to 0.5-μm thick coating on all the limestone particles and smaller sorbent mass with progressively greater Mn content downstream.

Figure S7 (continued). Comparison of measured (symbols) and simulated (curves) values for pH, Fe^{II}, Mn^{II}, Al, Pco_2, and Po_2 during treatment of AMD at the Pine Forest passive treatment system, December 2015. Simulations used the PHREEQ-N-AMDTreat sequential model with initial water chemistry, specified values for $k_{L,CO2}a$, FeOB rate factor, and sorbent mass and composition (Fig. S6). The black dotted curves show results for abiotic conditions without specified sorbent. The red dashed curves show results for enhanced FeOB activity (2X default FeOB rate) and specified sorbent mass in the ALD equivalent to 0.5-μm thick coating on all the limestone particles and smaller sorbent mass with progressively greater Mn content downstream.

DO & Nitrate

Dissolved oxygen

Nitrate-N

DOC & Humate

Dissolved organic carbon

Humate

Sulfate

☐ Measured values

⋯⋯ No FeOB, no added surfaces

– – 2X FeOB + Specified HFO+HMO

TDS

Figure S7 (continued). Comparison of measured (symbols) and simulated (curves) values for pH, Fe^{II}, Mn^{II}, Al, P_{CO_2}, and P_{O_2} during treatment of AMD at the Pine Forest passive treatment system, December 2015. Simulations used the PHREEQ-N-AMDTreat sequential model with initial water chemistry, specified values for $k_{L,CO_2}a$, FeOB rate factor, and sorbent mass and composition (Fig. S6). The black dotted curves show results for abiotic conditions without specified sorbent. The red dashed curves show results for enhanced FeOB activity (2X default FeOB rate) and specified sorbent mass in the ALD equivalent to 0.5-μm thick coating on all the limestone particles and smaller sorbent mass with progressively greater Mn content downstream.

S3.4. Sequential Treatment by Cascades, Oxidation/Settling Ponds, and Aerobic Wetlands

Field and laboratory water quality plus sediment chemistry were measured at points within a passive treatment system for the Silver Creek discharge during winter 2015 and summer 2016 (Ashby, 2017; this paper). The untreated AMD was anoxic with pH 5.9-6.0 and concentrations of Fe^{II}, Mn^{II}, and Al of 17.0-20.0, 2.2-2.9, and 0.12-0.17 mg/L, respectively. This aerobic treatment system, constructed in 2008, consists of a sedimentation pond, two oxidation/settling ponds, and two aerobic wetlands, in series, with aeration cascades in between (Figs. S8-S11). During the winter sampling event, water temperature decreased through the system, whereas during the summer event, water temperature increased. Although influent to the sedimentation pond was clear

each visit, the second and third ponds were turbid orange-brown because of increased pH through the cascades followed by in-situ oxidation of Fe^{II} and slow settling of HFO-rich particles in the ponds. Simulation results where initial sorbent mass was specified with chemical composition of sampled sediments (to simulate suspended particles) and using the default value of 1 for FeOB rate factor (Figs. S8 and S10) resulted in values of pH, Fe^{II}, Mn^{II}, Al, P_{CO2}, and P_{O2} that generally reproduced the longitudinal trends for measured values (Figs. S9 and S11). Large changes in pH during the aeration steps resulted from rapid CO_2 outgassing, which affected the rates of Fe^{II} oxidation in subsequent steps. Eventual removal of Mn^{II} in the wetland treatment steps were simulated by the specification of accumulated sorbent having greater HMO content, as measured in the sediment. Higher measured values for Fe (assumed to be Fe^{II}) than simulated values for summer 2018, may reflect a substantial Fe^{III} colloidal fraction in the 0.45-μm filtered sample and/or short circuiting associated with thermal stratification.

In addition to data on the rates of change in water temperature, DO, pH, alkalinity, and solute concentrations used to calibrate these models, sediment chemistry at the outflow of each treatment step at the Silver Creek system were available to estimate the sorbent composition (Ashby, 2017). For the Silver Creek models, the CO_2 outgassing rate ($k_{La,CO2}$) and sorbent mass and composition (HMeO.mg, Fe%, Mn%, Al%) at each step were the only kinetics variables adjusted to achieve a reasonable match between empirical and simulated values for dynamic changes in pH, Fe, Mn, Al, and associated solute concentrations. Shallow, wide aeration cascades and long riprap runs were highly effective at facilitating gas exchange and rapid increases in pH, followed by Fe^{II} oxidation in large ponds with long retention times where gas exchange was limited by minimal advection. Greater mass and/or Mn content of sorbent increased Fe^{II} and Mn^{II} attenuation; most Mn was attenuated in wetlands at later treatment steps.

S3.4.1. Sequential Treatment by Cascades, Oxidation/Settling Ponds, and Aerobic Wetlands (Silver Creek, December 2015)
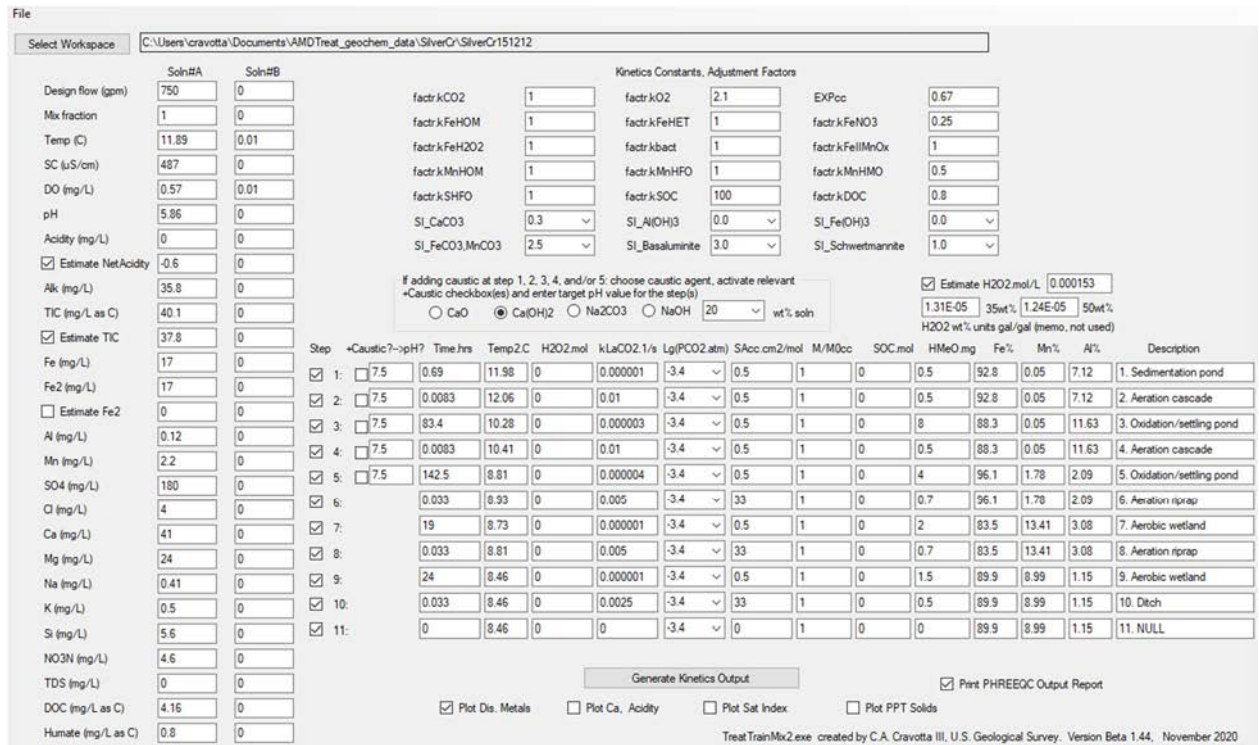
File

Select Workspace — C:\Users\cravotta\Documents\AMDTreat_geochem_data\SilverCr\SilverCr151212

	Soln#A	Soln#B
Design flow (gpm)	750	0
Mix fraction	1	0
Temp (C)	11.89	0.01
SC (uS/cm)	487	0
DO (mg/L)	0.57	0.01
pH	5.86	0
Acidity (mg/L)	0	0
☑ Estimate NetAcidity	-0.6	0
Alk (mg/L)	35.8	0
TIC (mg/L as C)	40.1	0
☑ Estimate TIC	37.8	0
Fe (mg/L)	17	0
Fe2 (mg/L)	17	0
☐ Estimate Fe2	0	0
Al (mg/L)	0.12	0
Mn (mg/L)	2.2	0
SO4 (mg/L)	180	0
Cl (mg/L)	4	0
Ca (mg/L)	41	0
Mg (mg/L)	24	0
Na (mg/L)	0.41	0
K (mg/L)	0.5	0
Si (mg/L)	5.6	0
NO3N (mg/L)	4.6	0
TDS (mg/L)	0	0
DOC (mg/L as C)	4.16	0
Humate (mg/L as C)	0.8	0

Kinetics Constants, Adjustment Factors

factr.kCO2	1	factr.kO2	2.1	EXPcc	0.67
factr.kFeHOM	1	factr.kFeHET	1	factr.kFeNO3	0.25
factr.kFeH2O2	1	factr.kbact	1	factr.kFeIIMnOx	1
factr.kMnHOM	1	factr.kMnHFO	1	factr.kMnHMO	0.5
factr.kSHFO	1	factr.kSOC	100	factr.kDOC	0.8
SI_CaCO3	0.3	SI_Al(OH)3	0.0	SI_Fe(OH)3	0.0
SI_FeCO3,MnCO3	2.5	SI_Basaluminite	3.0	SI_Schwertmannite	1.0

If adding caustic at step 1, 2, 3, 4, and/or 5: choose caustic agent, activate relevant +Caustic checkbox(es) and enter target pH value for the step(s)
○ CaO ◉ Ca(OH)2 ○ Na2CO3 ○ NaOH 20 wt% soln

☑ Estimate H2O2.mol/L 0.000153
1.31E-05 35wt% 1.24E-05 50wt%
H2O2 wt% units gal/gal (memo, not used)

Step	+Caustic?->pH?	Time.hrs	Temp2.C	H2O2.mol	kLaCO2.1/s	Lg(PCO2.atm)	SAcc.cm2/mol	M/M0cc	SOC.mol	HMeO.mg	Fe%	Mn%	Al%	Description
☑ 1:	☐ 7.5	0.69	11.98	0	0.000001	-3.4	0.5	1	0	0.5	92.8	0.05	7.12	1. Sedimentation pond
☑ 2:	☐ 7.5	0.0083	12.06	0	0.01	-3.4	0.5	1	0	0.5	92.8	0.05	7.12	2. Aeration cascade
☑ 3:	☐ 7.5	83.4	10.28	0	0.000003	-3.4	0.5	1	0	8	88.3	0.05	11.63	3. Oxidation/settling pond
☑ 4:	☐ 7.5	0.0083	10.41	0	0.01	-3.4	0.5	1	0	0.5	88.3	0.05	11.63	4. Aeration cascade
☑ 5:	☐ 7.5	142.5	8.81	0	0.000004	-3.4	0.5	1	0	4	96.1	1.78	2.09	5. Oxidation/settling pond
☑ 6:		0.033	8.93	0	0.005	-3.4	33	1	0	0.7	96.1	1.78	2.09	6. Aeration riprap
☑ 7:		19	8.73	0	0.000001	-3.4	0.5	1	0	2	83.5	13.41	3.08	7. Aerobic wetland
☑ 8:		0.033	8.81	0	0.005	-3.4	33	1	0	0.7	83.5	13.41	3.08	8. Aeration riprap
☑ 9:		24	8.46	0	0.000001	-3.4	0.5	1	0	1.5	89.9	8.99	1.15	9. Aerobic wetland
☑ 10:		0.033	8.46	0	0.0025	-3.4	33	1	0	0.5	89.9	8.99	1.15	10. Ditch
☑ 11:		0	8.46	0	0	-3.4	0	1	0	0	89.9	8.99	1.15	11. NULL

Generate Kinetics Output   ☑ Print PHREEQC Output Report

☑ Plot Dis. Metals   ☐ Plot Ca, Acidity   ☐ Plot Sat Index   ☐ Plot PPT Solids

TreatTrainMix2.exe created by C.A. Cravotta III, U.S. Geological Survey. Version Beta 1.44, November 2020

Figure S8. UI for PHREEQ-N-AMDTreat model exhibiting input values for simulations of sequential treatment steps at the Silver Creek treatment system, December 2015, which consists of a small sedimentation pond, two large oxidation/settling ponds, and two aerobic wetlands, with aeration cascades in between. Results of simulations are shown in Figure S9.
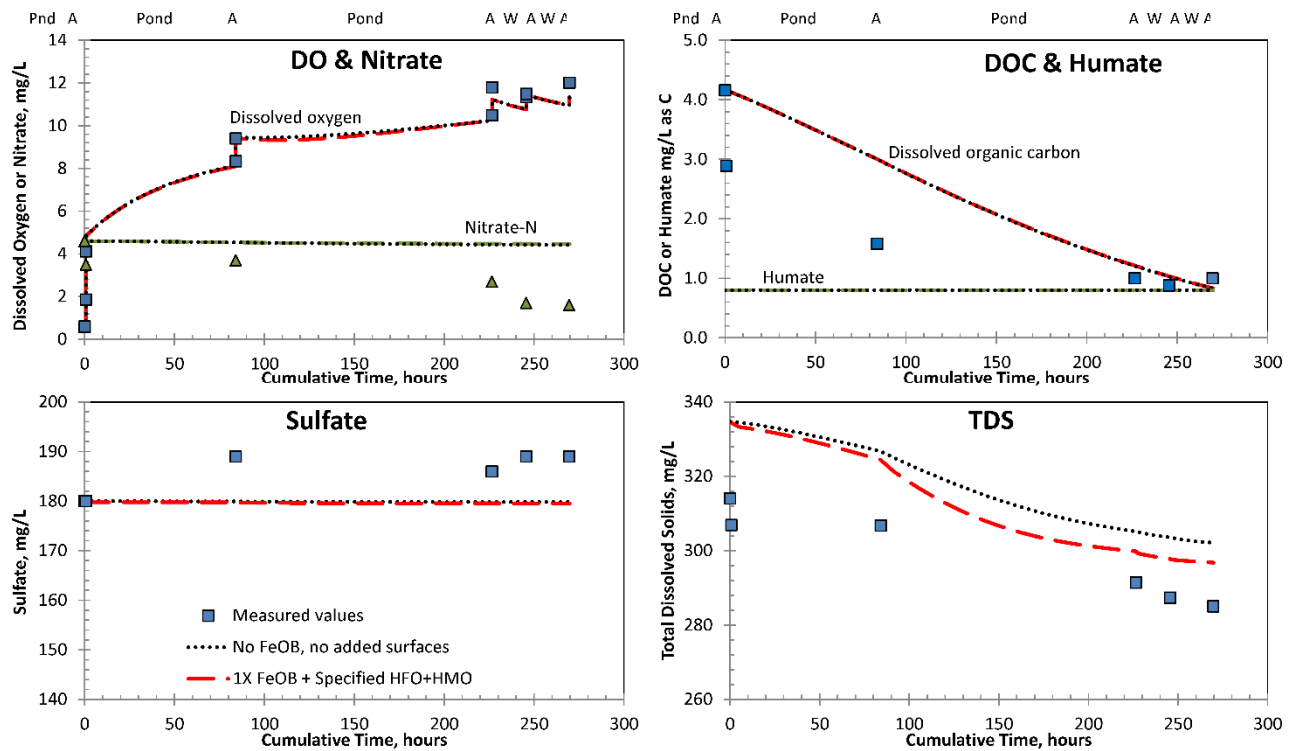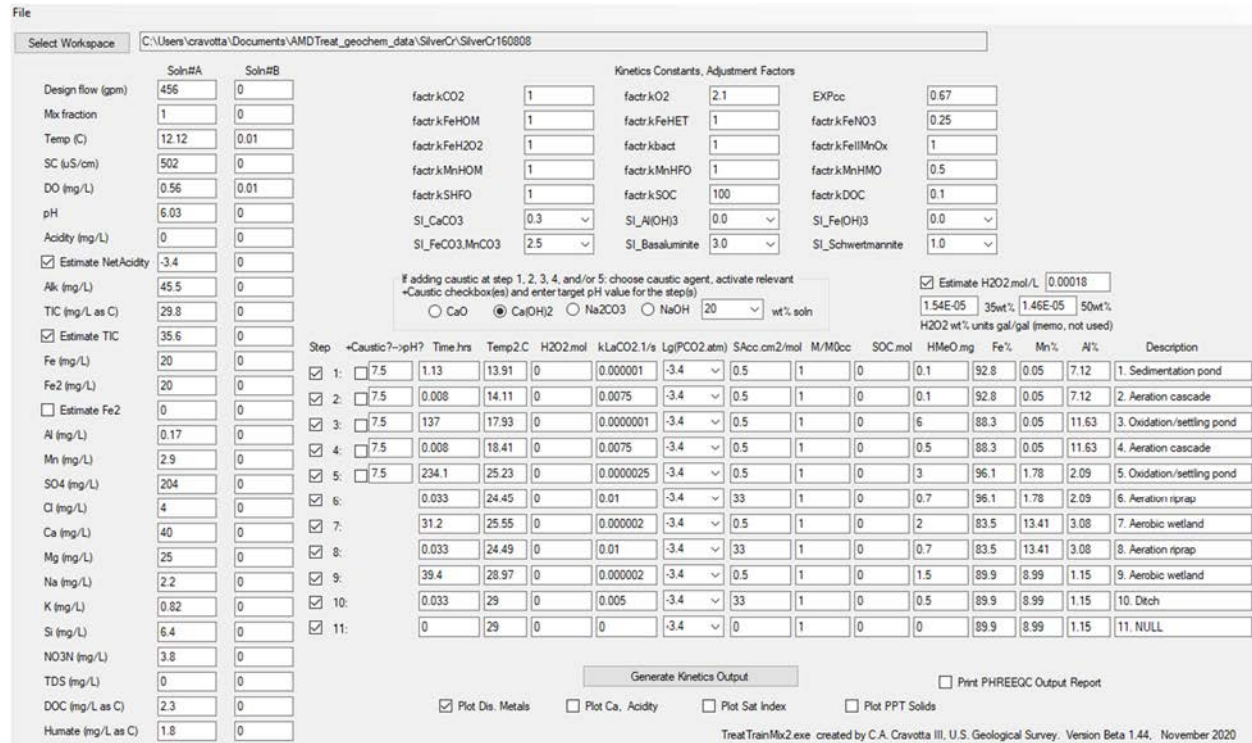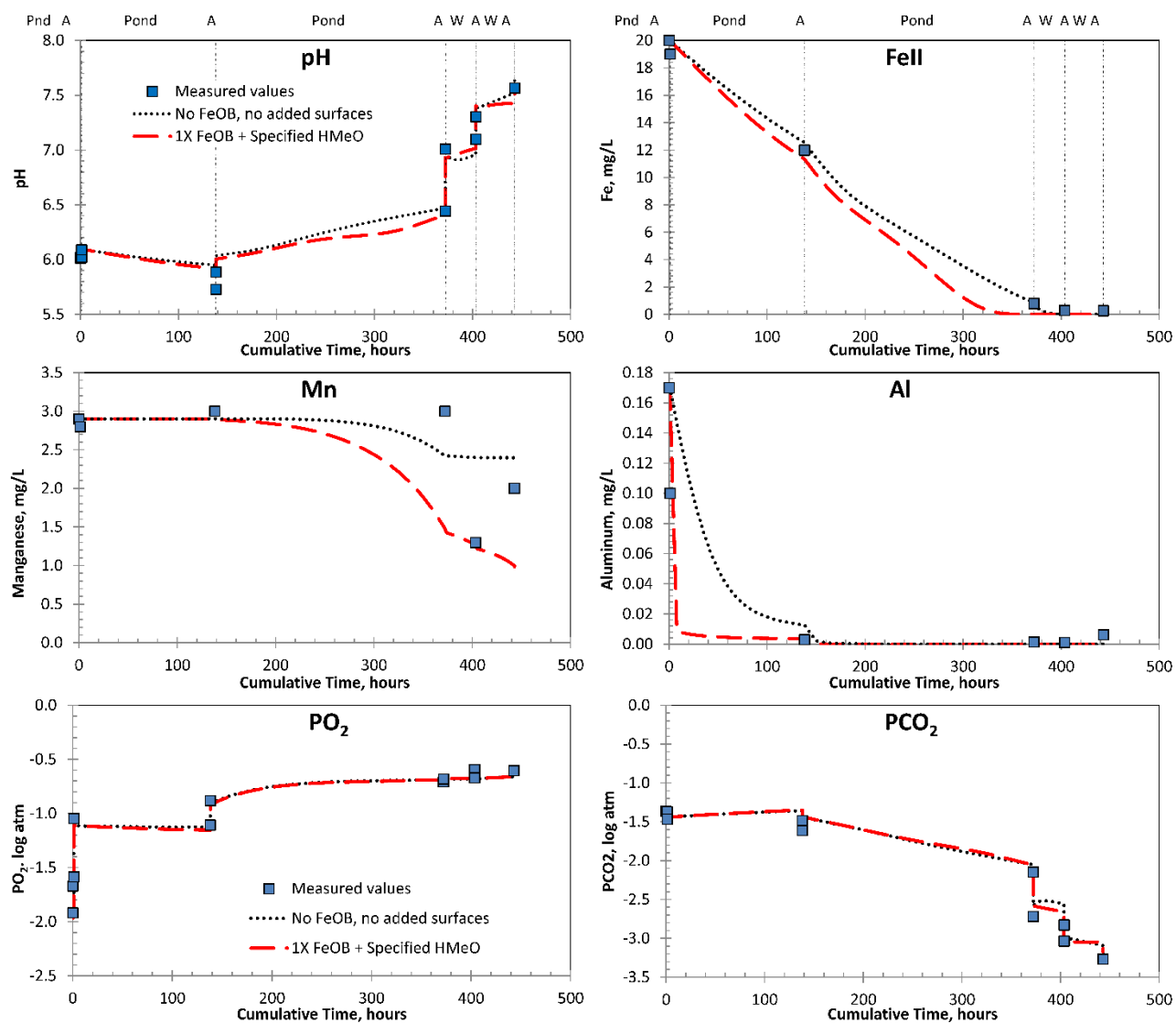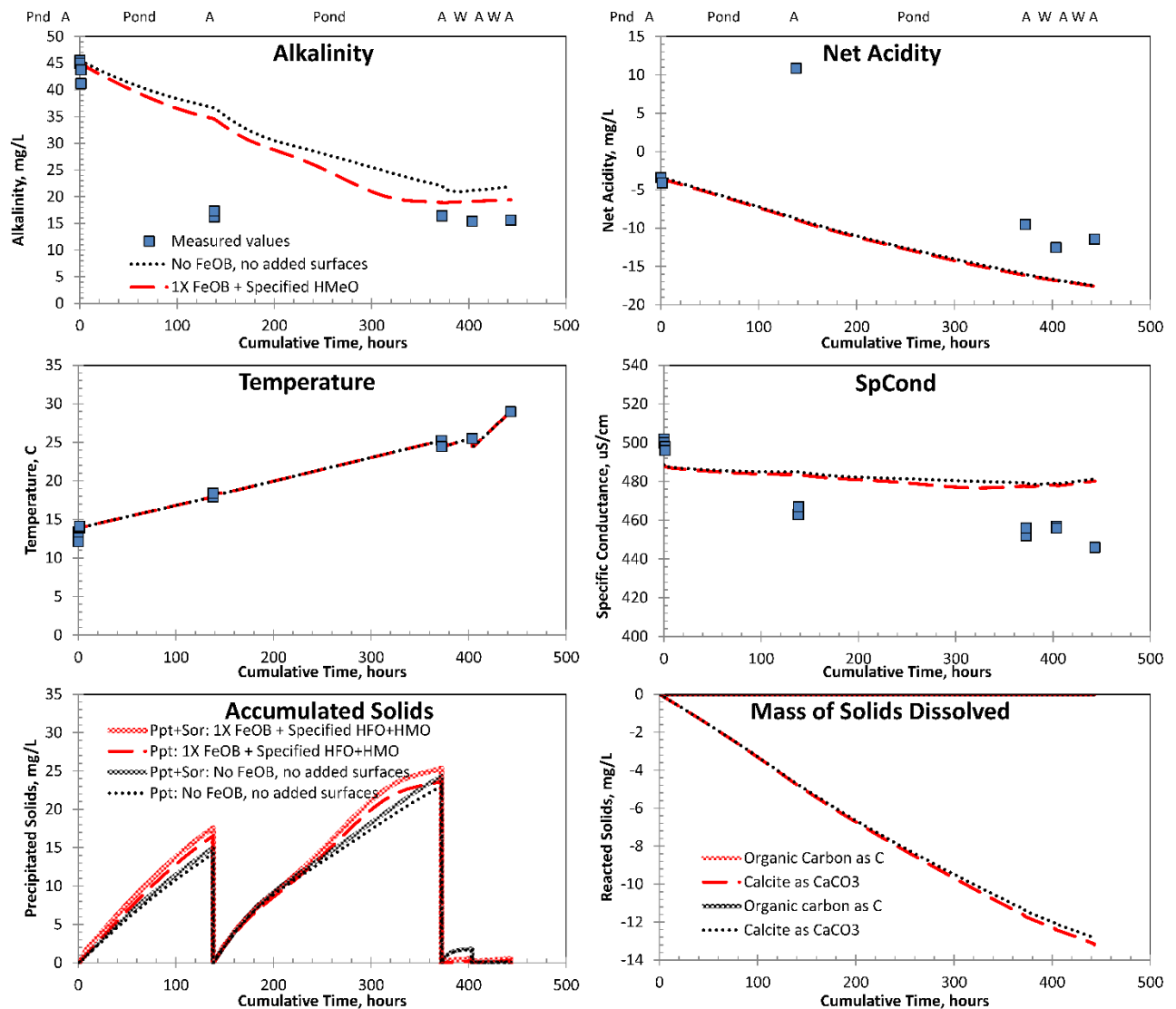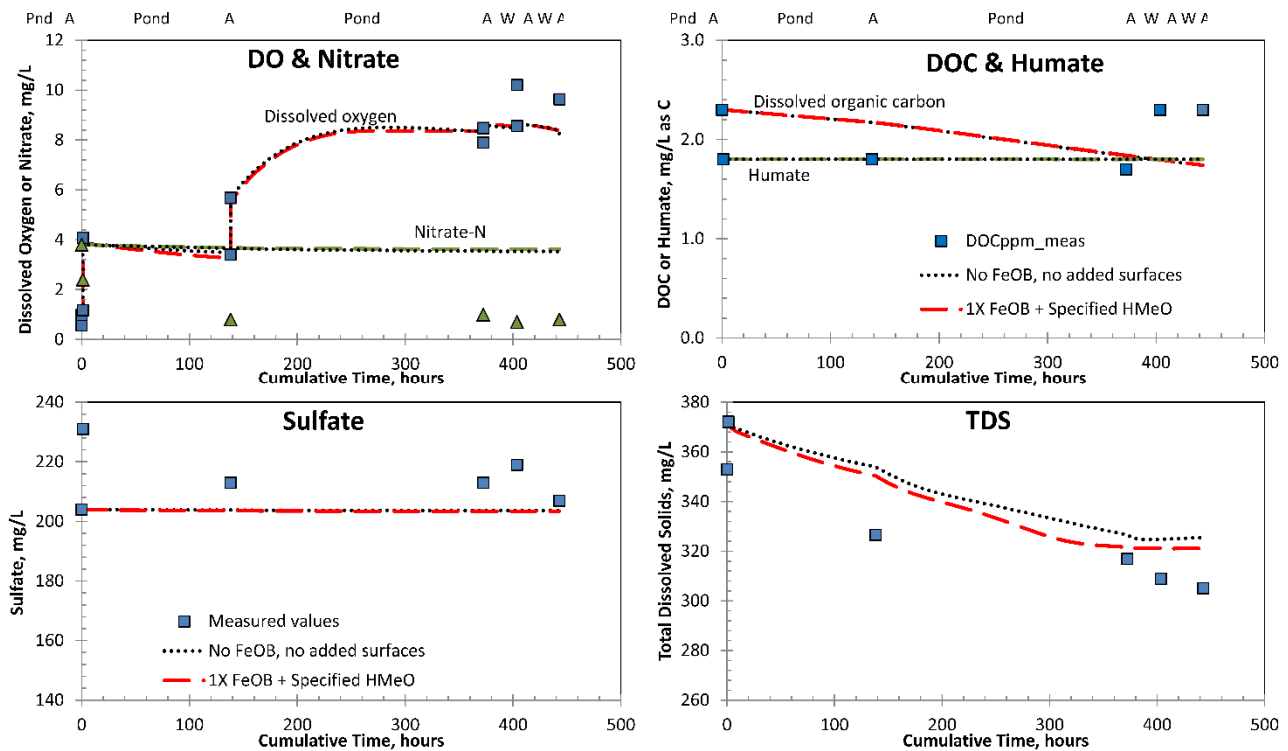
Figure S9. Comparison of measured (symbols) and simulated (curves) values for pH, Fe^{II}, Mn^{II}, Al, P_{CO_2}, and P_{O_2} during treatment of AMD at the Silver Creek passive treatment system, December 2015. Simulations used the PHREEQ-N-AMDTreat sequential model with initial water chemistry, specified values for $k_{L,CO_2}a$, and specified sorbent (Fig. S8). The red dashed curves show results for values in Figure S8, with specified sorbent representative of suspended solids having Fe-Mn-Al composition of sediment samples. The black dotted curves show results for conditions without FeOB catalysis or specified sorbent (values of 0).

Figure S9 (continued). Comparison of measured (symbols) and simulated (curves) values for pH, Fe^{II}, Mn^{II}, Al, P_{CO2}, and P_{O2} during treatment of AMD at the Silver Creek passive treatment system, December 2015. Simulations used the PHREEQ-N-AMDTreat sequential model with initial water chemistry, specified values for $k_{L,CO2}a$, and specified sorbent (Fig. S8). The red dashed curves show results for values in Figure S8, with specified sorbent representative of suspended solids having Fe-Mn-Al composition of sediment samples. The black dotted curves show results for conditions without FeOB catalysis or specified sorbent (values of 0).

Figure S9 (continued). Comparison of measured (symbols) and simulated (curves) values for pH, Fe^{II}, Mn^{II}, Al, P_{CO2}, and P_{O2} during treatment of AMD at the Silver Creek passive treatment system, December 2015. Simulations used the PHREEQ-N-AMDTreat sequential model with initial water chemistry, specified values for $k_{L,CO2}a$, and specified sorbent (Fig. S8). The red dashed curves show results for values in Figure S8, with specified sorbent representative of suspended solids having Fe-Mn-Al composition of sediment samples. The black dotted curves show results for conditions without FeOB catalysis or specified sorbent (values of 0).

S3.4.2. Sequential Treatment by Cascades, Oxidation/Settling Ponds, and Aerobic Wetlands (Silver Creek, August 2016)

Figure S10. UI for PHREEQ-N-AMDTreat sequential model exhibiting input values for simulations of sequential steps at the Silver Creek treatment system, August 2016. Results are shown in Figure S11.

Figure S11. Comparison of measured (symbols) and simulated (curves) values for pH, Fe^{II}, Mn^{II}, Al, Pco_2, and Po_2 during treatment of AMD at the Silver Creek passive treatment system, August 2016. Simulations used the PHREEQ-N-AMDTreat sequential model. The red dashed curves show results for values shown in Figure 8, with specified sorbent representative of suspended solids having Fe-Mn-Al composition of sediment samples. The black dotted curves show results for conditions without FeOB catalysis or specified sorbent (values of 0).

Figure S11 (continued). Comparison of measured (symbols) and simulated (curves) values for pH, Fe^{II}, Mn^{II}, Al, Pco_2, and Po_2 during treatment of AMD at the Silver Creek passive treatment system, August 2016. Simulations used the PHREEQ-N-AMDTreat sequential model. The red dashed curves show results for values shown in Figure 8, with specified sorbent representative of suspended solids having Fe-Mn-Al composition of sediment samples. The black dotted curves show results for conditions without FeOB catalysis or specified sorbent (values of 0).

Figure S11 (continued). Comparison of measured (symbols) and simulated (curves) values for pH, Fe^{II}, Mn^{II}, Al, Pco$_2$, and Po$_2$ during treatment of AMD at the Silver Creek passive treatment system, August 2016. Simulations used the PHREEQ-N-AMDTreat sequential model. The red dashed curves show results for values shown in Figure 8, with specified sorbent representative of suspended solids having Fe-Mn-Al composition of sediment samples. The black dotted curves show results for conditions without FeOB catalysis or specified sorbent (values of 0).

S4. Hypothetical Scenarios--Assessment of Potential Passive and Active Treatment Strategies

In this section, the TreatTrainMix2 sequential kinetics tool is used to assess hypothetical passive and active treatment strategies that may achieve equivalent effluent quality, with near-neutral pH and dissolved metals concentrations approaching 0. These simulated treatment scenarios demonstrate important effects of neutralization, oxidation-reduction, and precipitation processes during treatment steps. The modeled retention times for the treatment steps are then used to indicate the approximate sizes for comparison of the physical requirements of proposed treatment systems and to estimate generalized costs for installation, operation, and maintenance.

S4.1. Evaluation of Treatment Alternatives for Net-Acidic AMD

For the first case, the TreatTrainMix2 tool was used to evaluate potential chemical changes in the Morea AMD resulting from (1) passive treatment with a VFP followed by two oxidation ponds,

aerobic wetland, and manganese removal bed or (2) active treatment with hydrated lime, settling pond, and wetland. Median water-quality characteristics were considered for the untreated influent (Figs. S12, S13, S14, and S15). System components were simulated as a "treatment train" with retention times and other system properties adjusted to achieve desired water quality for each step.

The Morea mine discharges a large volume (7387 gal min^{-1}, 466 L s^{-1}) of net acidic (pH 3.4 to 3.8; hot acidity 32.6 to 57.8 mg/L as $CaCO_3$) AMD that has elevated concentrations of aluminum (3.1 to 3.8 mg/L), iron (5.0 to 8.7 mg/L), and manganese (1.3 to 1.7 mg/L) that could cause rapid fouling of a limestone bed if introduced directly. For passive treatment of such net-acidic water quality, a VFP, which consists of an organic rich compost layer containing dispersed limestone fines overlying a flushable bed of limestone aggregate, may be effective for the removal of initial Fe^{III} and Al with the addition of alkalinity early in the treatment scheme, followed by oxidation and removal of Fe^{II} and Mn^{II} in aerobic ponds and wetlands, and limestone-filled Mn-removal bed (e.g. Skousen et al., 2017; Watzlaf et al., 2000, 2004). Active lime dosing is an alternative treatment for such water quality (e.g. Cravotta et al., 2015; Skousen et al., 2019), which also requires some sort of settling ponds and/or wetlands to remove the precipitated solids. The active treatment system would require frequent site access for chemical delivery and system maintenance, whereas the passive treatment system would require less frequent access and maintenance and thus could have lower operation and maintenance costs than an active treatment system.

The Morea AMD passive treatment simulation (Fig. S12 and S13) indicates that during the cumulative retention time of 15 hours, pH increases from 3.5 to 7.5 while DO increases to near saturation, with corresponding decreases in dissolved Al, Fe, and Mn. Progressive dissolution of limestone fines within the compost bed of the VFP during 3-hr retention time (step 3) results in pH 6.0 to 6.5 and dissolved Al at a steady-state minimum; most of the initial Al and Fe^{III} accumulate as Al(OH)$_3$ and Fe(OH)$_3$ in the compost layer. Greater retention time in the compost (not shown) leads to more extensive sulfate reduction and the precipitation of a fraction of dissolved Fe^{II} as FeS. Otherwise, dissolved Fe^{II} and Mn concentrations are transported conservatively through the limestone bed of the VFP and are not attenuated until the aerobic ponds (steps 6 and 8), wetland (step 10), and Mn-removal bed (step 11). Aeration between these treatment steps is important for CO_2 outgassing and increasing pH that facilitate oxidation and adsorption processes. Simulations indicate two oxidation ponds with an intermediate aeration step are more efficient for Fe^{II} oxidation and require less space combined than a single, larger pond. After the ponds, remaining dissolved Fe is attenuated in wetlands, which also remove suspended HMeO solids (not modeled) and a small

fraction of dissolved Mn. Attenuation of Mn results mainly from adsorption by HMO-coated limestone surfaces within the Mn removal bed (step 11, HMeO 20 mg consisting of 99 wt% Mn and 1 wt% Fe). The adsorbed Mn is presumed to oxidize in place, aided by microbial activity (e.g. Burté et al., 2019; Means and Rose, 2005; Robbins et al., 1999a, 1999b; Santelli et al., 2010; Tan et al., 2010).

File

Select Workspace: C:\Users\cravotta\Documents\AMDTreat_geochem_data\MillCreek\Morea

Input	Soln#A	Soln#B
Design flow (gpm)	7387	0
Mix fraction	1	0
Temp (C)	10	0.01
SC (uS/cm)	455	0
DO (mg/L)	4.79	0.01
pH	3.54	0
Acidity (mg/L)	41.4	0
☑ Estimate NetAcidity	48.8	0
Alk (mg/L)	0	0
TIC (mg/L as C)	0	0
☑ Estimate TIC	1.2	0
Fe (mg/L)	7.26	0
Fe2 (mg/L)	5.64	0
☐ Estimate Fe2	0	0
Al (mg/L)	3.12	0
Mn (mg/L)	1.4	0
SO4 (mg/L)	129	0
Cl (mg/L)	7.77	0
Ca (mg/L)	20.1	0
Mg (mg/L)	7.52	0
Na (mg/L)	7.77	0
K (mg/L)	1.11	0
Si (mg/L)	7.77	0
NO3N (mg/L)	0.11	0
TDS (mg/L)	0	0
DOC (mg/L as C)	1.11	0
Humate (mg/L as C)	0.1	0

Kinetics Constants, Adjustment Factors

factr.kCO2	1	factr.kO2	2.1
factr.kFeHOM	1	factr.kFeHET	1
factr.kFeH2O2	1	factr.kbact	1
factr.kMnHOM	1	factr.kMnHFO	1
factr.kSHFO	1	factr.kSOC	100

EXPcc	0.67
factr.kFeNO3	0.25
factr.kFeIIMnOx	1
factr.kMnHMO	0.5
factr.kDOC	1

SI_CaCO3: 0.3 SI_Al(OH)3: 0.0 SI_Fe(OH)3: 0.0
SI_FeCO3,MnCO3: 2.5 SI_Basaluminite: 3.0 SI_Schwertmannite: 1.0

If adding caustic at step 1, 2, 3, 4, and/or 5: choose caustic agent, activate relevant +Caustic checkbox(es) and enter target pH value for the step(s)
○ CaO ● Ca(OH)2 ○ Na2CO3 ○ NaOH 20 ▼ wt% soln

☑ Estimate H2O2.mol/L 5.1E-05
4.4E-06 35wt% 4.1E-06 50wt%
H2O2 wt% units gal/gal (memo, not used)

Step	+Caustic?->pH?	Time.hrs	Temp2.C	H2O2.mol	kLaCO2.1/s	Lg(PCO2.atm)	SAcc.cm2/mol	M/M0cc	SOC.mol	HMeO.mg	Fe%	Mn%	Al%	Description
☑ 1:	☐7.5	0.25	12.1	0	0.000005	-3.4	0	1	0	1	100	0	0	1. Sedimentation pond
☑ 2:	☐7.5	1	12.1	0	0.000005	-3.4	0	1	0	1	100	0	0	2. VFP water layer
☑ 3:	☐7.5	3	15.1	0	0	-3.4	444	0.25	20	5	10.0	0	90.0	3. VFP compost layer
☑ 4:	☐7.5	5	15.1	0	0	-3.4	72	1	0	0.1	98.9	0.1	1.0	4. VFP limestone layer
☑ 5:	☐7.5	0.05	15.5	0	0.01	-3.4	0	1	0	0.1	97.0	3.0	0	5. Aeration cascades
☑ 6:		2	16.5	0	0.000005	-3.4	0	1	0	1	97.0	3.0	0	6. Oxidation/settling pond
☑ 7:		0.05	16.6	0	0.01	-3.4	0	1	0	1	97.0	3.0	0	7. Aeration cascades
☑ 8:		2	17	0	0.000005	-3.4	0	1	0	1	95.0	5.0	0	8. Oxidation/settling pond
☑ 9:		0.00833	17	0	0.005	-3.4	33	1	0	1	70.0	30.0	0	9. Aeration riprap
☑ 10:		1	17	0	0.00005	-3.4	72	0.1	0.1	1	70.0	30.0	0	10. Aerobic wetland
☑ 11:		0.5	17	0	0.0005	-3.4	72	1	0	20	1.0	99.0	0	11. Mn removal bed

Generate Kinetics Output

☐ Print PHREEQC Output Report

☑ Plot Dis. Metals ☐ Plot Ca, Acidity ☐ Plot Sat Index ☐ Plot PPT Solids

TreatTrainMix2.exe created by C.A. Cravotta III, U.S. Geological Survey. Version Beta 1.44, November 2020

Figure S12. UI showing values of input variables for TreatTrainMix2 simulation of passive treatment of net-acidic AMD at Morea Mine through (1) sedimentation pond; (2-4) vertical flow pond (VFP); (6, 8) oxidation/settling ponds; (10) aerobic wetlands; and (11) manganese removal bed with intermediate aeration steps (5 7 9 11). Results are shown in Figure S13.

Figure S13. TreatTrainMix2 simulation results for passive treatment of Morea AMD by (1) VFP (consisting of a 0.61-m (2-ft) deep water layer, 0.61-m (2-ft) thick compost layer composed of 25 % limestone fines and 75% organic matter having 45% porosity, 0.91-m (3-ft) thick limestone layer having 45% porosity), (2) 1.52-m (5-ft) deep aerobic pond, (3) 0.30-m (1-ft) deep wetlands, and (3) 0.30-m (0.5-ft) deep "manganese" removal limestone bed. Aeration steps are included between each of the major treatment stages.

The Morea AMD active treatment simulation (Fig. S14 and S15) indicates that during a cumulative retention time of 6.8 hours, the pH increases from 3.5 to 7.6 while DO increases to near saturation, with corresponding decreases in dissolved Al, Fe, and Mn. The Al, Fe, and Mn are indicated to accumulate as amorphous $Al(OH)_3$, $Fe(OH)_3$, and $MnOOH$ in the lime-mixing tank that included 100 mg/L recirculated solids (HMeO of 100 mg consisting of 61 wt% Fe, 12 wt% Mn, and 27 wt% Al). The large sorbent mass combined with high pH (8.5) promoted removal of the metals by adsorption, heterogeneous oxidation, and precipitation from solution. The aerobic pond and wetland that follow are primarily intended for settling of the metal-rich particles. Wetlands are included as "polishing" steps where suspended HMeO particles may be attenuated for both passive and active treatment systems. The PHREEQ-N-AMDTreat simulations do not evaluate particle transport or effects of HMeO accumulation on decreasing the retention times (owing to volume reduction) or limestone dissolution rates (owing to armoring or clogging).

Various sizing adjustments or maintenance may be considered to compensate for potential declines in performance as the systems age (e.g. Cravotta, 2003, 2008c; Hedin et al., 1994; Rose, 2004; Watzlaf et al., 2004; Wolfe et al., 2010).

Figure S14. UI showing values of input variables for TreatTrainMix2 simulation of active treatment of net-acidic AMD at Morea Mine through (1) sedimentation pond; (3) lime dosing and sludge recirculation; (4) aerobic pond; and (6) aerobic wetlands with aeration steps (2 5 7). Results are shown in Figure S15.

Figure S15. TreatTrainMix2 simulation results for active treatment of AMD at Morea Mine by (1) hydrated lime dosing and recirculation of sludge, including HMeO solids and unreacted lime, (2) 1.52-m (5-ft) deep aerobic pond, and (3) 0.30-m (1-ft) deep wetlands. Aeration steps are included between each of the major treatment stages. Results are shown as a function of the cumulative retention time within the treatment system.

Although the physical site characteristics are not explicitly considered in the PHREEQ-N-AMDTreat modeling tools, the retention time values for a model may be used to compute system sizing (Table S8). The volume for a treatment step in the kinetic model, such as pond or wetland, is computed as the product of flow rate and the retention time; area is computed as the volume divided by depth. For a pond, appropriate depths may be 2 to 4 m, whereas depths for a wetland generally may be 0.5 to 1 m, and less for aeration cascades (e.g. Hedin et al., 1994; Geroni et al., 2013; Skousen et al., 2017). For the VFP, volumes and depths for each of the three overlying layers (steps 2-4 in Table S8) are summed before computing area. Masses of limestone and compost also may be computed as the product of their respective volume and bulk density (Table S8).

Table S8. Estimated size of passive or active treatment systems for Morea AMD based on retention times used in TreatTrainMix2 simulations and 90th percentile flow.

Step	Treatment	flow rate, m^3/s	reten-tion time, sec	reten-tion time, hr	depth, m	porosity	volume, m^3	area of water surface, m^2	area of water surface, hectares	lime-stone particle size, AASHTO	CaCO3 fraction in bulk, M/M0cc	lime-stone mass, tonnes	compost organics mass, tonnes
	VFP, oxidation+settling pond, aerobic wetlands, and Mn bed												
1	Sedimentation pond	0.466	900	0.25	0.91	1.00	419	459	0.05		1.00	0	0
2	VFP water	0.466	3600	1.00	0.61	1.00	1678				1.00	0	0
3	VFP compost	0.466	10800	3.00	0.91	0.45	11185			8	0.25	4084	8265
4	VFP limestone	0.466	18000	5.00	0.91	0.45	18642	12920	1.29	3	1.00	27230	0
5	Aeration cascades	0.466	180	0.05	0.03	0.45	186	6116	0.61		1.00	272	0
6	Oxidation/settling pond	0.466	7200	2.00	1.52	1.00	3356	2202	0.22		1.00	0	0
7	Aeration cascades	0.466	180	0.05	0.03	0.45	186	6116	0.61		1.00	272	0
8	Oxidation/settling pond	0.466	7200	2.00	1.52	1.00	3356	2202	0.22		1.00	0	0
9	Aeration riprap	0.466	30	0.01	0.03	0.45	31	1019	0.10	R-3	1.00	45	0
10	Aerobic wetland	0.466	3600	1.00	0.30	0.90	1864	6116	0.61	3	0.10	50	272
11	Mn removal bed	0.466	1800	0.50	0.30	0.45	1864	6116	0.61	3	1.00	2723	0
1 to 11 Total:			14.86	7.10				43266	4.33			34676	8537
	Hydrated lime, oxidation+settling pond, and aerobic wetlands												
1	Sediment pond	0.466	900	0.25	0.91	1.00	419	459	0.05		1.00	0	0
2	Aeration Tank	0.466	90	0.03	1.52	1.00	42	28	0.00		1.00	0	0
3	Lime+recirculated sludge	0.466	1800	0.50	1.52	1.00	839	550	0.06		1.00	0	0
4	Oxidation/settling pond	0.466	14400	4.00	1.52	1.00	6711	4404	0.44		1.00	0	0
5	Aeration riprap	0.466	119	0.03	0.03	0.45	123	4037	0.40	R-3	1.00	180	0
6	Aerobic wetland	0.466	7200	2.00	0.30	0.90	3728	12232	1.22	3	0.10	99	543
7	Ditch	0.466	119	0.03	0.15	0.45	123	807	0.08	R-3	1.00	180	0
8	NULL	0.466	0	0.00	0.00	1.00	0	0	0.00		1.00	0	0
9	NULL	0.466	0	0.00	0.00	1.00	0	0	0.00		1.00	0	0
10	NULL	0.466	0	0.00	0.00	1.00	0	0	0.00		1.00	0	0
11	NULL	0.466	0	0.00	0.00	1.00	0	0	0.00		1.00	0	0
1 to 11 Total:			6.84	5.97				22516	2.25			458	543

AASHTO average particle diameter: R-3, 10.16 cm (4 inch); 3, 3.81 cm (1.5 inch); 8, 0.69 cm (0.25 inch). See table S7.

The estimated land area required for construction of the passive VFP and active lime treatment systems for the Morea discharge are given in Table S8. The passive treatment system water surface area is estimated at 4.33 ha, whereas that for the active treatment system is estimated at 2.25 ha. Considering a multiplier of 1.5 for clearing and grubbing, berms, and slopes, the total area increases to 6.5 ha for the passive treatment system and 3.4 ha for the active system. In general, site access, land ownership, and flooding potential would be considered as part of the feasibility analysis. For example, parts of two undeveloped adjoining parcels bordering the drainage channel below the Morea AMD site could be utilized for the construction and operation of the treatment system. Space is adequate to locate a passive or active treatment system outside the mapped flood zone. An existing gravel road could accommodate access for construction, delivery of lime and other chemicals, removal of sludge, and operations and maintenance.

To judge the potential cost-effectiveness of different treatment strategies, the sizing estimates from the PHREEQ-N-AMDTreat models may be considered with corresponding cost estimates for site development and system operations. Using the system sizing estimates given in Table S8 with

AMDTreat 5.0+ (Office of Surface Mining Reclamation and Enforcement, 2017), the approximate costs of construction (capital) plus annual costs of operation (labor, chemicals, sludge disposal) and maintenance (4 % of capital costs) were computed for the Morea AMD. Using default values for unit costs and assuming inflation of 5 % per year over 20 years (Pennsylvania Department of Environmental Protection, 2016), the net present value for the active treatment of Morea AMD is approximately US$2.7 million. Because of greater capital costs and relatively high annual costs based on a percentage of the capital costs, the net present value for the passive system is US$3.9 million using the same net worth factor. Thus, considering equivalent, acceptable effluent quality is predicted for both systems, the active treatment system would be considered the more cost-effective option for the Morea AMD.

S4.2. Evaluation of Treatment Alternatives for Combined AMD from Two Sources

Cravotta et al. (2014) and Cravotta (2015) reported field, laboratory, and modeling results for the headwaters of Schuylkill River, where AMD from the Pine Knot tunnel (PKN) and the Oak Hill boreholes (OAK) accounted for a majority of the streamflow to the West Branch during low-flow conditions. These two AMD sources contribute greater loadings of metals to the Schuylkill River than all the other dozens of AMD sources combined. Both AMD sources are net alkaline with comparable loads of dissolved Fe^{II}; however, the PKN was more dilute with approximately three times the flow volume and one-third the Fe concentration of OAK.

Cravotta (2015) described PHREEQC kinetic models for 1:3 mixtures of the two AMD sources (OAK:PKN) to simulate the observed downstream characteristics in the West Branch based on compositions for low-flow and high-flow end-member samples. Based on these calibrated models, Cravotta proposed a restoration strategy that could involve treatment of OAK and PKN at a single facility constructed on land outside the flood plain using enhanced aeration or H_2O_2 addition to decrease iron concentrations and maintain circumneutral pH of the net-alkaline AMD mixture. Pumping from the Oak Hill mine, which underlies the PKN tunnel outlet, would be conducted at a rate greater than or equal to that of the OAK discharge in order draw down the groundwater level in the Oak Hill mine, thus eliminating the current discharge. The abundant alkalinity of OAK could augment that of PKN, ensuring net-alkaline influent to the treatment plant.

Using the PHREEQ-N-AMDTreat "TreatTrainMix2" model, treatment alternatives were evaluated herein for the median 1:3 OAK:PKN mixtures using multiple treatment steps with variable aeration rates. Each treatment alternative is simulated to produce acceptable water quality

with near-neutral pH and low concentrations dissolved Fe, Al, and Mn. The first scenario considers a passive treatment strategy with aeration cascades (Figs. S16-S17), the second considers active treatment with forced aeration (S18-S19), and the third considers H_2O_2 addition without sludge recirculation (S20-S21). As a modification of the H_2O_2 treatment scenario, sludge recirculation was simulated by the inclusion of HMeO = 50 mg/L consisting of 100% Fe, during the step with H_2O_2 addition (e.g. Fig. S20); the had negligible effect on Mn removal. To attenuate dissolved Mn remaining in effluent after prior steps, a Mn-removal bed (e.g. Means and Rose, 2005) was added as the final step for each of the passive and active treatment models.

File

Select Workspace: C:\Users\cravotta\Documents\AMDTreat_geochem_data\WestBranch\OAK+PKN

Parameter	Soln#A	Soln#B
Design flow (gpm)	2830	8976
Mix fraction	0.24	0.76
Temp (C)	14.7	10.9
SC (uS/cm)	1000	570
DO (mg/L)	2	9.9
pH	6.3	6.4
Acidity (mg/L)	-111	-20
☑ Estimate NetAcidity	-110.7	-19.9
Alk (mg/L)	150	34
TIC (mg/L as C)	0	0
☑ Estimate TIC	73.3	15.7
Fe (mg/L)	18	5.15
Fe2 (mg/L)	18	5.15
☐ Estimate Fe2	0	0
Al (mg/L)	0.06	0.07
Mn (mg/L)	3.7	2.45
SO4 (mg/L)	390	240
Cl (mg/L)	8.8	17.5
Ca (mg/L)	99	40.5
Mg (mg/L)	55	42
Na (mg/L)	32	10
K (mg/L)	1.74	1.77
Si (mg/L)	5.72	5.72
NO3N (mg/L)	0.1	0.1
TDS (mg/L)	0	0
DOC (mg/L as C)	0.1	0
Humate (mg/L as C)	0.1	0

Kinetics Constants, Adjustment Factors

factr.kCO2	1	factr.kO2	2.1
factr.kFeHOM	1	factr.kFeHET	1
factr.kFeH2O2	1	factr.kbact	1
factr.kMnHOM	1	factr.kMnHFO	1
factr.kSHFO	1	factr.kSOC	100
EXPcc	0.67		
factr.kFeNO3	0.25		
factr.kFeIIMnOx	1		
factr.kMnHMO	0.5		
factr.kDOC	1		

SI_CaCO3	0.3	SI_Al(OH)3	0.0
SI_FeCO3,MnCO3	2.5	SI_Basaluminite	3.0
SI_Fe(OH)3	0.0	SI_Schwertmannite	1.0

If adding caustic at step 1, 2, 3, 4, and/or 5: choose caustic agent, activate relevant +Caustic checkbox(es) and enter target pH value for the step(s)
○ CaO ● Ca(OH)2 ○ Na2CO3 ○ NaOH 20 wt% soln

☑ Estimate H2O2.mol/L 0.00007411
6.4E-06 35wt% 6E-06 50wt%
H2O2 wt% units gal/gal (memo, not used)

Step	+Caustic?->pH?	Time.hrs	Temp2.C	H2O2.mol	kLaCO2.1/s	Lg(PCO2.atm)	SAcc.cm2/mol	M/M0cc	SOC.mol	HMeO.mg	Fe%	Mn%	Al%	Description
☑ 1:	☐ 7.5	0.25	14.7	0	0.000005	-3.4	0	1	0	0	100	0	0	1. Sedimentation pond
☑ 2:	☐ 7.5	0.05	14.7	0	0.01	-3.4	0	1	0	0	100	0	0	2. Aeration cascades
☑ 3:	☐ 7.5	8	15.1	0	0.000005	-3.4	0	1	0	3	998	0.1	0.1	3. Oxidation/settling pond
☑ 4:	☐ 7.5	0.01667	15.1	0	0.005	-3.4	33	1	0	2	99.8	0.1	0.1	4. Aeration riprap
☑ 5:	☐ 7.5	2	15.5	0	0.000005	-3.4	144	0.1	0.1	2	95	5	0	5. Aerobic wetland
☑ 6:		0.0333	15.5	0	0.005	-3.4	33	1	0	2	95	5	0	6. Aeration riprap
☑ 7:		0.5	16	0	0.0005	-3.4	72	1	0	20	10	90	0	7. Mn removal bed
☑ 8:		0.01667	17	0	0.005	-3.4	33	1	0	1	100	0	0	8. Ditch
☑ 9:		0	17	0	0	-3.4	0	1	0	0	100	0	0	9. NULL
☑ 10:		0	17	0	0	-3.4	0	1	0	0	100	0	0	10. NULL
☑ 11:		0	17	0	0	-3.4	0	1	0	0	100	0	0	11. NULL

Generate Kinetics Output   ☐ Print PHREEQC Output Report

☑ Plot Dis. Metals ☐ Plot Ca, Acidity ☐ Plot Sat Index ☐ Plot PPT Solids

TreatTrainMix2.exe created by C.A. Cravotta III, U.S. Geological Survey. Version Beta 1.44. November 2020

Figure S16. UI for PHREEQ-N-AMDTreat model exhibiting input values for simulations of hypothetical treatment using passive aeration after mixing of AMD from the Oak Hill boreholes (Soln#A) and Pine Knot tunnel (Soln#B). Treatment consists of a small sedimentation pond, aeration cascades, oxidation/settling pond, aerobic wetland, and Mn removal bed with aeration steps in between. Results of simulations are shown in Figure S17.
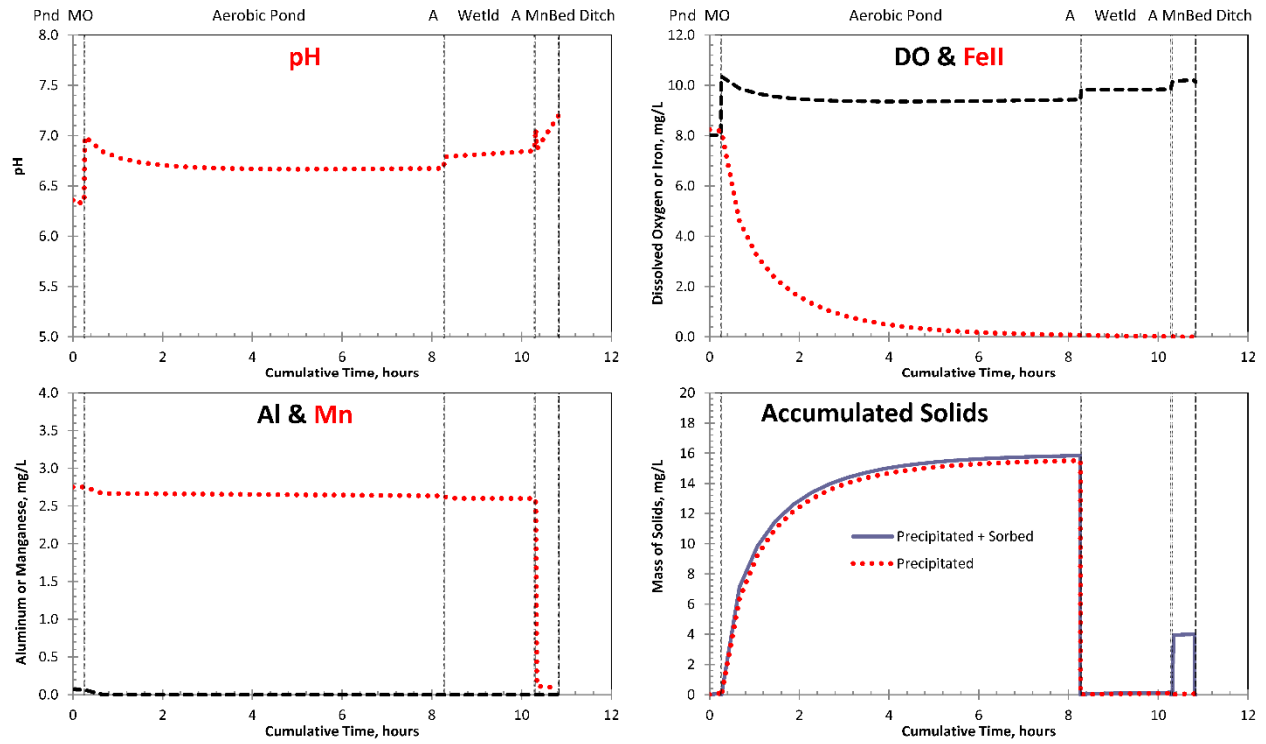
Figure S17. Simulation results for passive treatment of combined Oak Hill boreholes + Pine Knot tunnel AMD by aeration cascades, oxidation+settling pond, aerobic wetlands, and Mn-removal bed.

Figure S18. UI for PHREEQ-N-AMDTreat model exhibiting input values for simulations of hypothetical treatment using aggressive aeration after mixing of AMD from the Oak Hill boreholes (Soln#A) and Pine Knot tunnel (Soln#B). Treatment consists of a small sedimentation pond, Maelstrom Oxidizer®, oxidation/settling pond, aerobic wetland, and Mn removal bed with aeration steps in between. Results of simulations are shown in Figure S19.

Figure S19. Simulation results for passive treatment of combined Oak Hill boreholes + Pine Knot tunnel AMD by Maelstrom Oxidizer®, oxidation+settling pond, aerobic wetlands, and Mn-removal bed.

Figure S20. UI for PHREEQ-N-AMDTreat model exhibiting input values for simulations of hypothetical treatment using H₂O₂ after mixing of AMD from the Oak Hill boreholes (Soln#A) and Pine Knot tunnel (Soln#B). Treatment consists of a small sedimentation pond, H₂O₂ without sludge recirculation, oxidation+settling pond, aerobic wetlands, and Mn-removal bed with aeration steps in between. Results of simulations are shown in Figure S21.
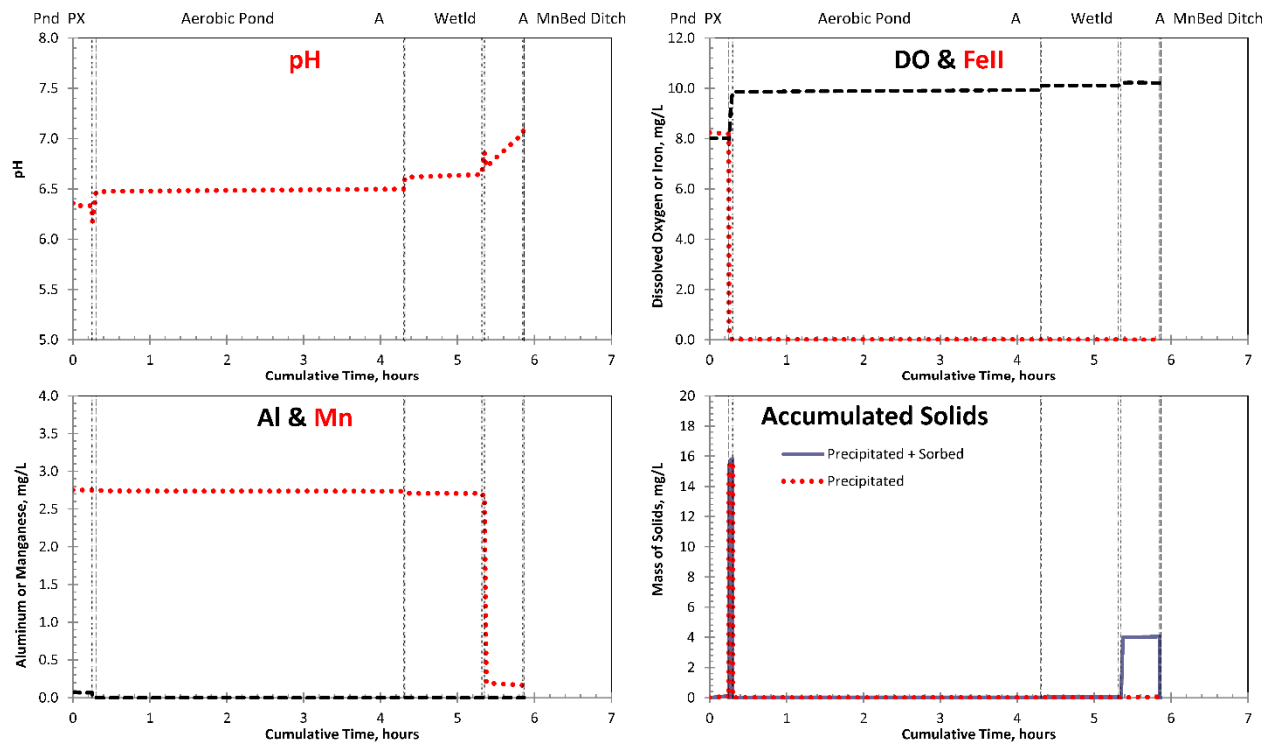
Figure S21. Simulation results for passive treatment of combined Oak Hill boreholes + Pine Knot tunnel AMD by H_2O_2 without sludge recirculation, oxidation+settling pond, aerobic wetlands, and Mn-removal bed. Note that if 100 % HFO sludge concentration of 50 mg/L is recirculated at step 2, almost all the original Mn remains in solution. Increased Mn content of the solids and increased pH as simulated for the Mn removal bed promote Mn attenuation.

Although the amount of retention time and, hence, land area required for treatments decreased for active treatment versus passive treatment, the costs for active treatment increased because of added expenses for electricity and pumping or H_2O_2 for active treatments. The passive aeration treatment system water surface area is estimated at 7.6 ha, whereas the estimates for the Maelstrom Oxidizer® and the H_2O_2 treatment systems are 7.5 ha and 4.8 ha, respectively. A multiplier of 1.5 for clearing and grubbing, berms, and slopes, increases the total acreage required for construction. Using the system sizing estimates given by the PHREEQ-N-AMDTreat TreatTrainMix2 simulations with the AMDTreat 5.0+ software (Cravotta et al., 2015), the approximate capital costs plus annual costs of operation and maintenance (4% of capital costs) for the passive and active treatment systems were computed. Capital costs were estimated to be US$1.2M, US$2.4M, and US$1.9M for the passive aeration, Maelstrom Oxidizer®, and H_2O_2 treatment systems, respectively. The corresponding annual cost for operation and maintenance of the passive aeration,

Maelstrom Oxidizer®, and H_2O_2 treatment systems were estimated to be US$0.014, US$0.019, and US$0.027 per 3785 L (1000 gallons), respectively. Assuming inflation of 5% per year over 20 years, the net present value for the passive treatment of the combined discharges is US$2.7M. Although it has smaller capital costs, H_2O_2 treatment has larger annual costs than the Maelstrom Oxidizer®. The net present value of active treatment with the Maelstrom Oxidizer® is US$4.3 million and that for active treatment with peroxide is US$4.7 million. Such cost estimates are preliminary and imprecise; site-specific information is essential for feasibility analysis and design of the selected treatment system.

S5. References for Supplementary Data

Appelo, C.A.J., Van Der Weiden, M.J.J., Tournassat, C., and Charlet, L., 2002. Surface complexation of ferrous iron and carbonate on ferrihydrite and the mobilization of arsenic. Environ. Sci. Technol. 36, 3096-3103.

Ashby, E.J., 2017. Biogeochemical mechanisms of rare earth element enrichment in mining-affected aqueous environments. University of Ottawa, Canada, M.S. thesis, 133 p.

Ball, J.W., and Nordstrom, D.K., 1991. User's manual for WATEQ4F, with revised thermodynamic data base and test cases for calculating speciation of major, trace, and redox elements in natural waters. U.S. Geol. Surv. Open-File Report 91-183.

Bigham, J.M., Schwertmann, U., Traina, S.J., Winland, R.L., and Wolf, M., 1996. Schwertmannite and the chemical modeling of iron in acid sulfate waters. Geochim. Cosmochim. Acta 60, 2111-2121. DOI: 10.1016/0016-7037(96)00091-9

Burrows, J.E., Cravotta, C.A. III, and Peters, S.C., 2017. Enhanced Al and Zn removal from coal-mine drainage during rapid oxidation and precipitation of Fe oxides at near-neutral pH: Appl. Geochem. 78, 194-210. DOI: 10.1016/j.apgeochem.2016.12.019

Charlton, S.R., and Parkhurst, D.L., 2011. Modules based on the geochemical model PHREEQC for use in scripting and programming languages. Computers & Geosciences 37, 1653-1663.

Cravotta, C.A. III, 2003. Size and performance of anoxic limestone drains to neutralize acidic mine drainage: J. Env. Qual., 32, 1277-1289. (https://doi.org/10.2134/jeq2003.1277)

Cravotta, C.A. III, 2008a. Dissolved metals and associated constituents in abandoned coal-mine discharges, Pennsylvania, USA -- 1. Constituent concentrations and correlations. Appl. Geochem. 23, 166-202.

Cravotta, C.A. III, 2008b. Dissolved metals and associated constituents in abandoned coal-mine discharges, Pennsylvania, USA -- 2. Geochemical controls on constituent concentrations. Appl. Geochem. 23, 203-226.

Cravotta, C.A. III, 2008c. Laboratory and field evaluation of a flushable oxic limestone drain for treatment of net-acidic, metal-laden drainage from a flooded anthracite mine, Pennsylvania, USA. Appl. Geochem. 23, 3404-3422.

Cravotta, C.A. III, 2015. Monitoring, field experiments, and geochemical modeling of FeII oxidation kinetics in a stream dominated by net-alkaline coal-mine drainage, Pennsylvania, U.S.A. Appl. Geochem. 62, 96-107.

Cravotta, C.A. III, 2020a. Interactive PHREEQ-N-AMDTreat water-quality modeling tools to evaluate performance and design of treatment systems for acid mine drainage. Appl. Geoch. https://doi.org/10.1016/j.apgeochem.2020.104845 .

Cravotta, C.A. III, 2020b. Interactive PHREEQ-N-AMDTreat water-quality modeling tools to evaluate performance and design of treatment systems for acid mine drainage (software download). U.S. Geological Survey Software Release https://doi.org/10.5066/P9QEE3D5 https://code.usgs.gov/water/phreeq-n-amdtreat/-/archive/v1.44/phreeq-n-amdtreat-v1.44.zip

Cravotta, C.A. III, and Trahan, M.K., 1999. Limestone drains to increase pH and remove dissolved metals from acidic mine drainage. Appl. Geochem. 14, 581-606.

Cravotta, C.A. III, and Watzlaf, G.R., 2003. Design and performance of limestone drains to increase pH and remove metals from acidic mine drainage, in Naftz, D.L., Morrison, S.J., Fuller, C.C., and Davis, J.A., eds., Handbook of groundwater remediation using permeable reactive barriers--Application to radionuclides, trace metals, and nutrients: San Diego, Ca., Academic Press, p. 19-66. (http://dx.doi.org/10.1016/B978-012513563-4/50006-2)

Cravotta, C.A. III, Means, B., Arthur, W., McKenzie, R., and Parkhurst, D.L., 2015. AMDTreat 5.0+ with PHREEQC titration module to compute caustic chemical quantity, effluent quality, and sludge volume. Mine Water Environ. 34, 136-152.

Cravotta, C.A. III, Ward, S.J., and Hammarstrom, J.M., 2008. Downflow limestone beds for treatment of net-acidic, oxic, iron-laden drainage from a flooded anthracite mine, Pennsylvania, USA--Laboratory evaluation: Mine Water Environ. 27, 86-99. (http://dx.doi.org/10.1007/s10230-008-0031-y).

Dzombak, D.A., and Morel, F.M.M., 1990. Surface complexation modeling: Hydrous ferric oxide. John Wiley and Sons, New York, NY, USA.

Geroni, J.N., Cravotta, C.A. III, and Sapsford, D.J., 2012. Evolution of the chemistry of Fe bearing waters during CO_2 degassing. Appl. Geochem. 27, 2335-2347.

Giffaut, E., Grivé, M., Blanc, P., Vieillard, P., Colàs, E., Gailhanou, H., Gaboreau, S., Marty, N., Madé, B., and Duro, L., 2014. Andra thermodynamic database for performance assessment: ThermoChimie. Appl. Geochem. 49, 225-236. doi.org/10.1016/j.apgeochem.2014.05.007

Hedin, R.S., Nairn, R.W., and Kleinmann, R.L.P., 1994. Passive treatment of coal mine drainage. U.S. Bureau of Mines Information Circular 9389, 35 p.

Jageman, T.C., Yokley, R.A., and Heunisch, H.E., 1988. The use of preaeration to reduce the cost of neutralizing acid mine drainage. U.S. Bureau of Mines Information Circular 9183, Pittsburgh, PA, p 131-135

Karamalidis, A.K., and Dzombak, D.A., 2010. Surface complexation modeling: Gibbsite. John Wiley & Sons, Inc., Hoboken, NJ, USA.

Kirby, C.S., and Cravotta, C.A., III, 2005. Net alkalinity and net acidity 2: Practical considerations. Appl. Geochem. 20, 1941-1964.

Liger, E., Charlet, L., Cappellen, P.V., 1999. Surface catalysis of uranium(VI) reduction by iron(II). Geochim. Cosmochim. Acta 63, 2939-2955.

Lozano, A., Ayora, C., and Fernández-Martínez, A., 2020. Sorption of rare earth elements on schwertmannite and their mobility in acid mine drainage treatments. Appl. Geochem. 113, 104499. doi.org/10.1016/j.apgeochem.2019.104499

Majzlan, J., Navrotsky, A., and Schwertmann, U., 2004. Thermodynamics of iron oxides. Part III. Enthalpies of formation and stability of ferrihydrite ($\sim Fe(OH)_3$), schwertmannite ($\sim FeO(OH)_{3/4}(SO_4)_{1/8}$), and e-$Fe_2O_3$. Geochim. Cosmochim. Acta 68, 1049-1059.

Means, B., and Hilton, T., 2004. Comparison of three methods to measure acidity of coal-mine drainage. Proceedings of the 2004 National Meeting of the American Society of Mining and Reclamation and the 25th West Virginia Surface Mine Drainage Task Force, p. 1249-1277.

Means, B., and Rose, A.W., 2005. Manganese removal in limestone bed systems. Proceedings of the 2005 National Meeting of the American Society of Mining and Reclamation, p. 702-717.

Means, B., Beam, R., and Charlton, D., 2013. Operational and financial studies of hydrogen peroxide versus hydrated lime and hydrogen peroxide versus sodium hydroxide at two

Pennsylvania mine drainage treatment sites. West Virginia Mine Drainage Task Force, 2013 Symposium https://wvmdtaskforce.files.wordpress.com/2016/01/13-means-paper.doc

Means, B., Parker, B., and Beam, R., 2015. Decarbonating at the St. Michael Treatment plant: Effect on cost, sludge, and sedimentation. West Virginia Mine Drainage Task Force, 2013 Symposium https://wvmdtaskforce.files.wordpress.com/2016/01/15-means-paper.docx

Myneni, S.C.B., Traina, S.J., and Logan, T.J., 1998. Ettringite solubility and geochemistry of the $Ca(OH)_2$-$Al_2(SO_4)_3$-H_2O system at 1 atm pressure and 298K. Chem. Geol. 148, 1-19.

Office of Surface Mining Reclamation and Enforcement, 2017. AMDTreat.(last updated 2017). https://amd.osmre.gov/ accessed August 24, 2020.

Parkhurst, D.L., and Appelo, C.A.J., 2013. Description of input and examples for PHREEQC version 3—A computer program for speciation, batch-reaction, one-dimensional transport, and inverse geochemical calculations. U.S. Geol. Surv. Techniques Methods 6-A43, 497 p. https://pubs.er.usgs.gov/publication/tm6A43 https://www.usgs.gov/software/phreeqc-version-3/

Peiffer, S., dos Santos Afonso, M., Wehrli, B., and Gachter, R., 1992. Kinetics and mechanism of the reaction of H_2S with lepidocrocite. Environ. Sci. Technol. 26, 2408-2412.

Robbins, E.I., Cravotta, C.A. III, Savela, C.E., and Nord, G.L. Jr., 1999a. Hydrobiogeochemical interactions in "anoxic" limestone drains for neutralization of acidic mine drainage. Fuel 78, 259-270.

Robbins, E.I., Brant, D.L., and Ziemkiewicz, P.F., 1999b. Microbial, algal, and fungal strategies for manganese oxidation at a Shade Township coal mine, Somerset County, Penna, in Proceedings American Society of Mining and Reclamation, Scottsdale, AZ, August 13-19, 1999, p. 634-640. DOI: 10.21000/JASMR99010634.

Rose, A.W., 1999. Chemistry and kinetics of calcite dissolution in passive treatment systems, in Proceedings American Society of Mining and Reclamation, Scottsdale, AZ, August 13-19, 1999, p. 634-640. DOI: 10.21000/JASMR99010599.

Rose, A.W., 2004. Vertical flow systems-Effects of time and acidity relations, in Proceedings American Society of Mining and Reclamation, Morgantown, WV, April 18-24, 2004, p 1595-1616. DOI: 10.21000/JASMR04011595.

Sajih, M., Bryan, N., Livens, F., Vaughan, D., Descostes, M., Phrommavanh, V., Nos, J., and Morris, K., 2014. Adsorption of radium and barium on goethite and ferrihydrite: A kinetic and surface complexation modelling study. Geochim. Cosmochim. Acta, 146: 150-163.

Skousen, J.G., Zipper, C.E., Rose, A.W., Ziemkiewicz, P.F., Nairn, R., McDonald, L.M., and Kleinmann, R.L., 2017. Review of passive systems for acid mine drainage treatment. Mine Water Environ. 36, 133-153.

Swedlund, P.J., and Webster, J.G., 1999. Adsorption and polymerisation of silicic acid on ferrihydrite, and its effect on arsenic adsorption. Water Research 33 3413-3422.

Tan, H., Zhang, G., Heaney, P.J., Webb, S.M., Burgos, W.D., 2010. Characterization of manganese oxide precipitates from Appalachian coal mine drainage treatment systems. Appl. Geochem. 25, 389-399. DOI: 10.1016/j.apgeochem.2009.12.006

Thomas, R.C., and Romanek, C.S., 2002a. Passive treatment of low-pH, ferric dominated acid rock drainage in a vertical flow wetland--I. Acidity neutralization and alkalinity generation, in Proceedings American Society of Mining and Reclamation, Lexington, Kentucky, June 9-13, 2002, p. 723-748. DOI: 10.21000/JASMR02010723

Thomas, R.C., and Romanek, C.S., 2002b. Passive treatment of low-pH, ferric dominated acid rock drainage in a vertical flow wetland--II. Metal removal, in Proceedings American Society of Mining and Reclamation, Lexington, Kentucky, June 9-13, 2002, p. 752-775. DOI: 10.21000/JASMR02010752

Tonkin, J.W., Balistrieri, L.S., and Murray, J.W., 2004. Modeling sorption of divalent metal cations on hydrous manganese oxide using the diffuse double layer model. Appl. Geochem. 19, 29-53.

Van Geen, A., Robertson, A.P., and Leckie, J.O., 1994. Complexation of carbonate species at the goethite surface: Implications for adsorption of metal ions in natural waters. Geochim. Cosmochim. Acta 58, 2073-2086.

Watzlaf, G.R., Schroeder, K.T., Kleinmann, R.L.P., Kairies, C.L., and Nairn, R.W., 2004. The passive treatment of coal mine drainage. U.S. Department of Energy DOE/NETL-2004/1202 (accessed June 15, 2020 at http://www.bobkleinmann.com/images/2004_DOEPassiveTreatment_of_Coal_Mine_Drainage_NETL-1202.pdf)

Wolfe, N., Hedin, R.S., and Weaver, T., 2010. Sustained treatment of AMD containing Al and Fe^{3+} with limestone aggregate, in International Mine Water Association 2010 Symposium, Sydney, Nova Scotia, Canada, p. 237-241. https://www.imwa.info/docs/imwa_2010/IMWA2010_Hedin_490.pdf

Additional relevant references used for the model development are included in the main paper by Cravotta (2020a).